THE UNIVERSITY *of* EDINBURGH

Dynamical evolution of idealised star cluster models

Philip Breen

Doctor of Philosophy
University of Edinburgh
2012

Declaration

I declare that this thesis was composed by myself and that the work contained therein is my own, except where explicitly stated otherwise in the text.

(*Philip Breen*)

To my wife Clodagh

Abstract

This thesis is concerned with the dynamical evolution of globular star clusters modelled as the classical gravitational N-body problem. The models in this thesis are idealised in order to allow the detailed study of particular dynamical aspects of the cluster evolution. Examples of properties which tend to be omitted are stellar evolution, primordial binaries and the effect of an external tidal gravitational field. The methods used in this thesis are gas models, N-body models and physical arguments.

One of the main topics in this thesis is gravothermal oscillations in multicomponent star clusters. The evolution of one-component globular clusters, systems with equal particle masses, is quite well understood. However, the evolution of more realistic globular clusters, with a range of particle masses, is a much more complicated matter. The condition for the on-set of gravothermal oscillations in a one-component system is simply that the number of stars is greater than a certain number ($\approx$ 7000). In a multi-component system the relationship between the number of stars at which the gravothermal oscillations first appear and the stellar mass distribution of a cluster is a complex one. In order to investigate this phenomenon two different types of multi-component systems were studied: two-component systems (the simplest approximation of a mass spectrum, Chapter 2) and ten-component systems (which were realisations of continuous power law IMFs, Chapter 3). In both cases the critical number of stars at which gravothermal oscillations first appear are found empirically for a range of stellar mass distributions. The nature of the oscillations themselves are investigated and it is shown that the oscillations can be understood by focusing on the behaviour of the heavier stars within the cluster. A parameter N_{ef} (definined M_{tot}/m_{max} where M_{tot} is the total mass and m_{max} is the maximum stellar mass) acts as an approximate stability boundary for multicomponent systems.The stability boundary was found to be at $N_{ef} \simeq 12000$.

In this Chapter 4, globular star clusters which contain a sub-system of stellar-mass black holes (BH) are investigated. This is done by considering two-component models, as these are the simplest approximation of more realistic multi-mass systems, where one component represents the BH population and the other represents all the other stars. These systems are found to undergo a long phase of evolution where the centre of the system is dominated by a BH sub-system. After mass segregation has driven most of the BH into a compact sub-system, the evolution of the BH sub-system is found to be influenced by the cluster in which it is contained. The BH sub-system evolves in such a way as to satisfy the energy demands of the whole cluster, just as the core of a one component system must satisfies the energy demands of the whole cluster. The BH sub-system is found to exist for a significant amount of time. It takes approximately $10t_{rh,i}$, where $t_{rh,i}$ is the initial half-mass relaxation time, from the formation of the compact BH sub-system up until the time when 90% of the sub-system total mass is lost (which is of order 10^3 times the half-mass relaxation time of the BH sub-system at its time of formation). Based on theoretical arguments the rate of mass loss from the BH sub-system ($\dot{M}_2$) is predicted to be $(\beta\zeta M)/(\alpha t_{rh})$: where M is the total mass, t_{rh} is the half-mass relaxation time, and α, β, ζ are three dimensionless parameters. (see Section 4.3 for details). An interesting consequence of this is that the rate of mass loss from the BH sub-system is approximately independent of the stellar mass ratio (m_2/m_1) and the total mass ratio (M_2/M_1) (in the range $m_2/m_1 \gtrsim 10$ and $M_2/M_1 \approx 10^{-2}$, where m_1, m_2 are the masses of individual low-mass and high-mass particles respectively, and M_1, M_2 are the corresponding total mass). The theory is found to be in reasonable agreement with most of the results of a series of N-body simulations, and all of the models if the value of ζ is suitable adjusted. Predictions based on theoretical arguments are also made about the structure of BH sub-systems. Other aspects of the evolution

are also considered such as the conditions for the onset of gravothermal oscillation.

The final chapter (Chapter 5) of the thesis contains some concluding comments as well as a discussion on some possible future projects, for which the results in this thesis would be useful.

Acknowledgements

In presenting this thesis, I would like to acknowledge the help and support I have received throughout my PhD.

First and foremost, I would like to express my deepest gratitude to my supervisor, Professor Douglas Heggie, for his guidance and support during the course of my PhD. I sincerely appreciate the time and energy that was put into my supervision.

Secondly, many thanks to both the administration and support staff at the School of Mathematics, University of Edinburgh, that contributed to making my PhD programme proceed smoothly.

Some of the hardware used for the N-body simulations in the thesis was purchased using a Small Project Grant awarded to Professor Douglas Heggie and Dr. Maximilian Ruffert by the University of Edinburgh Development Trust and I am most grateful for access to the hardware.

I would also like to acknowledge the Science and Technology Facilities Council for providing the studentship which supported me throughout my PhD.

Finally, I would like to thank my wife Clodagh for her invaluable support and encouragement throughout the course of my PhD.

Contents

Chapter 1

Introduction

1.1 Globular star clusters

Globular star clusters consist of between roughly 10^4 to 10^6 stars which are nearly spherically distributed. These clusters are found in orbit around galaxies. There are at least 150 known globular star clusters (Harris, 1996) in our own galaxy, the Milky Way, while large elliptical galaxies may have thousands. In the case of our galaxy, these clusters are very old and are believed to be relics from the formation of our galaxy. The centres of star clusters are very dense with typical values of $10^4 M_\odot pc^{-3}$, especially when compared with the local solar neighbourhood ($0.05 M_\odot pc^{-3}$, Binney & Tremaine (2008)). Therefore it is not surprising that it is often remarked that globular clusters make the ideal test bed for stellar dynamics. As an example an image of one of the galactic globular clusters (47 Tucanae) is given in Figure 1.1[1].

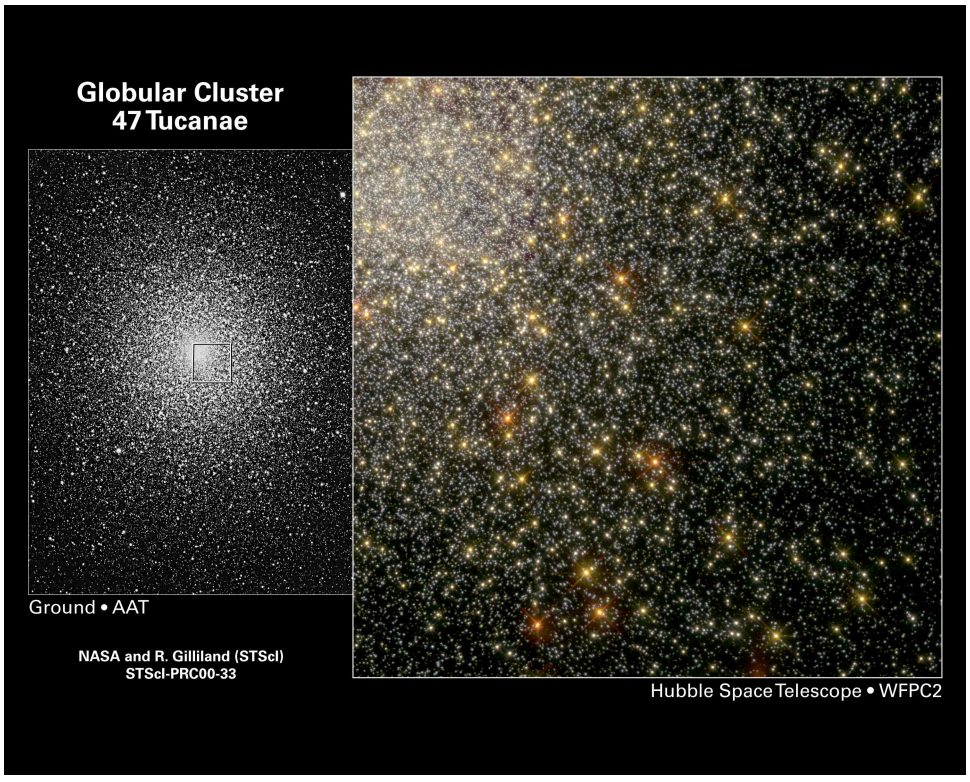

Figure 1.1: Globular cluster 47 Tucanae

[1]Credits for image: NASA and Ron Gilliland (Space Telescope Science Institute) and David Malin, Anglo-Australian Observatory

Globular clusters are normally characterised by three radii, the core radius r_c, the half mass radius r_h and tidal radius r_t. A table containing all the notation used in the present thesis is given in Appendix A. The tidal radius is the radius at which the gravitation force of the cluster equals the tidal gravitation force of the galaxy. The half mass radius, as the name suggests, is the radius of a sphere (centred at the cluster centre) containing half the total mass of the system. There are many different ways to define r_c. A dynamical definition (Heggie & Hut, 2003; Binney & Tremaine, 2008) which is commonly used in the present thesis is

$$r_c = \sqrt{\frac{9\sigma_c^2}{4\pi\rho_c}}$$

where ρ_c is the central density and σ_c is the one dimensional velocity dispersion. However the direct N-body code NBODY6 (see 1.3 and Aarseth (2012)), which is also frequently used in the present thesis uses a different definition of r_c. Observational astronomers also use a different definition for r_c, where r_c as the radius at which the surface brightness drop off by half its central value. Observational astronomers also tend to use the projected half light radius, the radius which contains half the surface brightness in projection, in place of r_h. To give the reader an idea of the usual values of r_c, r_h and r_t for globular clusters associated with our galaxy, the median values are $1pc$, $3pc$ and $35pc$ respectively (Binney & Tremaine, 2008; Harris, 1996).

1.2 Dynamics

This section briefly introduces some of the relevant aspects of stellar dynamics, specifically focusing on the core concepts needed to understand the basic dynamical evolution of globular star clusters. Given the high central mass densities of globular star clusters it is perhaps not surprising that two body encounters (gravitational encounters between two stars which alter the stars' velocities) have an effect on the structure of the system. In fact stellar dynamics can be divided into two types: collisionless stellar dynamics, where the effects of two body encounters are negligible and collisional stellar dynamics[2] where the accumulated effects of two body encounters are important. For a more detailed introduction to stellar dynamics see the textbooks Heggie & Hut (2003), Spitzer (1987) and Binney & Tremaine (2008).

1.2.1 Relaxation time and crossing time

The process by which two body encounters have an effected the system is know as relaxation or two body relaxation. Normally the relaxation time within r_h is used as a global time scale for relaxation, which is referred to as the half-mass relaxation time (t_{rh}). This is typically defined as follows

$$t_{rh} = \frac{0.138N^{\frac{1}{2}}r_h^{\frac{3}{2}}}{(G\bar{m})^{\frac{1}{2}}\ln\Lambda}, \tag{1.1}$$

where N is the number of stars, $\bar{m}$ is the average stellar mass, G is Newtons constant and $\ln\Lambda$ is the coulomb logarithm (Spitzer, 1987). The median value of (t_{rh}) for the Milky way globular clusters is $1.17 \times 10^9 yr$ (Heggie & Hut, 2003).

The relaxation time in the core of the system is also of interest, as the system's mass density is at its highest within r_c. The core relaxation time (t_{rc}) can be defined as

$$t_{rc} = \frac{0.34\sigma_c^3}{G^2\bar{m}_c\rho_c\ln\Lambda}, \tag{1.2}$$

[2]The word collisional in this context can be a bit misleading. Whilst physical collisions can occur in dense stellar systems, the term refers to the spread of heat (kinetic energy) through two body encounters. There is an analogy with molecular dynamics where the molecules exchange energy through two body encounters though in this case the encounters are actually physical collisions.

where the subscript c indicates that the properties of the value correspond to those of the core. As the core has a higher density than within r_h, the relaxation time in the core is considerably shorter than t_{rh}. For the Milky Way globular clusters the median value of t_{rc} is $3.4 \times 10^8 yr$, which is about an order of magnitude smaller than the median value of t_{rh}.

Another important time scale is the crossing time t_{cr}; this time scale is used little in the present thesis but has been included here for completeness. It is defined as the time it takes for a particle to cross the system. It is usually significantly shorter than the local relaxation time (by approximately a factor $0.1N/logN$ (Binney & Tremaine, 2008)). The importance of the crossing time is that it is the timescale at which the system achieves virial equilibrium. A system is said to be in virial equilibrium if the condition $2K + W = 0$ is satisfied, where K is the total kinetic energy of system and W is the total potential energy of the system. Therefore if a system is disturbed from virial equilibrium, it will evolve back towards it on the crossing time scale.

1.2.2 Core collapse

The temperature of a star cluster can be defined in terms of the mean-square velocity $\bar{v}^2$, where $\bar{v}^2 = 3\sigma^2$. If we cool a star cluster by removing energy from the star cluster, the stars would sink in the gravitational potential well. There the stars would be subject to a stronger gravitational force, which in turn would increase the stars' velocities. Thus as you cool a star cluster its temperature increase. Alternative if energy is added to a star cluster it expands, the gravitational potential reduces and therefore the velocities of the stars also reduce (i.e. the temperature drops). This odd behaviour results from the fact that star clusters have a negative heat capacity. In fact any bound, finite gravitational system has a negative heat capacity (another example being a star itself).

If there is a temperature gradient between the inner and outer parts of a cluster, heat flows from the inner part of the cluster to the other part of the system, causing the inner part to contract and heat up, increasing the temperature gradient. This leads to a runaway process where the core of the system continuously loses energy, contracts and heats up. The phenomenon is known as core collapse or more dramatically the gravothermal catastrophe Lynden-Bell & Wood (1968). The collapse of the core if it is sufficiently deep, the structure of the core approaches a self-similar model (Lynden-Bell & Eggleton, 1980).

Ultimately the flow of heat from the core must be balanced by a source of energy generation otherwise the central density would become infinite in finite time (Hénon, 1965, 1975). What the energy source could be is a point which will discussed in the next section. Figure 1.2 shows the process of core collapse in a cluster with $N = 10^4$ equal mass stars, calculated using a gas code (see section 1.3).

The core collapse time t_{cc} for a single component cluster with Plummer model initial conditions (Plummer, 1911) has been found to be approximately $15.5t_{i,rh}$ (Binney & Tremaine, 2008; Heggie & Hut, 2003) using various methods. Takahashi (1995) found a longer t_{cc} of $17.6t_{rh,i}$ with a single component anisotropic Fokker-Planck code. However, the presence of a range of stellar masses can have a dramatic effect on the collapse time (Chernoff & Weinberg, 1990; Murphy et al, 1990) because the process of mass segregation speeds up the collapse of the core (see section 1.2.3).

1.2.3 Mass segregation

Each component in a multi-component systems try to achieve kinetic energy equipartition (i.e $m_i\bar{v}_i^2 \rightarrow m_j\bar{v}_j^2$, where $i \neq j$), which causes the more massive stars to have low velocities and to sink towards the centre. This can lead to an instability in which the heavier stars continuously lose energy to the lighter stars causing the heavier stars to sink in the gravitational well, where they are subject to stronger gravitational forces, heat up and bring the system further from equipartition of kinetic energy. This instability is known as the equipartition instability or Spitzer instability (Spitzer, 1987). The equipartition instability is self limiting as once the density of heavier star dominates the centre, the density of the lighter component becomes significantly smaller, reducing the heat flow from the heavy component. At this point the gravothermal instability takes over and the core will continue to collapse. As mass segregation

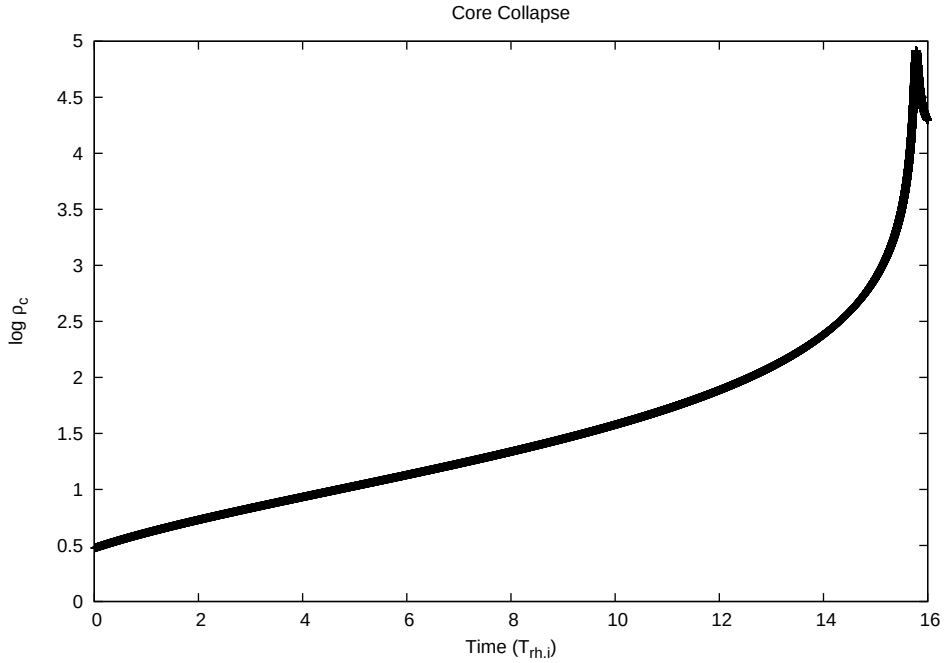

Figure 1.2: Central density (ρ_c) vs time (in units of the initial relaxation time $t_{rh,i}$) calculated using a gas code with $N = 10^4$ equal mass stars.

enhances the central density, the time of core collapse is shorter in multi-component systems than for the one component case.

Spitzer (1987) gave an analytical criterion for two-component system, to determine whether it is possible for a two component system to achieve equipartition of kinetic energy. Spitzer (1987) found that it is possible for energy equipartition to be achieved if

$$\frac{M_2}{M_1}\Big(\frac{m_2}{m_1}\Big)^{\frac{3}{2}} < 0.16 \tag{1.3}$$

where M_1 and M_2 are the total masses in light and heavy components and m_1 and m_2 are the stellar masses of each component, respectively. However, a more recent study by Watters, Joshi & Rasio (2000), using Monte Carlo simulations, found that a more reliable criterion was

$$\frac{M_2}{M_1}\Big(\frac{m_2}{m_1}\Big)^{2.4} < 0.32. \tag{1.4}$$

An example of mass segregation in a two-component model is shown in Fig 1.3. This was calculated using a two component model which will be described in Section 1.3 (also see Chapter 2). The effect of mass segregation for a range of two-component models has been studied using direct N-body methods by Khalisi et al (2007).

1.2.4 Post collapse evolution

Core collapse was a major research topic in the area of star cluster dynamics in the 1970's and 1980's. Researchers often used idealised models in which the effects of stellar evolution, escaping stars,the galactic tidal and stellar mass spectrum were simplified or ignored altogether. For example, there has been much research completed using models in which all the stars had identical masses. This was done in order to isolate the dynamic processes one wished to study. Through this research core collapse became a rather well understood phenomenon and the focus of researchers moved to gaining an understanding of the effect of more realistic models and post collapse evolution.

Core collapse is ultimately terminated by the generation of energy in the core (Heggie & Hut,

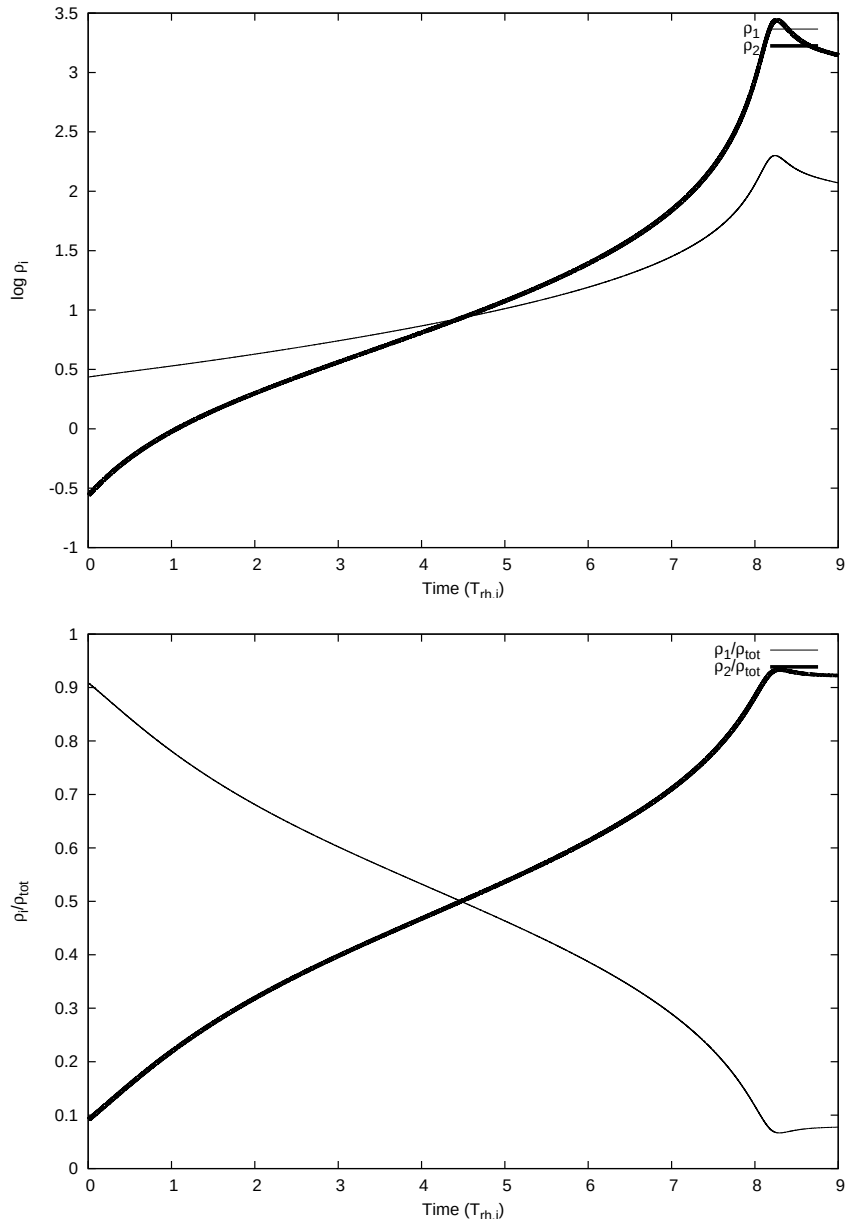

Figure 1.3: Mass segregation in a two component model with total mass ratio $M_2/M_1 = 0.1$ and stellar mass ratio $m_2/m_1 = 2$. Top: Central density of each component (ρ_i) vs time. Bottom: Contribution of each component to the total central density ($\frac{\rho_i}{\rho_1+\rho_2}$) vs time. In both figures the thick line corresponds to the heavy component and the thin line corresponds to the light component.

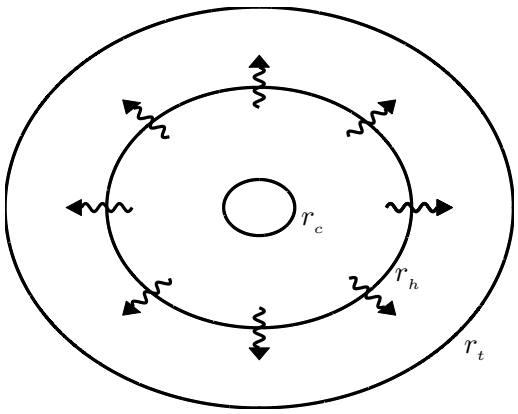

Figure 1.4: **Hénon's Principle:** The core of the system evolves to produce enough energy to balance the outward flux of kinetic energy across r_h. The rate of energy production in the core is regulated as follows: if too much energy is being generated, not enough kinetic energy is being removed and the core expands causing a drop in the rate of energy generation. Alternatively if not enough energy is being generated, the outward flux at r_h is still the same, which causes the core to contract, increasing the rate of energy generation.

2003, and references therein). Possible energy sources included stellar evolution (Gieles, 2012), an intermediate mass black hole (Baumgardt et al, 2005), primordial binaries (McMillan et al, 1990; Heggie & Hut, 2003; Heggie & Aarseth, 1992) and dynamically formed binaries (Heggie, 1975). It is only the last one of these (dynamically formed binaries) which is considered in the present chapter. Dynamically formed binaries are formed in three body encounters, where one body binds the other two by removing kinetic energy from them. The binary than generates more energy through encounters with other stars in the system. (The energy generated by a black hole binary is discussed in detail in Chapter 4). Energy generation heats the cluster causing it to expand on the time scale proportional to t_{rh}.

We will now consider a concept used frequently in the present thesis, Hénon's Principle (Hénon, 1965), which is thought to govern the post collapse evolution of a star cluster. Hénon's Principle states that the core evolves to produce energy generation in such a way as to balance the outward flux of kinetic energy at r_h. Hénon's Principle is illustrated in Fig 1.4. Hénon's Principle is a really powerful concept, as we do not even need to know the nature of the power source to know exact how much energy will be generated. The energy source will simply adjust itself to produced the require amount of energy (providing that there is some mechanism by which the cluster can regulate the energy source).

If N is small enough and the system is isolated (i.e. there is no external tidal field) the cluster undergoes a smooth self similar expansion. Therefore it would be expected that r_c increases smoothly and r_c/r_h is constant. However, whilst studying the post-collapse evolution of star clusters using a gas model, Bettwieser & Sugimoto (1985) found large oscillations in density. This was in sharp contrast to the predicted steady post-collapse evolution of star clusters. This phenomenon was called gravothermal oscillation and the condition for the onset of the instability in multicomponent models is the main topic of Chapters 2 & 3. The condition for the one-component system is quite well established (Goodman, 1987; Makino , 1996; Cohn et al, 1989). See the introduction sections in Chapters 2 & 3 for more details.

1.2.5 Mass loss by escape, external tides and stellar evolution

As the stars in a globular cluster near the end of their lives they often lose a large amount of mass. The mass lost by stars is normally travelling fast enough to escape the cluster and thus the cluster itself loses mass. As the more massive stars age more quickly than less massive stars and as they tend to be concentrated in the central region of the cluster due to mass segregation,

the mass loss can have a dramatic effect on the dynamics of the cluster (see for example Lamers et al (2005)). The stars can also experience a velocity kick as a result of stellar evolution which can give the star enough speed to escape the cluster.

Mass can also be lost from a cluster because of the escape of the stars themselves. The stars in a cluster tend to achieve a Maxwellian distribution of velocity, which continuously generates stars with speeds above the escape speed, which results in mass loss on the relaxation time scale (Spitzer, 1987). In fact the escape of stars from a cluster is actually more complicated then this simple picture (Fukushige & Heggie, 2000; Baumgardt, 2001).

Globular clusters normally experience an external tidal field from their host galaxies. During the post collapse evolution, the cluster expands and loses mass as the stars are stripped away by the host galaxy (for example see Küpper et al (2010)). Gieles et al (2011) found that roughly 1/3 of the galactic globular cluster are tidally limited systems and the other 2/3 are in an expansion-dominated phase evolution.

1.3 Models

There are many different methods of modelling star clusters from computationally costly direct N-body codes to simple analytical models.

The most detailed way, which is also the most computationally costly, is using direct N-body codes such as the NBODY6 (Aarseth, 2003) or starlab (www.sns.ias.edu/∼starlab/starlab.html). Direct N-body codes use a variety of sophisticated methods to improve the performance such as individual time steps and regularization. Improvements in hardware also helped improve the number of stars that it is possible to simulate (e.g Graphical Processing Units). However, it still is currently not feasible to run direct N-body simulations of large star clusters ($N \sim 10^6$). In this thesis all direct N-body simulations were conducted using NBODY6 enabled for use with Graphical Processing Units (GPU) (Nitadori & Aarseth, 2012). NBODY6 has a range of features and options such as individual time steps which make it an excellent direct N-body code. NBODY6 is written in FORTRAN and is publicly available for download from www.ast.cam.ac.uk/∼ sverre/web/pages/nbody.htm.

Another more approximate method is the gas models which is useful because it is computationally cheap. Therefore, it is possible to complete a large number of simulations in a short period of time. As gas models are one of the main methods used in the present thesis, the equations of the one component model are discussed in section 1.3.1. Although only the simplest kind of one component gas model is considered in section 1.3.1 a lot of the fundamental aspects of star cluster dynamics are captured by this model. More complicated gas models do exist, for example the multi-component gas model used in Chapter 3. Even gas models which have stochastic energy generation source have been developed (Takahashi & Inagaki, 1995).

Other methods of Modelling star clusters include Monte-Carlo methods (Hénon, 1971), Fokker-Planck models (Cohn, 1979) and semi analytical models (Alexander & Gieles, 2012).

1.3.1 Equations of the one component gas model

The stars in a star cluster can be thought of in a similar way as molecules in a gas. For example, in Section 1.2.2 it was stated that the temperature of a cluster can be thought of as its mean squared velocity. This idea can be extended to create a complete model of a star cluster (Lynden-Bell & Wood, 1968). We will now explain the equations to construct a one-component gas model (for a two component model see section 2.3). The first equation is a simple but necessary statement of mass conservation, i.e.

$$\frac{\partial M}{\partial r} = 4\pi\rho r^2,$$

where $M(r)$ is the mass inside radius r. Next, in a self gravitating gas the gravitational force must be balanced by its pressure, otherwise the gas would collapse. If the star cluster is thought of as an ideal gas the pressure could be defined as $p = \rho\sigma^2$, where σ is the one dimensional

velocity dispersion. This gives the equation of hydrostatic support:

$$\frac{\partial p}{\partial r} = -\frac{GM(r)}{r^2}\rho.$$

The temperature gradient is equal to the energy flux times an appropriate term for the thermal conductivity of the cluster. The thermal conductivity of a star cluster is quite different from a gas. The molecules of a gas only move short distances before colliding with other molecules. The stars in a cluster can travel large distances along their orbits before an encounter with another star occurs. Thus the heat flux L of a star cluster must be inversely proportional to the relaxation time (t_r), resulting in:

$$\frac{\partial \sigma^2}{\partial r} = -\frac{\sigma L}{12\pi C G m_i r^2 \rho \ln \Lambda},$$

where C is a constant. The final equation needed is the flux equation. The net flux across a shell of radius r is the amount of energy lost by the growth in entropy plus a term to take into account energy generation, and so

$$\frac{\partial L}{\partial r} = -4\pi r^2 \rho \Big[\sigma^2 \Big(\frac{D}{Dt}\Big) \ln \Big(\frac{\sigma^3}{\rho}\Big) + \epsilon\Big],$$

where

$$\epsilon = 85\frac{G^5 m^5 n^2}{\sigma_c^7}.$$

The ϵ term represents energy generation by the formation of binary stars in three body encounters and subsequent encounters of binaries with single stars; see Heggie & Hut (2003) for the full derivation.

1.4 Outline

This thesis is laid out as follows: Chapter 2 is concerned with conditions for the onset of gravothermal oscillation in two-component systems. This is done by investigating a series of two-component models with a range of different stellar mass ratios and total component mass ratios. In chapter 3, the results and conclusions obtained in chapter 2 are extended to the problem of the conditions for the onset of gravothermal oscillations in more realistic multi-component models of star clusters. In chapter 4 we turn to a different problem, the more general evolution of a cluster containing a significant population of black holes. In order to make the problem more tractable only two-component models are considered, where one component represents the black holes and the other component the other stars in the system. In chapter 4 a theoretical approach is first taken and then this theory tested by conducting a range of simulations. Finally in chapter 5 the main results are summarised and a few possible future projects are discussed.

1.4.1 Publications

Chapters 2 & 3 have appeared, in a slightly altered format, as publications in Monthly Notices of the Royal Society (MNRAS). All references to chapters 2 & 3 in this thesis are accompanied by citations to the published version of the chapter. The published version of chapter 2 is Breen & Heggie (2012a) and chapter 3 is Breen & Heggie (2012b). Therefore all citations to Breen & Heggie (2012a) and Breen & Heggie (2012b) can be regarded as references to Chapter 2 and Chapter 3 repetitively. Chapter 4 has also been accepted for publication in MNRAS in a slightly altered format. Chapters 2, 3 & 4 are stand alone and can be read independently from one another, because they were written in the same format as research publications. However the research in each chapter builds on the previous (particularly in the case of chapters 2 & 3) and so it is recommended that the chapters are read in the order in which they appear.

Chapter 2

Gravothermal oscillations in two-component models of star clusters

2.1 Chapter summary

In this Chapter, gravothermal oscillations are investigated in two-component clusters with a range of different stellar mass ratios and total component mass ratios. The critical number of stars at which gravothermal oscillations first appeared is found using a gas code. The nature of the oscillations is investigated and it is shown that the oscillations can be understood by focusing on the behaviour of the heavier component, because of mass segregation. It is argued that, during each oscillation, the re-collapse of the cluster begins at larger radii while the core is still expanding. This re-collapse can halt and reverse a gravothermally driven expansion. This material outside the core contracts because it is losing energy both to the cool expanding core and to the material at larger radii. The core collapse times for each model are also found and discussed. For an appropriately chosen case, direct N-body runs were carried out, in order to check the results obtained from the gas model, including evidence of the gravothermal nature of the oscillations and the temperature inversion that drives the expansion.

2.2 Introduction

Gravothermal oscillations are one of the most interesting phenomena which may arise in the post-collapse evolution of a star cluster. The inner regions of a post collapse cluster are approximately isothermal and are subject to a similar instability as the one found in an isothermal sphere in a spherical container, as studied by Antonov (1962) and Lynden-Bell & Wood (1968). Gravothermal oscillations, which are thought to be a manifestation of this instability, were discovered by Bettwieser & Sugimoto (1984) whilst studying the post-collapse evolution of star clusters using a gas model. For a gas model of a one-component cluster it was found that gravothermal oscillations first appear when the number of stars N is greater than 7000 (Goodman, 1987). This value of N has also been found with Fokker-Planck calculations (Cohn et al, 1989) and by direct N-body simulations (Makino , 1996). However, in a multi-component cluster the situation is more complicated. The presence of different mass components introduces different dynamical processes to the system such as mass stratification. Multi-component systems try to achieve kinetic energy equipartition between the components, which causes the heavier stars to move more slowly and sink towards the centre. This can lead to the Spitzer instability (Spitzer, 1987) in which the heavier stars continuously lose energy to the lighter stars without ever being able to reach equipartition. Murphy et al (1990) found that the post-collapse evolution for multi-component models was stable to much higher values of N than in the case of the one-component system and that the value of N at which gravothermal oscillations appeared varied with different mass functions.

In order to gain a deeper understanding of gravothermal oscillations, it is desirable to work with simpler models in which some of the effects which are present in real star clusters are ignored or simplified. For example, real star clusters have a range of stellar masses present, but in the current Chapter, the stellar masses are limited to two. Gaseous models are often used in this kind of research (Bettwieser & Sugimoto, 1984; Goodman, 1987; Heggie & Aarseth, 1992) because they are computationally efficient. Kim, Lee & Goodman (1998) have already completed research in this area using Fokker-Planck models. However, their research was limited to mostly Spitzer stable models and only a small range of stellar mass ratios. The study in the present Chapter looks at the more general Spitzer unstable models using various stellar mass and total mass ratios.

There is also evidence of gravothermal oscillations in real star clusters. Giersz & Heggie (2009) modelled the cluster NGC 6397 using Monte Carlo models and found fluctuation in the core radius. Their timescale suggests that they are gravothermal. Subsequently, they confirmed these fluctuations using direct N-body methods with initial conditions generated from the Monte Carlo model (Heggie & Giersz , 2009).

Two-component clusters may seem very unrealistic but there is reason to believe that they may be a good approximation to multi-component systems. Kim & Lee (1997) were able to find good approximate matches for half-mass radius r_h, central velocity dispersion v_c, core density ρ_c and core collapse time t_{cc} between two-component models and eleven-component models which were designed to approximate a power law IMF. Also see Kim, Lee & Goodman (1998) for a discussion of the realism of two-component models.

This Chapter is structured as follows. In Section 2, we describe the models which are used. This is followed by Section 3, in which the results concerning gravothermal oscillations are given. Section 4 is concerned with the results of the core collapse times. In Section 5, the results of N-body simulations are given. Finally Section 6 consists of the conclusions and a discussion.

2.3 Models

2.3.1 Gas model

Basic equations and Notation

In our model, we ignore primordial binaries and stellar evolution, and assume that the energy generating mechanism is the formation of binary stars in three body encounters and subsequent encounters of binaries with single stars. In a one-component model the rate of energy generation per unit mass is approximately

$$\epsilon = 85\frac{G^5 m^5 n^2}{\sigma_c^7} \tag{2.1}$$

(Heggie & Hut, 2003), where m is the stellar mass, n is the number density, σ_c is the one dimensional velocity dispersion of the core and G is the gravitational constant. Goodman (1987), whose results on the 1-component model we shall occasionally refer to, used a similar formula, with a coefficient which is, in effect, in the range 140–170 (depending on the value of N).

The equations of the two-component gas model (Heggie & Aarseth, 1992) are given below:

$$\frac{\partial M_i}{\partial r} = 4\pi\rho_i r^2 \tag{2.2}$$

$$\frac{\partial p_i}{\partial r} = -\frac{G(M_1+M_2)}{r^2}\rho_i \tag{2.3}$$

$$\frac{\partial \sigma_i^2}{\partial r} = -\frac{\sigma_i L_i}{12\pi C m_i \rho_i r^2 \ln\Lambda} \tag{2.4}$$

Table 2.1: Notation (the subscript i corresponds to the i^{th} component, $i = 2$ refers to the more massive component)

r	radius
ρ	mass density
σ	one dimensional velocity dispersion
m	stellar mass
M	total mass (within radius r)
C	Constant (see text)
L	energy flux
N	number of stars
$\ln\Lambda$	coulomb logarithm ($\Lambda = 0.02N$)
$\frac{D}{Dt}$	Lagrangian derivative (at fixed M)
$\frac{\partial}{\partial r}$	radial derivative (at fixed t)

$$\frac{\partial L_i}{\partial r} = -4\pi r^2 \rho_i \Big[\sigma_i^2 \Big(\frac{D}{Dt}\Big) \ln\Big(\frac{\sigma_i^3}{\rho_i}\Big) + \delta_{i,2}\epsilon + 4(2\pi)^{\frac{1}{2}} G^2 \ln\Lambda \Big[\frac{\rho_{3-i}}{(\sigma_1^2+\sigma_2^2)^{\frac{3}{2}}}\Big](m_{3-i}\sigma_{3-i}^2 - m_i\sigma_i^2)\Big] \tag{2.5}$$

where $i = 1, 2$. This model in turn is ultimately inspired by the one-component model of Lynden-Bell & Eggleton (1980).

The meaning of the symbols can be found in Table 2.1. The major difference between the above equations and those for the one-component model is the last term of equation 2.5, which involves the exchange of kinetic energy between the two components. See Spitzer (1987, p.39) for information on this term. As the heavier component dominates in the core of the cluster, it is assumed that all of the energy is that generated from the second component. Hence the Kronecker delta $\delta_{2,i}$ in the last equation. There are two constants in the gas code which can be adjusted: C and the coefficient λ of N in $\Lambda = \lambda N$. The value of $\lambda = 0.02$ was used as it was found to provide a good fit for multi-component models (Giersz & Heggie , 1996). The value of C used was 0.104 (Heggie & Ramamani , 1989). This value of C results from the comparison of core collapse between gas and Fokker-Planck models of single component systems and it is not clear if it applies accurately to post-collapse two-component models.

The role of N in the gas code

This section places emphasis on the role of N in evolution, but it is not clear what role N plays in equations (2.2) – (2.5). For fixed structure (i.e. $\rho_i(r)$, etc), N appears explicitly in Λ (where its role is rather insignificant), and in the individual masses m_i. These appear in equations (2.4) and (2.5). In a system with fixed structure, equation (2.4) shows

$$L_i \propto m \ln\Lambda \propto \frac{\ln\lambda N}{N},$$

reflecting the fact that the flux L is caused by two-body relaxation, and its time scale is proportional to $N/\ln\lambda N$. In equation (2.5) N plays a similar role in the last term on the right, which governs the approach to equipartition. It also appears implicitly through ϵ, because of the m dependence in equation (2.1). For a system of given structure, its contribution to L in equation (2.5) is proportional to N^{-3} (as we are assuming that $\rho = mn$ is fixed and so ϵ in equation (2.1) is proportional to m^3). It would seem as though this term is insignificant for large N. In practice, however, the system compensates by increasing the central density so that ϵ plays a comparable role to the relaxation terms (see Section 2.4.2).

Table 2.2: Critical value of N (N_{crit}) in units of 10^4

$\frac{M_2}{M_1} \backslash \frac{m_2}{m_1}$	**2**	**3**	**4**	**5**	**10**	**20**	**50**
1.0	1.7	2.0	2.4	2.8	5.0	8.5	18
0.5	2.2	2.8	3.5	4.0	7.2	13	30
0.4	2.3	3.2	3.8	4.6	8.2	15	33
0.3	2.6	3.6	4.6	5.4	10	18	42
0.2	3.0	4.4	5.5	7.0	12	22	55
0.1	3.8	6.0	8.5	10	22	36	100

2.3.2 Direct N-body

Direct N-body simulations were conducted using the NBODY6 code (Aarseth, 2003) enabled for use with Graphical Processing Units (GPU). NBODY6 has a range of features and options such as individual time steps which make it an excellent direct N-body code. NBODY6 is written in FORTRAN and is publicly available for download from www.ast.cam.ac.uk/∼sverre/web/pages/nbody.htm .

2.4 Critical Value of N

If the value of N is not too large, then, after core collapse, the cluster expands at a steady rate (Fig. 2.1, top). However, at a larger value of N the central density (ρ_c) was found to oscillate (Fig. 2.1, bottom). Goodman (1987) showed that for one-component models the steady expansion is unstable for large values of N and found that the value at which oscillations first appeared is $N = 7000$. In the present chapter, the case of two-component models is investigated.

2.4.1 Results of the gas code

In all cases, the initial conditions used were Plummer models (Plummer, 1911; Heggie & Hut, 2003). The initial velocity dispersions of both components were equal and the initial ratio of density of each component was equal at all locations. The initial conditions were constructed with different stellar mass ratios $m_2/m_1 = 2, 3, 4, 5, 10, 20, 50$ and for each of these mass ratios, a model with total mass ratios $M_2/M_1 = 0.1, 0.2, 0.3, 0.4, 0.5$ and 1 was constructed. A python script was used to run the gas model code over a range of values of N for each of the pairs of mass ratios. Each run terminated when the time value reached 30 initial relaxation times ($t_{i,rh}$).The value of the central density was checked for an increase in value of 5 percent or more in any interval over the time period between $20t_{i,rh}$ and $30t_{i,rh}$. If an increase was found, the run was deemed to be unstable and the range of N was refined. This process continued until the critical value of N (N_{crit}) at which oscillations first appeared was determined (correct to ten percent). The values of N_{crit} were also visually confirmed from the output of the gas code. The obtained values of N_{crit} in units of 10^4 are given in Table 2.2. Fig. 2.2 shows a contour plot of $\log_{10} N_{crit}$.

2.4.2 Interpretation of the results

In order to attempt to interpret the results in the previous subsection, it is helpful to illustrate the mass density distribution of each component within the cluster and this is done in Fig. 2.3.

Firstly, let us consider models in which $m_2/m_1 \gg 1$. In a region where both components are present at comparable densities, there is a strong tendency towards mass segregation. Therefore, in the region at which $\rho_2/\rho_1 \sim 1$, the ratio ρ_2/ρ_1 is a rapidly decreasing function of the radius, i.e. the transition region is narrow. Inside this region, m_2 dominates, and m_1 dominates outside. Clearly the radius at which this region is located increases with M_2/M_1, and must be near r_h when $M_2/M_1 = 1$ (Fig. 2.4). Finally, for models in which $m_2/m_1 \not\gg 1$, the tendency towards mass segregation decreases, the decrease of ρ_2/ρ_1 with r is more gradual, and the transition

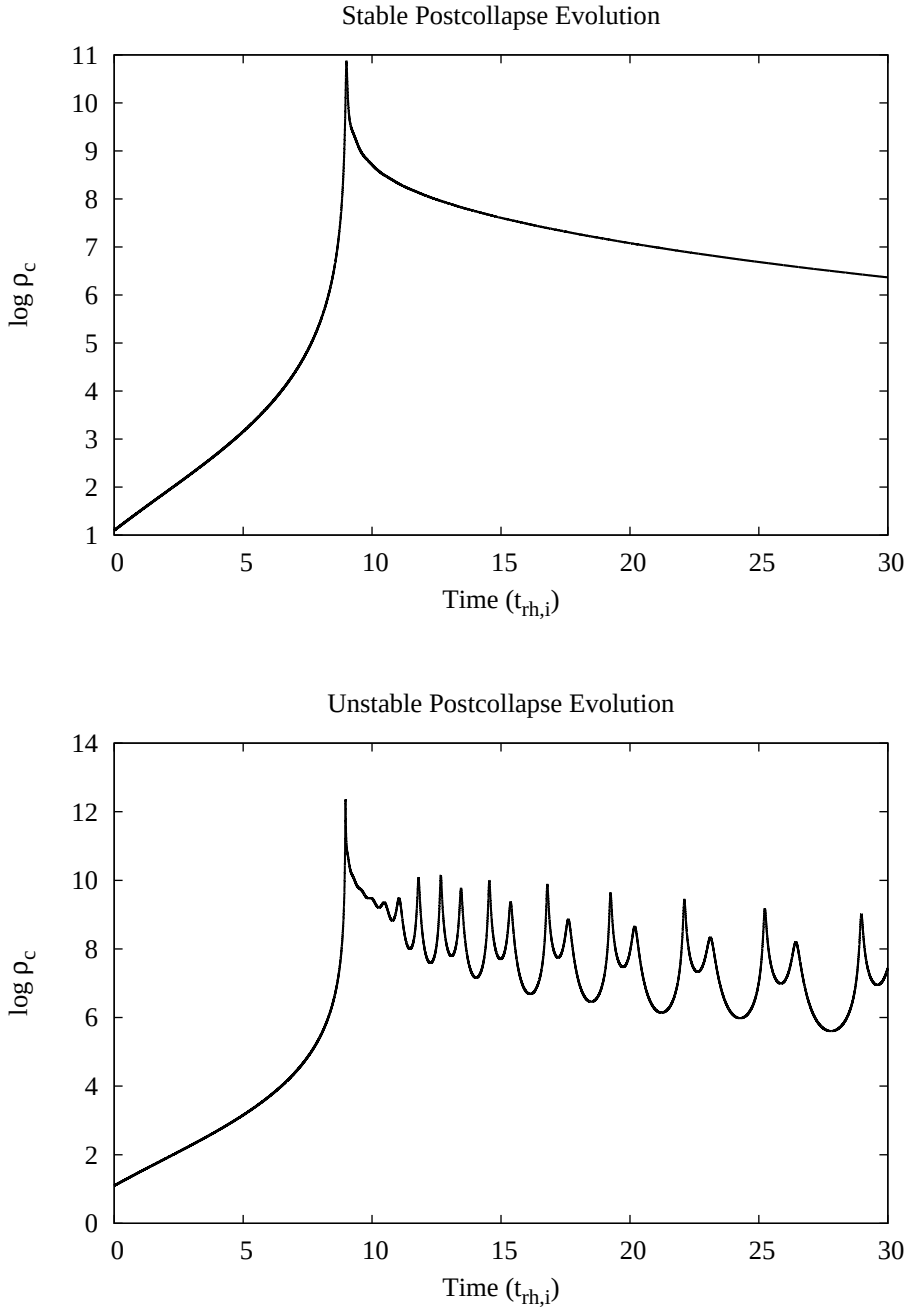

Figure 2.1: Logarithm of the central density vs time (in units of the initial value of t_{rh}) for a two-component gas model, $m_2/m_1 = 2$, $M_2/M_1 = 1$, top: $N = 1.5 \times 10^4$ (stable), bottom: 2.5×10^4 (unstable). For initial conditions see Section 2.4.1

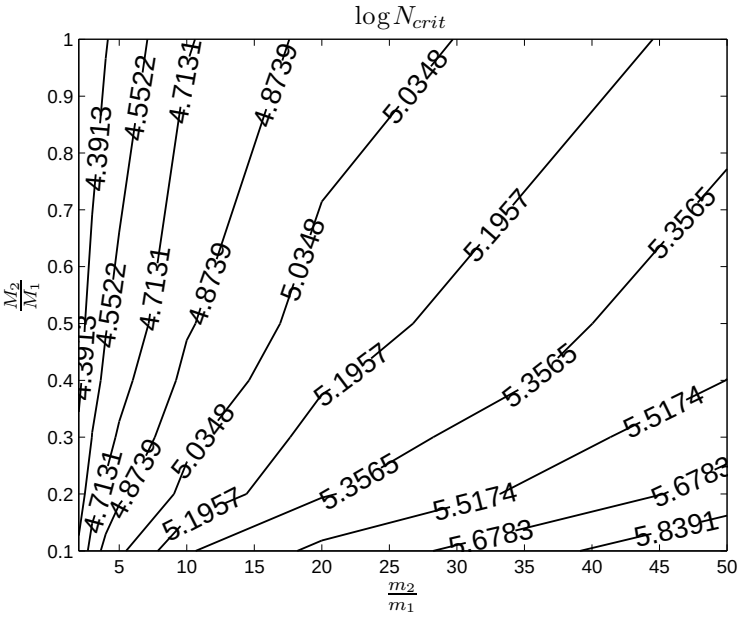

Figure 2.2: Contours of $\log_{10}(N_{crit})$

Table 2.3: Number of heavy stars (N_2) at N_{crit} in units of 10^4

$\frac{M_2}{M_1} \backslash \frac{m_2}{m_1}$	**2**	**3**	**4**	**5**	**10**	**20**	**50**
1.0	0.57	0.50	0.48	0.47	0.45	0.41	0.35
0.5	0.44	0.40	0.39	0.36	0.34	0.32	0.30
0.4	0.38	0.38	0.35	0.34	0.36	0.29	0.26
0.3	0.34	0.33	0.32	0.31	0.29	0.27	0.25
0.2	0.27	0.28	0.26	0.27	0.24	0.22	0.22
0.1	0.18	0.19	0.21	0.20	0.22	0.18	0.20

region is more extensive (Fig. 2.5). For the same reason the regions dominated by a single component are more restricted than when $m_2/m_1 \gg 1$.

Dependence on the number of heavy stars N_2

The values of N_2 at N_{crit} are given in Table 2.3. The variation in N_2 is considerably less than that of N_{crit}. For large m_2/m_1 and fixed M_2/M_1, the value of N_2 has approximately the same value, independent of m_2/m_1. Now, we give a possible interpretation of this empirical finding that the stability of the system is dominated by the heavy component.

Firstly, let us consider the case of $M_2/M_1 \gtrsim 1$ and $m_2/m_1 \gg 1$ (Fig. 2.4, left). Within r_h the heavy component dominates and most of the light component is removed to the outer halo. In this case, the light component acts as a container for the heavy component. Here, the stellar mass of the light component is not the most important factor, rather the most important factor is the overall mass of the container. If we were to replace this by an equal mass of stars with stellar mass m_2, the behaviour of the stars inside r_h would be nearly the same, and so the value of N_2 at the stability boundary would be roughly the same as for a one-component model. Indeed, since part of the container consists of stars of mass m_1, this could also explain why the values of N_2 are in fact somewhat less than the value of N_{crit} for a one-component system (i.e. 7000, Goodman (1987)) and, in fact, why the critical value of N_2 is decreasing with decreasing M_2/M_1. On the other hand, the fact that the critical value of N_2 is less than 7000 may also partly be due to the fact that the energy generation rate, equation (2.1), is smaller than that used by Goodman. In his paper (Goodman, 1987, equation II.26) he shows implicitly that the critical value of N is approximately proportional to the square root of the numerical

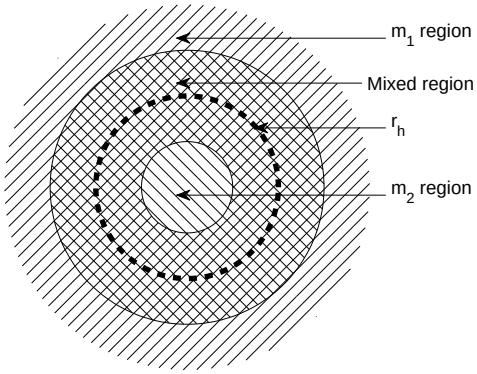

Figure 2.3: Illustration of mass distribution in star clusters. The dashed line represents r_h, the lines at 135 degrees in the centre represent the area dominated by the heavy component (i.e $\rho_2/\rho_1 \gg 1$), the lines at 45 degrees in the far halo represent the area dominated by the light component (i.e $\rho_2/\rho_1 \ll 1$), the crossed section represents the area where there is a mixture of heavy and light components (i.e. $\rho_2/\rho_1 \sim 1$)

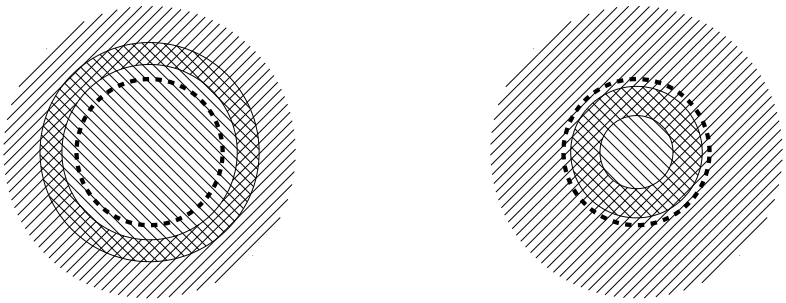

Figure 2.4: Left: System with $M_2/M_1 \gtrsim 1$ and with large enough m_2/m_1 to remove most of the light component from within the half mass radius. Right: System with $M_2/M_1 < 1$ and $m_2/m_1 \gg 1$.

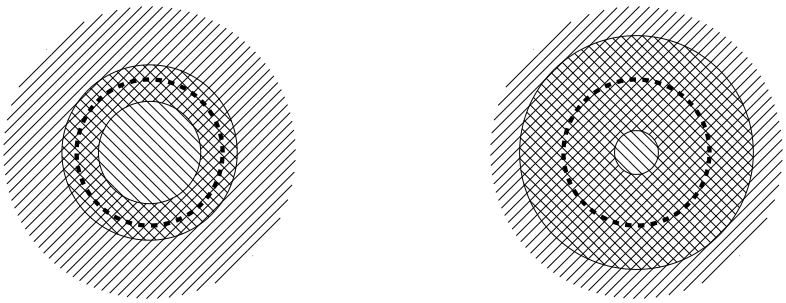

Figure 2.5: Effect of high and low values of m_2/m_1 for a fixed value of $M_2/M_1 \sim 1$. Left: high value of m_2/m_1. Right: low value of m_2/m_1. The mixed region grows with decreasing m_2/m_1 and decreases with increasing m_2/m_1, because of the enhanced effect of mass segregation.

coefficient in ϵ. At any rate, the arguments we have presented are consistent with the results in the uppermost rows of Table 2.3.

Secondly, consider the case $M_2/M_1 \lesssim 1$ (Fig. 2.4, right). If the system is Spitzer unstable, the heavy component decouples from the light component and forms its own subsystem. This heavy subsystem can itself become gravothermally unstable and exhibit a temperature inversion in the same way as a one-component model. In this case, however, there is not enough mass in the heavy component to dominate throughout the region within r_h, and so it is not quite as easy to relate this to the one-component case. Rather, we assume that the heavy component behaves like a detached one-component model. However, the basic conclusion is still the same, the stability of the model is determined by the heavy component. Since the heavy component is again sitting in the potential well of the lighter stars, it is easier for a nearly isothermal region to be set up in the heavier stars than if the entire system consisted of heavy stars, and we again expect N_{crit} to correspond to a lower value of N_2 than in the one-component case.

There is also a noticeable increase in the values of N_2 with decreasing m_2/m_1 in the top rows of Table 2.3. There is currently no clear interpretation of this effect but it may possibly be related to the effect of mass segregation, as the region dominated by the heavy component is larger for larger m_2/m_1 (see Fig. 2.5).

Goodman's stability parameter

Goodman (1993) suggested that the quantity

$$\epsilon \equiv \frac{E_{tot}/t_{rh}}{E_c/t_{rc}} \tag{2.6}$$

should indicate the stability universally, where $\log_{10}\epsilon \sim -2$ is the stability limit below which the cluster would become unstable. Here E_{tot} is the total energy, E_c is the energy of the core, t_{rc} is the core relaxation time and t_{rh} is the half mass relaxation time. Kim, Lee & Goodman (1998) carried out research using a Fokker-Planck model which seemed to support the condition, although the models they studied were all Spitzer stable.

We have compared the values of ϵ found by Kim, Lee & Goodman (1998) to results obtained from the gas code (Table 2.4). All the models compared in Table 2.4, which are the same as those studied by Kim, Lee & Goodman (1998), are stable in the post-collapse expansion as well as being Spitzer stable. An important difference between the Fokker-Planck model used by Kim, Lee & Goodman (1998) and the gas code used in this chapter is that Kim, Lee & Goodman (1998) included an energy generation term in both components, whereas the gas code only contains an energy generation term in the heavier component. Therefore, it would be expected, in the case of the gas code, that the core would have to collapse further in order to generate the required amount of energy (from Hénon's principle, see Section 2.4.3). This could explain the differences in the values of r_c/r_h in Table 2.4. However, as M_2/M_1 increases, the heavier component will dominate in the core and the energy generation of the lighter component will then become negligible. As can be seen in Table 2.4, there is good agreement between the two results for $\log_{10}\epsilon$ even though there are only small values of M_2/M_1. Also, it is possible that Kim, Lee & Goodman (1998) used a different definition of t_{rc} than the one used in this chapter (see equation 2.7). However, as there is such good agreement between the values in Table 2.4, it is unlikely that Kim, Lee & Goodman (1998) used a significantly different definition. Unlike the other models in the present chapter, the models in Table 2.4 are Spitzer stable. These runs have only been carried out in order to make a comparison of the calculation of ϵ and r_c/r_h using the gas code with the results of Kim, Lee & Goodman (1998). Next we will test the use of epsilon as a stability criterion for Spitzer unstable cases.

We tested the stability criterion based on equation (2.6) for the subset of models given in Table 2.5. For each fixed M_2/M_1 and m_2/m_1, the values of ϵ were found to decrease with increased N up until the post-collapse evolution became unstable. The values of $\log_{10}\epsilon$ given in Table 2.5 are the values for the run with the highest stable N. As can be seen from Table 2.5 the value of $\log_{10}\epsilon$ is indeed in the region of -2. However, the limiting value of stable ϵ varies with m_2/m_1 and to a much lesser extent with M_2/M_1.

Table 2.4: Comparison of values of ϵ and r_c/r_h

m_2/m_1	M_2/M_1	N	*Kim et al* $\log\epsilon$	*Gas model* $\log\epsilon$	*Kim et al* r_c/r_h	*Gas model* r_c/r_h
2	0.02	3×10^4	-1.620	-1.553	7.03×10^{-3}	4.86×10^{-3}
3	0.03	3×10^4	-1.224	-1.167	1.31×10^{-2}	0.91×10^{-2}
3	0.03	10^5	-1.597	-1.544	5.38×10^{-3}	3.93×10^{-3}

Table 2.5: Value of $\log\epsilon$ for largest stable run

$\frac{M_2}{M_1}\backslash\frac{m_2}{m_1}$	**2**	**5**	**10**	**50**
1.0	-1.65	-1.78	-2.15	-2.75
0.5	-1.68	-1.90	-2.15	-2.75
0.2	-1.65	-1.84	-1.95	-2.48

Now we shall try to improve upon the definition of ϵ. In equation (2.6), t_{rc} and t_{rh} are defined by

$$t_{rc} = \frac{0.34\sigma_{c,2}^3}{G^2 m_2 \rho_{c,2} \ln\Lambda} \tag{2.7}$$

and

$$t_{rh} = \frac{0.138 N^{\frac{1}{2}} r_h^{\frac{3}{2}}}{(G\bar{m})^{\frac{1}{2}} \ln\Lambda}. \tag{2.8}$$

Note that t_{rc} was defined using the properties of the heavy component in the core rather than the averages of both components, as the heavy component dominates in the core. However t_{rh} (equation (2.8)) depends on N and $\bar{m}$, which can vary dramatically with m_2/m_1 and M_2/M_1 for fixed N_2 whereas, as argued in Section 2.4.2, the important criterion is the number of heavy stars. We suggest that a modified version of the Goodman stability parameter could be constructed using a relaxation time based on the heavy component in place of t_{rh}. For example, if $M_2/M_2 \gtrsim 1$ and we assume that the heavier component dominates within r_h, then the properties of the system within r_h would be roughly similar to that of a one-component system with the same total mass. We can attempt to treat the system as if it consisted entirely of the heavy component with an effective number of stars $N_{ef} = M/m_2$. The half mass relaxation time of this one-component system would be

$$t_{rh,ef} = \frac{0.138 N_{ef}^{\frac{1}{2}} r_h^{\frac{3}{2}}}{(Gm_2)^{\frac{1}{2}} \ln\lambda N_{ef}} = \Big(\frac{1+\frac{M_2}{M_1}}{\frac{M_2}{M_1}+\frac{m_2}{m_1}}\Big)\Big(\frac{\ln\lambda N}{\ln\lambda N_{ef}}\Big) t_{rh}.$$

We can define a modified stability condition by replacing t_{rh} with $t_{rh,ef}$ in the definition of ϵ which would then give the following condition

$$\epsilon_2 \equiv \frac{E_{tot}/t_{rh,ef}}{E_c/t_{rc}}.$$

The values of $\log_{10}\epsilon$ and $\log_{10}\epsilon_2$ are compared in Table 2.6 for the case $M_2/M_1 = 1$. The values of $\log_{10}\epsilon_2$ are in much better agreement with each other than those of $\log_{10}\epsilon$ and suggest that a better stability condition is $\log_{10}\epsilon_2 \approx -1.5$ rather than $\log_{10}\epsilon \simeq -2$. For the cases with $M_2/M_1 \lesssim 1$ it is unclear how to define an appropriate relaxation time, and so we will not consider the modified stability condition for those cases.

To summarise, the values of ϵ (and especially ϵ_2) seem to give an indication of stability for the two-component models but the values of ϵ were found to change with different conditions (e.g m_2/m_1). The critical value of ϵ_2 is much less variable. The critical value of $\log_{10}\epsilon$ or $\log_{10}\epsilon_2$ for multi-component models will be investigated in the next chapter 3.

Table 2.6: $\log\epsilon$ and $\log\epsilon_2$ for the case $M_2/M_1 = 1$

$\frac{m_2}{m_1}$	**2**	**5**	**10**	**50**
$\log\epsilon$	-1.65	-1.78	-2.15	-2.75
$\log\epsilon_2$	-1.51	-1.39	-1.53	-1.56

2.4.3 Weak oscillations

Hénon (1975) suggested that the energy generation rate of the core is determined by the requirement that it meets the energy demands of the rest of the cluster. This demand is normally thought of in terms of the energy flux at the half mass radius. We shall refer to this as Hénon's principle. This principle, together with the notion of gravothermal instability, is the basis of the usual qualitative picture of gravothermal oscillations (Bettwieser & Sugimoto, 1984), which we now recap.

In a situation with very large N, the core has to collapse to a small size in order to meet the required energy generation. The steady state is gravothermally unstable, as there would be a large density contrast in a nearly isothermal region. If the core is generating more energy than can be conducted away, this would cause the core to expand, cool and reduce its rate of energy generation. If there is sufficient expansion, then the core would be cooler than its surroundings. This would result in the core starting to absorb heat. Since the core has a negative specific heat capacity, this would cause the core to expand further and became even cooler than before (Bettwieser & Sugimoto, 1984). Ultimately, however, the core must collapse again to meet the energy requirements of the rest of the cluster. Here, we adapt this explanation of gravothermal oscillations to the case of two-component clusters.

In one-component gas models, as N increases the instability first appears in the form of periodic oscillations[1] (Heggie & Ramamani , 1989). In order to study the instability for the case of weak or low amplitude oscillations in our two-component model, a model was chosen which demonstrated periodic oscillation with parameters $m_2/m_1 = 2$, $M_2/M_1 = 1$ and $N = 2.0 \times 10^4$ (the value of N_{crit} for $m_2/m_1 = 2$, $M_2/M_1 = 1$ is 1.7×10^3 from Table 2.2). Fig. 2.6 plots $\ln\rho$ at various fixed values of $\log r$ for this model. The total energy flux L is shown in Fig. 2.7 over the particular expansion phase from $24.54t_{i,rh}$ to $25.18t_{i,rh}$ and the contraction phase from $25.18t_{i,rh}$ to $26.52t_{i,rh}$. Fig. 2.8 shows the profiles of $\log\rho$ and $\log\sigma^2$ over the expansion phase from $24.54t_{i,rh}$ to $25.18t_{i,rh}$.

During the expansion of the core, the flux in the inner region (between r_c and r_h) drops and eventually becomes negative (Fig. 2.7, top) in a small range of the radius. At this point there is an inwards flux of energy to the core. Since the core has a negative heat capacity, it would be expected that this would enhance the negative flux and therefore the expansion. However, the expansion stops at this point. This is similar to behaviour observed by McMillan & Engle (1996). Now we explain why this happens. Hénon (1975) argues that the flux at r_h must be maintained, and we note that there is always a positive flux at the half-mass radius r_h. Since the flux from the core becomes negative at some radius between r_c and r_h, there must be a positive flux gradient in some region between the core and half mass radius. This can be seen in Fig. 2.7 (top) towards the end of the expansion and it continues into the early part of the contraction phase (Fig. 2.7, bottom).

The flux gradient can be related to density via equation (2.5). As the heavier component dominates in the inner regions (see Fig. 2.8), the main contribution to the flux is from the heavier component (i.e. $L \sim L_2$). Outside the core the energy generation will be negligible. Finally, the temporal change in $\ln\rho$ is greater than that in $\ln\sigma^3$. Taking all of this into account and rearranging equation (2.5) will result in the following:

$$\frac{1}{r^2\rho_2\sigma_2^2}\frac{\partial L}{\partial r} \simeq \left(\frac{D}{Dt}\right)\ln\left(\frac{\rho_2}{\sigma_2^3}\right) \simeq \left(\frac{D}{Dt}\right)\ln\left(\rho_2\right). \tag{2.9}$$

[1] Strictly, only periodic if one scales out the steady expansion

Table 2.7: Collapse time t_{cc} in units of the initial relaxation time

$\frac{M_2}{M_1} \backslash \frac{m_2}{m_1}$	**2**	**3**	**4**	**5**	**10**	**20**	**50**
1.0	8.95	7.80	4.78	3.87	2.0	1.1	0.5
0.5	7.80	4.78	3.45	2.75	1.38	0.72	0.35
0.4	7.58	4.43	2.89	2.49	1.23	0.66	0.31
0.3	7.44	4.17	2.88	2.24	1.1	0.55	0.20
0.2	7.42	3.89	2.65	1.97	0.91	0.47	0.16
0.1	8.1	3.95	2.4	1.7	0.75	0.38	0.13

Since all of the coefficients of the flux gradient are positive the sign of flux gradient must be the same as that of the Lagrangian derivative of the density. Thus a positive radial flux gradient in space implies that the density is increasing with time. This can be seen in Fig. 2.6, where the dashed lines mark the moment when the contraction becomes an expansion, and the solid lines mark the time when contraction resumes. It is clear that the contraction begins at large radii ($\log r \gtrsim -1.6$) while the core is expanding, and that this region of contraction propagates inwards at later times. This can be related to the position of the positive gradient in Fig. 2.7 via the above equation (as long as the density is low enough that energy generation is negligible). Therefore, the collapse of the parts of the cluster between the core and r_h starts while the core is expanding, and brings the expansion to a halt. Note that Fig. 2.6 is density plotted at fixed radius whereas time-derivatives in equation 2.9 are at fixed mass. Nevertheless in Fig. 2.6 we can also see that there are intermediate radii in which the density evolves in the opposite way from the core.

Although we have constructed the details of this description in the context of two-component models, nothing we have said depends entirely on this, and it is expected that similar ideas will apply to one-component and multi-component models.

.

2.5 Core Collapse Time

While it may seem that the study of core collapse times is inappropriate in the context of gravothermal oscillations, it can be argued that the collapse phase of a gravothermal oscillation is not essentially different from the phenomenon of core collapse. Furthermore, another reason for its inclusion is that the evolution of isolated two-component models is an interesting research topic in its own right, and with the aim of constructing a comprehensive approximate theory of these models, studying the core collapse time is an appropriate first step.

The core collapse time t_{cc} for a one-component cluster with Plummer model initial conditions has been found to be approximately $15.5t_{i,rh}$(Binney & Tremaine, 2008; Heggie & Hut, 2003) using various methods. Takahashi (1995) found a longer t_{cc} of $17.6t_{i,rh}$ with a one-component anisotropic Fokker-Planck code. However, the presence of a range of stellar masses can have a dramatic effect on the collapse time because of the process of mass segregation. The effect of mass segregation in multi-component models has been studied using Fokker-Planck calculations (Murphy et al, 1990; Chernoff & Weinberg, 1990) and Monte Carlo methods (Gürkan et al, 2004). The effect of mass segregation in two-component models has already been studied extensively using direct N-body methods (Khalisi et al, 2007).

For the gas model runs discussed in Section 3, Table 2.7 gives the values of the collapse time in units of the initial half mass relaxation time. Fig. 2.9 shows a contour plot of log t_{cc}. The fastest collapse times occur with models of low M_2/M_1 and high m_2/m_1.

For two-component systems, the timescale of mass segregation varies as m_1/m_2 (Fregeau et al, 2002, and references therein). As mass segregation enhances the central density, it is expected that the mass segregation timescale is comparable with the timescale of core collapse. Fig. 2.10 compares the variation of the timescale of core collapse with the expected timescale of mass segregation. For the case of $M_2/M_1 = 1.0$ (top line in Fig. 2.10) the collapse time indeed appears to vary as m_1/m_2. However, for lower values of M_2/M_1, the core collapse time decreases more quickly than for m_1/m_2. Khalisi et al (2007) also found a steeper decrease of

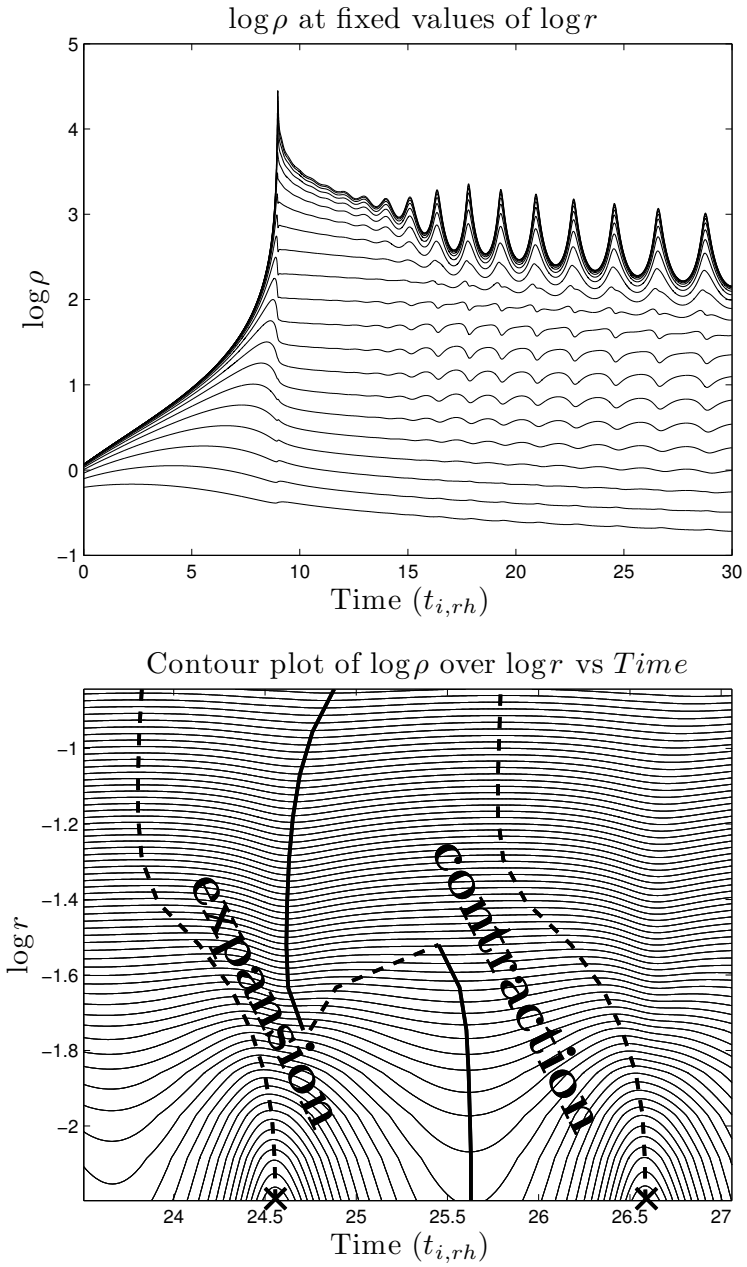

Figure 2.6: Values of $\log \rho$ at fixed values of $\log r$ in the range -2.7621 to -0.5038 in equal steps of size 0.1129, for two-component models with $m_2/m_1 = 2$, $M_2/M_1 = 1$ and $N = 2.0 \times 10^4$. Bottom: contour plot of $\log \rho$; the dashed lines represent the point of highest density reached locally over the time interval $23.5t_{i,rh}$ to $26.7t_{i,rh}$ and solid lines are the regions of lowest density reached between the dashed lines. $\times$ marks the points of core bounce, where the core stops contracting and starts expanding

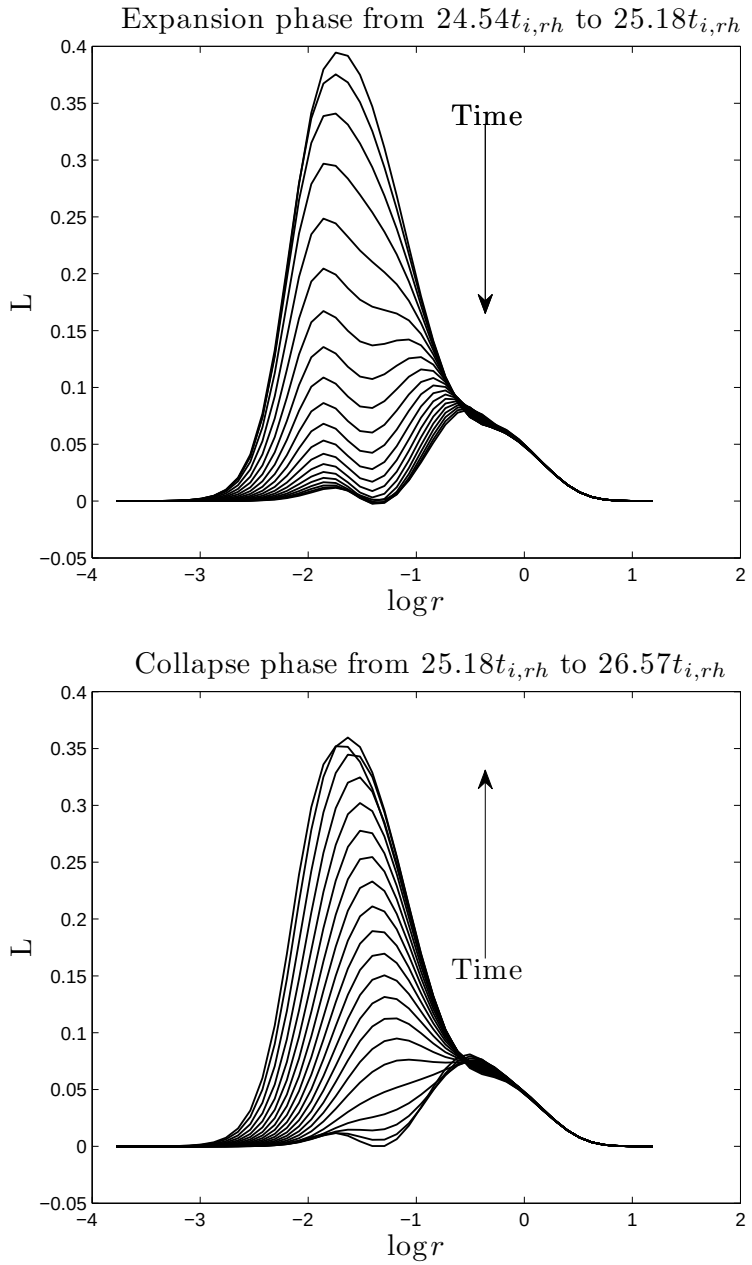

Figure 2.7: Total energy flux in a two-component model with $m_2/m_1 = 2$, $M_2/M_1 = 1$ and $N = 2.0 \times 10^4$. The expansion phase from $24.54t_{i,rh}$ to $25.18t_{i,rh}$ is on the top and the contraction phase from $25.18t_{i,rh}$ to $26.57t_{i,rh}$ is on the bottom

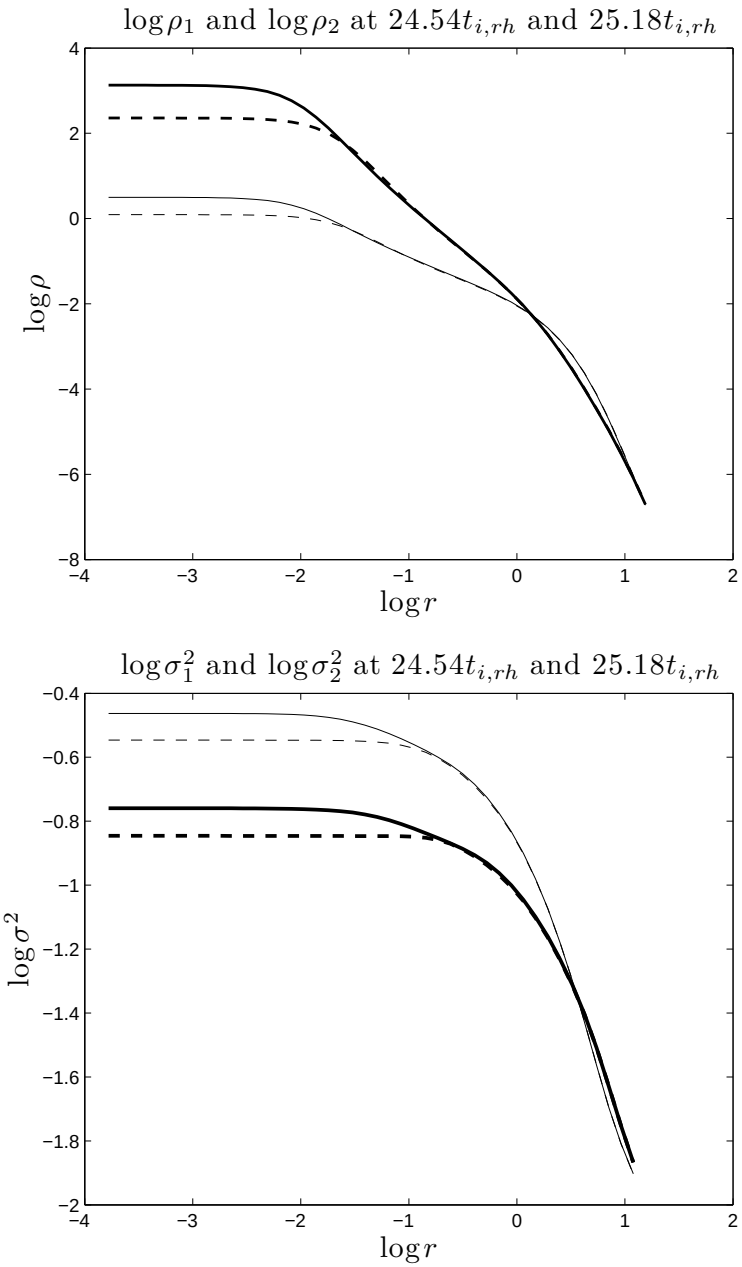

Figure 2.8: Profiles of $\log_{10}(\rho)$ (top) and $\log_{10}(\sigma^2)$ (bottom) for each component at maximum (dashed line) and minimum (solid line) expansion over times shown in Fig. 2.7. The heavy (light) curves refer to the more (less) massive component

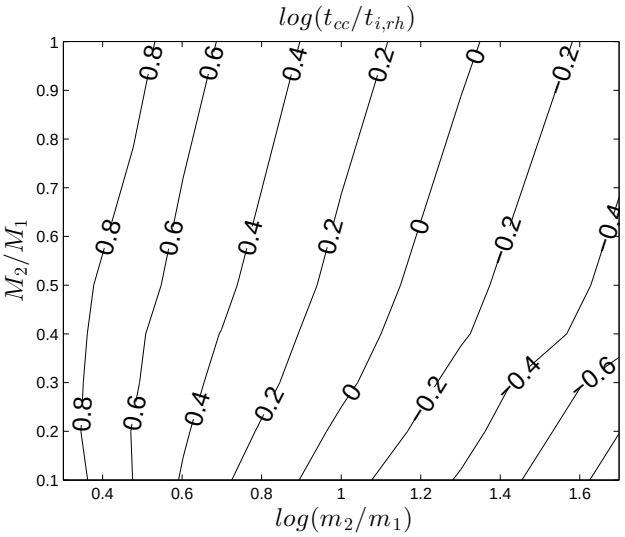

Figure 2.9: Contours of $\log(t_{cc}/t_{i,rh})$ as a function of M_2/M_1 and m_2/m_1.

the core collapse time in their study, for the case $M_2/M_{i,tot} = 0.1$, where $M_{i,tot}$ is the initial total cluster mass.

We can attempt to improve on these ideas at least qualitatively by considering in more detail a Spitzer unstable model. In that case, we can separate the pre-collapse evolution of the cluster into an initial mass segregation-dominated stage and a later gravothermal collapse-dominated stage, in which the centrally concentrated heavy component behaves almost as a one-component system thermally detached from the lighter component. We propose that this separation can be located via the minimum of the rate of change of central density ratio (i.e min $\{\frac{d}{dt}(\frac{\rho_2}{\rho_1})\}$). The reasoning behind this is as follows: as time passes, the increase in the density ratio caused by mass segregation starts to slow due to a combination of decreasing relative density and increasing temperature of the lighter component in the central regions. We assume that it is at this point that the gravothermal collapse of the heavier component becomes the dominant behaviour of the system. The gravothermal collapse in the heavy component increases the temperature of the heavy component, and because the light component absorbs energy from the heavy component, the collapse of the heavy component causes a deceleration in the collapse of the light component. This in turn enhances the rate of increase in the density ratio.

Fig. 2.11 shows the density ratio ρ_2/ρ_1 vs time for $N = 10000$ and $M_2/M_1 = 1, 0.1$. For the case of $m_2/m_1 = 2$ (the lowest curve) there is a clear distinction between the part before the point of inflection at about $t/t_{i,rh} = 5$ (i.e the initial mass segregation phase) and the part after the point of inflection (i.e the gravothermal collapse phase). As m_2/m_1 increases the initial phase dominated by mass segregation becomes more substantial and eventually the initial mass segregation phase brings the system all the way to core bounce. However, as N increases, binary energy generation becomes less efficient relative to the energy demands of the cluster (Goodman, 1987). Therefore, the core needs to reach a higher density at core bounce for larger N. As the initial phase of mass segregation is self limiting for the reason given above, mass segregation cannot increase the central density beyond a certain point. Therefore, it would be expected that the gravothermal collapse dominated phase must eventually return with increasing N for any given M_2/M_1 and m_2/m_1.

2.6 Direct N-body

Bettwieser & Sugimoto (1985) compared N-body systems to gaseous models using a direct $N = 1000$ model. Even though the value of N is small by today's standards there was still fair agreement during the pre-collapse phase. There were large statistical fluctuations in the post-collapse phase and this potentially due to the small particle number. However, it is still

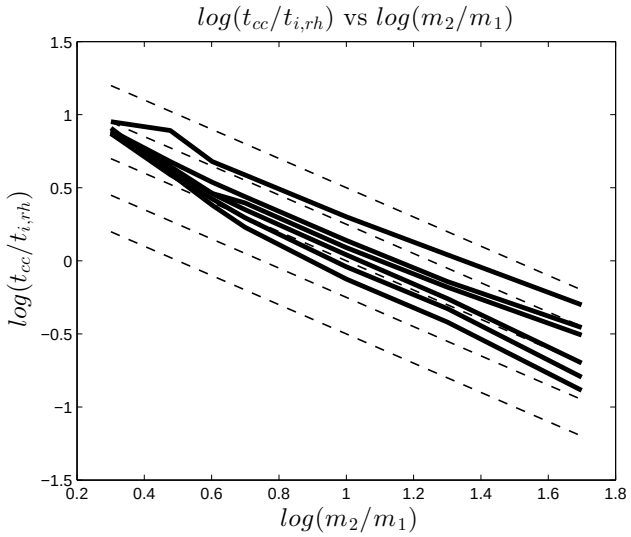

Figure 2.10: Solid lines are $\log(t_{cc}/t_{i,rh})$ vs $\log m_2/m_1$; from top to bottom $M_2/M_1 = 1.0, 0.5, 0.4, 0.3, 0.2$ and 0.1. Dashed lines are $\log(km_1/m_2)$ vs $\log m_2/m_1$ for various values of k.

Table 2.8: Collapse time t_{cc}

N	$8k$	$16k$	$32k$	$64k$
N-body units	1160	1990	3480	6380
$t_{i,rh}$	7.76	7.56	7.41	7.51

important to confirm a sample of the results of the gas model by using a direct N-body code.

The case of $m_2/m_1 = 2$ and $M_2/M_1 = 1$ was chosen because it had the smallest value of N_{crit}. The values of N used for these runs were $8k, 16k, 32k$ and $64k$. The collapse times of the runs in N-body units (see Heggie & Mathieu, 1986) and units of $t_{i,rh}$ are given in Table 2.8. The average collapse time measured in units of $t_{i,rh}$ is about 7.5 which is lower than the predicted value of 8.95 in Table 2.7. The difference in collapse time could be because of the approximate treatment of two-body relaxation in the gas model, the neglect of escape, or parameter choices in the gas code (Section 2.3.1).

For the case of the runs with N equal to $8k$ and $16k$ no behaviour was found which could be described as gravothermal oscillation. This is in agreement with the gas code, which gave $N_{crit} = 17000$. However, the $32k$ case does show a cycle of expansion and contraction of the core over the time interval 4500 to 5500 N-body units (see Fig. 2.12). In order to check that the expansion was not driven by sustained binary energy generation, we consider the evolution of the relative binding energy E_b/E, where E_b is the total binding energy of the binaries and E is the absolute value of the total energy of the cluster, over this time period. This is plotted in Fig. 2.13 along with the core radius. There are small changes in the binding energy of binaries over this period, decreases as well as increases, but this cannot fully account for the expansion phase that is observed, as there are other periods with similar binary activity in which no sustained expansion occurs. Also, the time scale of the expansion is much longer than the relaxation time in the core (~ 0.5 in N-body time units). Therefore, we assume that the expansion must be driven by phenomena outside the core, and gravothermal behaviour is a plausible explanation.

Several other pieces of evidence point to this conclusion. Fig. 2.14 shows the density in Lagrangian shells of the heavier component. As discussed in Section 2.4.3 (e.g. Fig. 2.6, top) the region further away from the core is seen to contract while the core expands. Also, in the cycle of $\ln \rho_c$ vs the core velocity dispersion $\log v_c^2$, the temperature is lower during the expansion where heat is absorbed and higher during the collapse where heat is released (Fig. 2.13, bottom). This is similar to the cycles found by Makino (1996) for one-component models

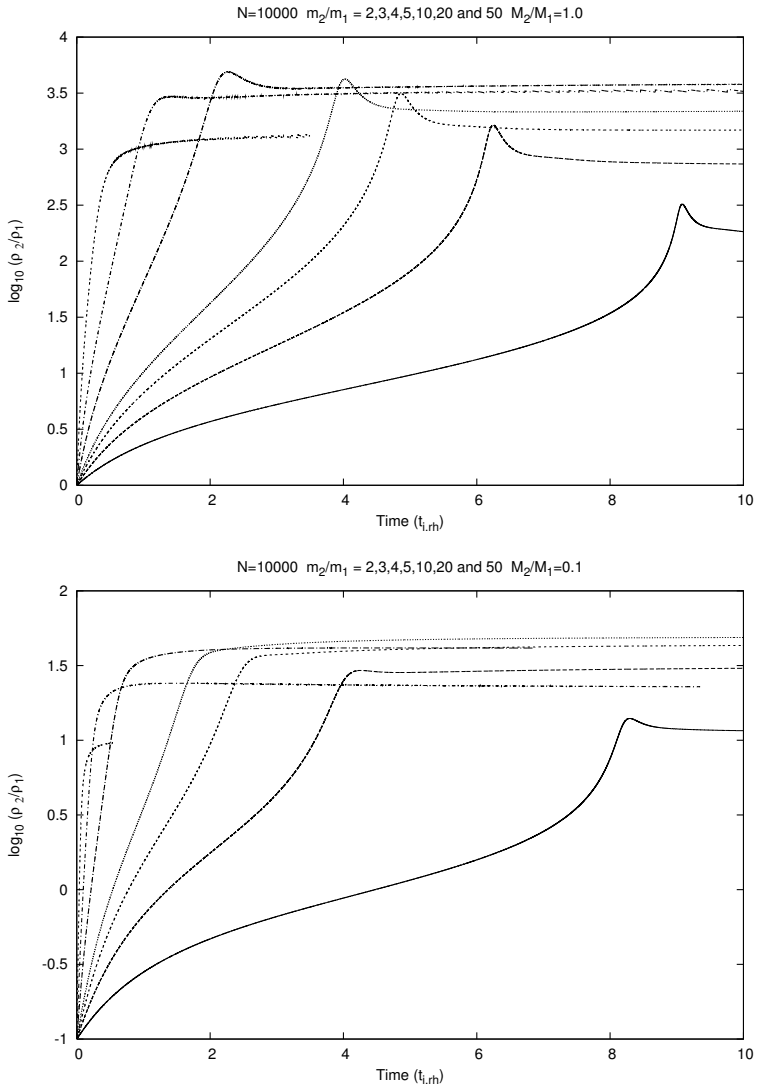

Figure 2.11: $\log_{10}(\rho_2/\rho_1)$ vs time (in units of $t_{i,rh}$) for the case of $M_2/M_1 = 1$ (top) and $M_2/M_1 = 0.1$ (bottom) Curves from bottom to top are $m_2/m_1 = 2, 3, 4, 5, 10, 20$ and 50

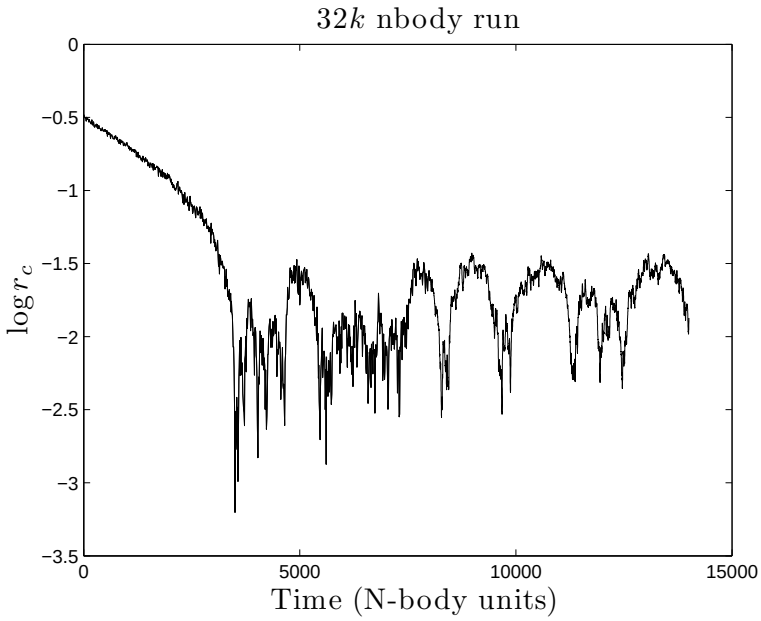

Figure 2.12: $\log_{10} r_c$ vs time, where r_c is defined as in NBODY6, $m_2/m_1 = 2$, $M_2/M_1 = 1$ and $N = 32k$.

and is another sign of gravothermal behaviour. The results from the $32k$ gas run are shown in Fig. 2.15 for comparison.

The $64k$ run shown in Figs. 2.16 and 2.17 has large amplitude oscillations. There is a part of the expansion which is shown in Fig. 2.17 between 7353 and 7390 in which the relative binding energy of binaries is nearly constant. Therefore binary activity cannot be what is driving the expansion. Fig. 2.17 (bottom) shows the evolution of the profile of $\log v^2$ over part of the expansion. A negative temperature gradient is visible towards the end of this expansion and this is what is driving the expansion. From the results of the $32k$ and $64k$ runs it seems that the value of $N_{crit} = 17000$ obtained by the gas code is a reasonable indicator of stability for the N-body case in the sense that none of the signs of gravothermal behaviour were found for $N \lesssim 16k$.

2.7 Conclusions and Discussion

The main focus of this chapter has been on the gravothermal oscillations of two-component systems. The critical value of N for the onset of instability has been found for a range of stellar mass ratios and total mass ratios using a gas model. The case of $M_2/M_1 = 1$ and $m_2/m_1 = 2$ was further investigated using the direct N-body code NBODY6. The value of N_{crit} obtained from the gas code seems to be a good indicator for stability in N-body runs for this case. Based on this, it is a reasonable assumption that the other N_{crit} values would give an indication of the stability for direct N-body systems. The values of N_{crit} for the two-component model were found to be much higher than for the one-component case and were found to vary with m_2/m_1 and M_2/M_1. However, the value of N_2 at the stability limit was found to vary much less than N itself. This seems to suggest that instability depends on the properties of the heavy component (see 2.4.2). A possible explanation of this is given in Section 2.4.2.

The physical manifestation of the oscillations was investigated for the case of small-amplitude periodic oscillations in the gas model. It has been pointed out that the collapse of the region between r_c and r_h is an important mechanism which can halt the expansion phase of a gravothermal oscillation. This mechanism should also be present in one-component models and it would be an interesting topic for future work to see how this mechanism would behave with different stellar mass functions.

Kim, Lee & Goodman (1998) argued that two-component clusters may be realistic approx-

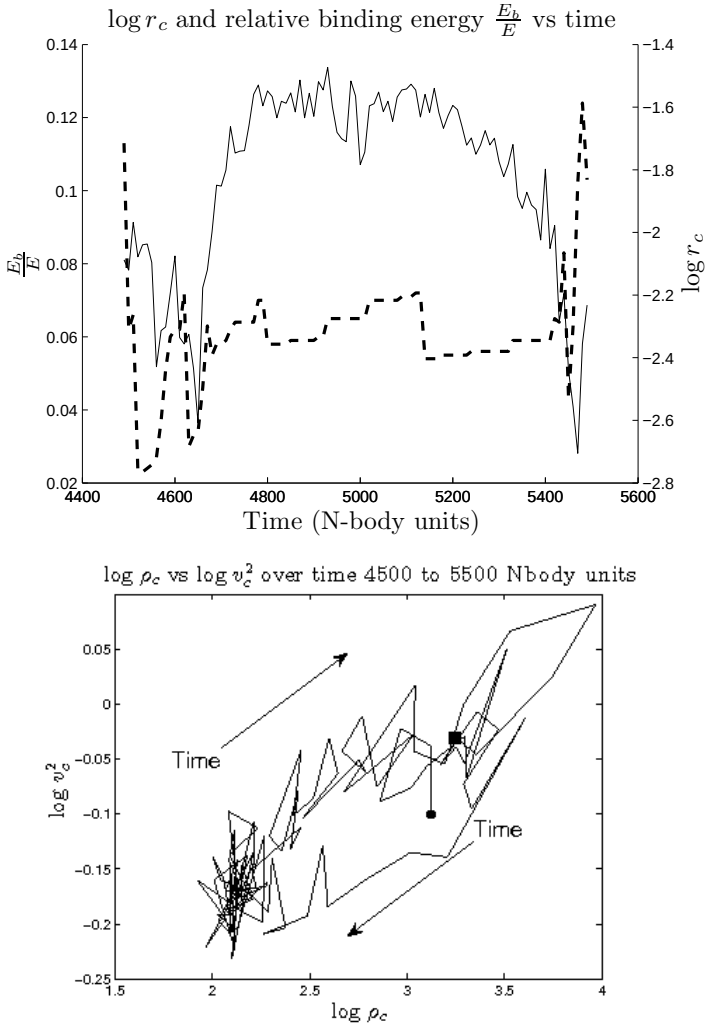

Figure 2.13: $32k$ N-body results. Top: relative binding energy E_b/E compared to $\log r_c$ over time 4500 to 5500 N-body units. Bottom: $\log r_c$ vs $\log v_c^2$ over the same time period, where, • and ■ represent the starting and finishing points.

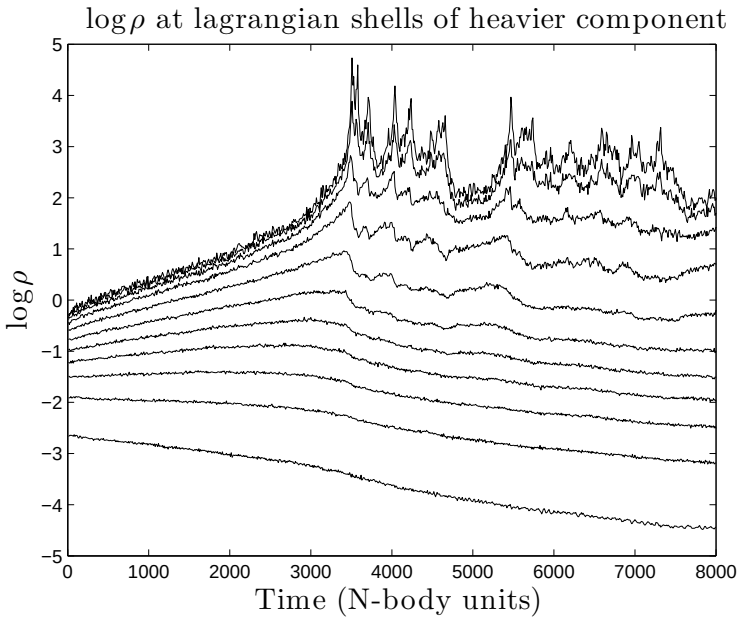

Figure 2.14: $32k$ N-body results. $\log \rho$ in Lagrangian shells of 1, 2, 5, 10, 20, 30, 40, 50, 62.5, 75 and 90 percent mass in the heavier component. It can be seen that the collapse at 5400 starts further out (while the core is still expanding) and propagates towards the core.

imations of multi-component clusters, where the two components are neutron stars and main sequence stars and the effect of white dwarfs (heavier than the turnoff mass) was assumed to be negligible. They also only studied cases that were Spitzer stable, which means that the components were able to achieve equipartition of kinetic energy. For the two-component case, it is only possible for it to be Spitzer stable if there is only a small amount of the heavier component present. As there is a significant range of stellar masses in a real star cluster, it is possible that some form of the Spitzer instability will be present.

To apply our ideas to a multi-component system, it may be possible to group the heavier components together if they are able to achieve approximate thermal equilibrium. This could be considered as a single heavier component which is Spitzer unstable with respect to the remaining components. This would help to reduce a multi-component system to the two-component case studied in this chapter.

Nevertheless, it is not clear quantitatively how the considerations of this research are to be applied to a multi-component cluster. Furthermore, we have ignored many things such as primordial binaries, tidal fields and stellar evolution and these are important in the evolution of a real star cluster. Further study is needed in order to understand the phenomenon that is gravothermal oscillation.

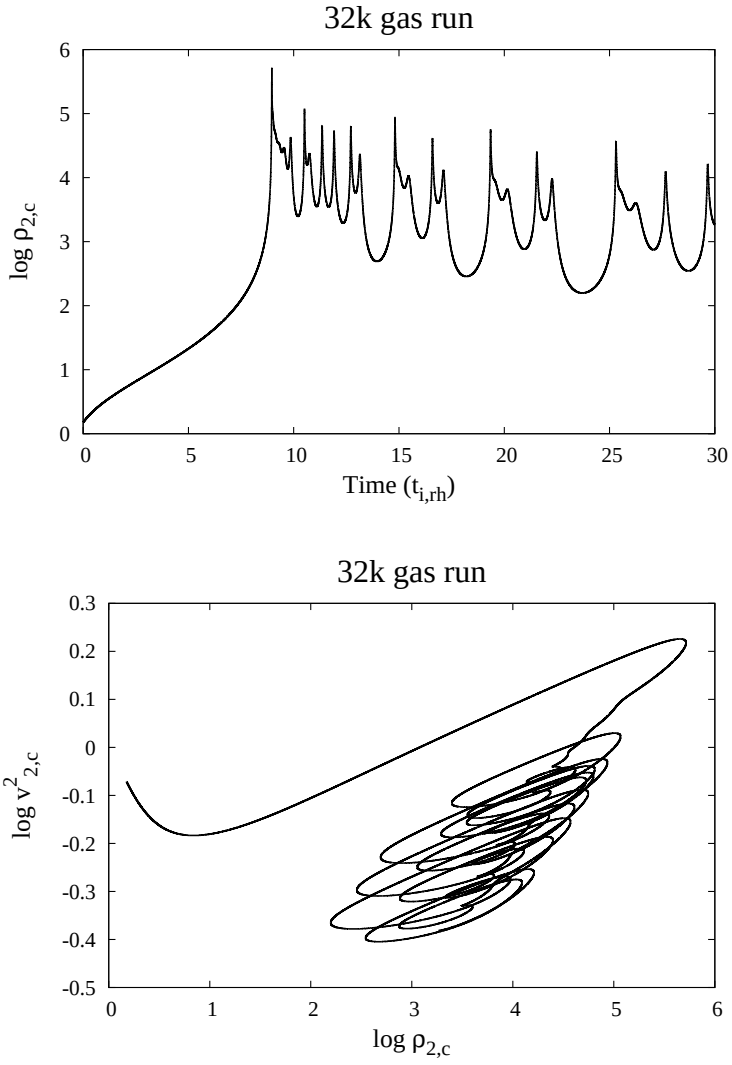

Figure 2.15: Evolution of the central properties of the heavy component in a 32k gas model. Top: $\log \rho_{2,c}$ vs time (units $t_{i,rh}$), bottom: $\log \rho_{2,c}$ vs $\log v_{2,c}^2$. All cycles are clockwise. The initial drop in $\log v_{2,c}^2$ results from the two components trying to achieve thermal equilibrium

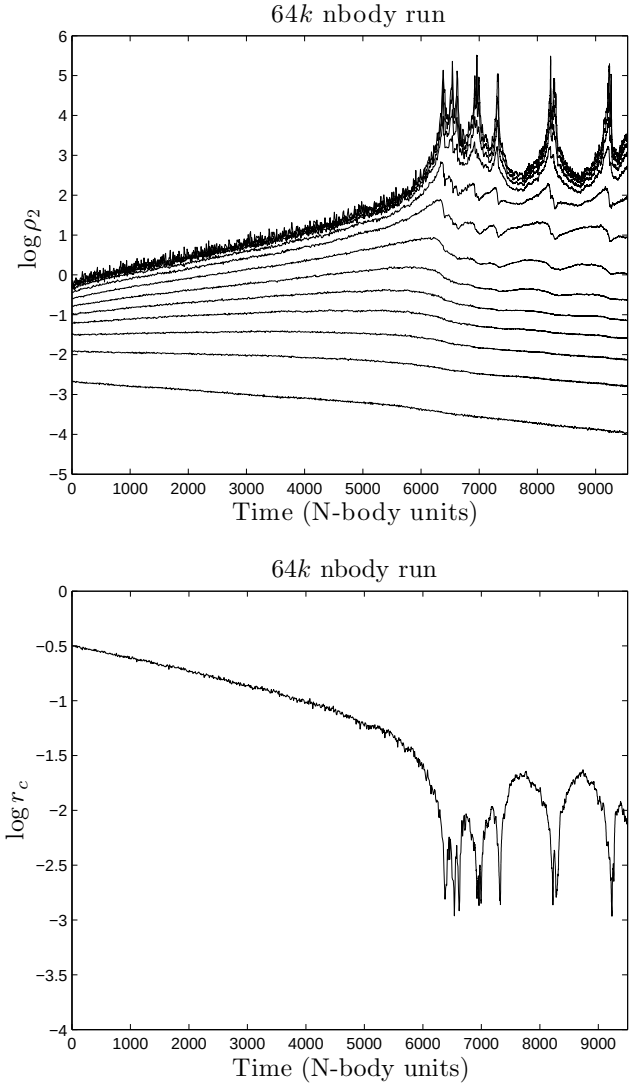

Figure 2.16: 64k N-body run. Top: $\log \rho_2$ at various Lagrangian shells in the heavier component, bottom: $\log r_c$ vs time

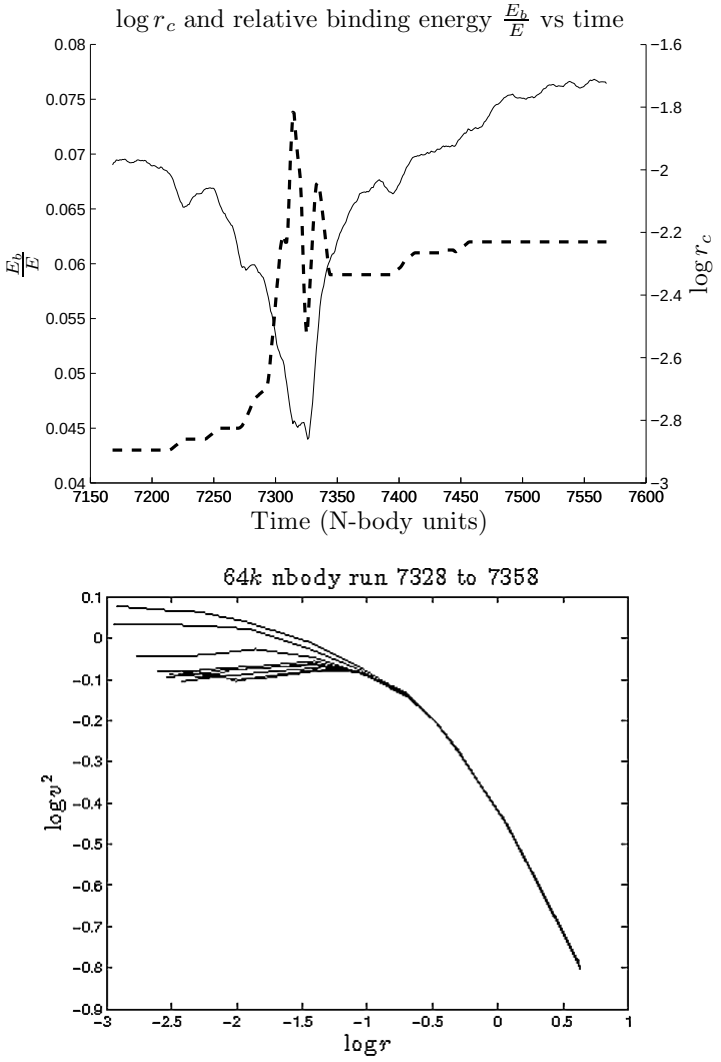

Figure 2.17: Top: evolution of the relative binding energy E_b/E and $\log r_c$. Bottom: $\log v_2^2$ measured at Lagrangian shells in the heavier component over part of the expansion of the core.

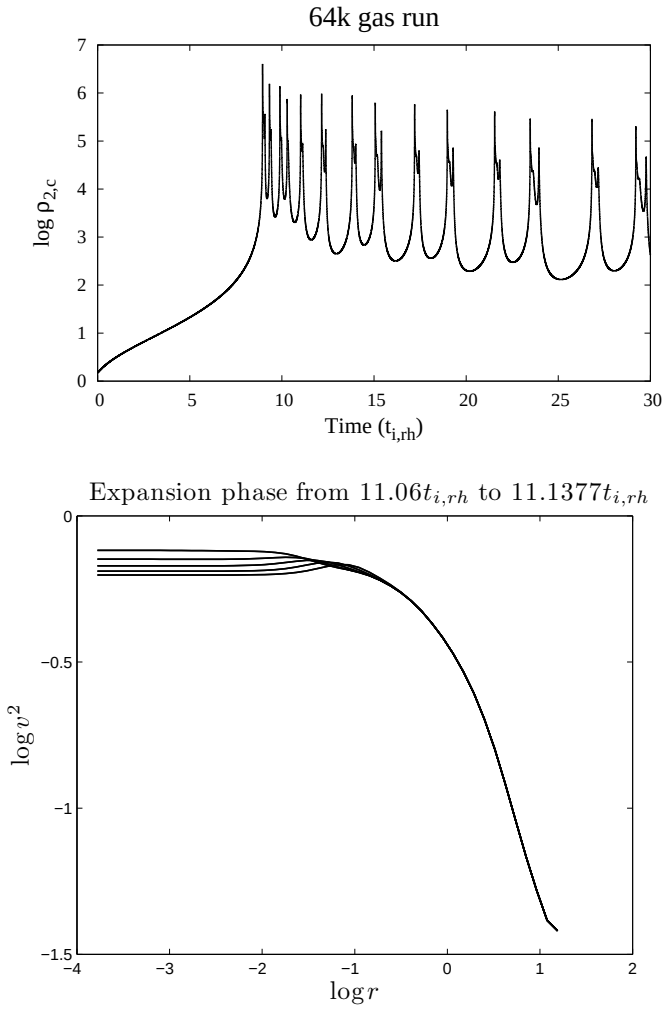

Figure 2.18: 64k gas model. Top: $\log \rho_{2,c}$ vs time ($units\ t_{i,rh}$), bottom: $\log v_2^2$ vs $\log r$ at different times during a gravothermal expansion.

Chapter 3

Gravothermal oscillations in multi-component models of star clusters

3.1 Chapter summary

In this chapter, gravothermal oscillations are investigated in multi-component star clusters which have power law initial mass functions (IMF). For the power law IMFs, the minimum masses (m_{min}) were fixed and three different maximum stellar masses (m_{max}) were used along with different power-law exponents (α) ranging from 0 to -2.35 (Salpeter). The critical number of stars at which gravothermal oscillations first appear with increasing N was found using the multi-component gas code SPEDI. The total mass (M_{tot}) is seen to give an approximate stability condition for power law IMFs with fixed values of m_{max} and m_{min} independent of α. The value $M_{tot}/m_{max} \simeq 12000$ is shown to give an approximate stability condition which is also independent of m_{max}, though the critical value is somewhat higher for the steepest IMF that was studied. For appropriately chosen cases, direct N-body runs were carried out in order to check the results obtained from SPEDI. Finally, evidence of the gravothermal nature of the oscillations found in the N-body runs is presented.

3.2 Introduction

The condition for the onset of gravothermal oscillations is best understood for the case of one-component star clusters, clusters consisting of stars of equal mass. Goodman (1987) found that gravothermal oscillations first appear when the number of stars N is greater than 7000. This condition has also been confirmed with Fokker-Planck calculations (Cohn et al, 1989) and by direct N-body simulations (Makino , 1996). However, the multi-component case is more complicated. This is due to the fact that the presence of several components introduces new dynamical processes into the system, and several additional parameters in addition to N.

Even for the two-component case, which is the simplest kind of mass spectrum, the condition for the onset of gravothermal oscillations is not so simple. Two-component models can be subdivided into Spitzer stable and Spitzer unstable cases depending on whether or not the two components can achieve equipartition of kinetic energy during core collapse (Spitzer, 1987). Kim, Lee & Goodman (1998) studied a range of Spitzer stable two-component models. Their research supported the applicability of the Goodman stability parameter ϵ (see Goodman, 1993) as a stability criterion. Breen & Heggie (2012a), whose research focused on the more general Spitzer unstable two-component case, indicated that the occurrence of gravothermal instability depends approximately on the number of stars in the heavier component. Breen & Heggie (2012a) also found that the critical value of ϵ depended on the parameters of the mass function (e.g. stellar mass ratio). However, by using a slightly modified version of ϵ, one with a modified definition of the half mass relaxation time, they found a nearly constant critical value.

Murphy et al (1990) found that the post-collapse evolution of multi-component models was stable to much higher values of N than in one-component models and that the value of N at which gravothermal oscillations appeared varied with different mass functions. They studied seven-component systems constructed to approximate evolved power law IMFs with masses ranging from 0.1 to $1.2M_{sun}$. The power law exponent that they considered ranged from -2 to -4.5. They found that gravothermal oscillations appeared when the total mass of the system (M_{tot}) was of order $8 \times 10^4 M_{sun}$ (see Murphy et al, 1990, Figure 6) and that the critical value of M_{tot} increased with decreasing power law exponent. They suggested that the appearance of oscillations depends on the number of heavier stars. However, this leads to the issue that in a multi-component system it is not clear what the definition of a heavy star should be (this point is discussed in Section 2).

The main aim of the present chapter is to provide a theoretical understanding of the onset of gravothermal oscillations in multi-component systems. As this present chapter follows on from the research in Chapter 2 (Breen & Heggie, 2012a) it is worthwhile attempting to extend the concepts developed in that chapter to the multi-component case. Although two-component systems may be realistic approximations of multi-component systems (Kim & Lee, 1997), it is best to have a better understanding of gravothermal oscillations in multi-component systems as real globular clusters contain a continuous mass spectrum. What is of particular importance is the effect of varying the maximum stellar mass (m_{max}) on the onset of instability as this was not studied by Murphy et al (1990).

The rest of this chapter is structured as follows. In Section 2, we state the results concerning gravothermal oscillations in gaseous models. This section also contains subsections on the Goodman stability parameter and a variant which used a modified relaxation timescale. This is followed by Section 3 in which the results of N-body simulations are given. Finally, Section 4 consists of the conclusion and discussion.

3.3 Critical Value of N

3.3.1 Results of gaseous models

In all cases, the initial conditions used were realisations of the Plummer model (Plummer, 1911; Heggie & Hut, 2003). The initial velocity dispersion of all components and the initial ratio of density of all components were equal at all locations. The initial conditions were constructed in order to approximate a continuous power law IMF with different exponents $\alpha = -0.0, -0.65, -1.3, -1.65, -2.00$ and -2.35. The multi-component gas code SPEDI[1] was used for all gaseous models in the present chapter. The power law IMFs were approximated by dividing the complete mass range into equal logarithmic steps. Alternative methods of discretization were also tried for certain cases in order to confirm the validity of the results, such as approximating the IMF using equal total masses in each of the components. The ranges of stellar masses (m_{max}, m_{min}) used in this chapter are $(1.0, 0.1)$, $(2.0, 0.1)$ and $(3.0, 0.1)$. The reason why higher values of m_{max} were not used is that it is customary to suppose that a cluster would be largely depleted in heavier stars by the time gravothermal oscillations manifest (Kim, Lee & Goodman, 1998). In Sec 3.6, however, we briefly discuss a possible exception.

The critical value of N (N_{crit}) at which oscillations in the central density (ρ_c) first appeared (as N increased) was determined (correct to ten percent). The obtained values of N_{crit} in units of 10^4 are given in Table 3.1.

3.3.2 Interpretation of results

Guided by the results of Murphy et al (1990), we first consider the values of M_{tot} at N_{crit} (M_{crit}). The values of M_{crit}, for the models considered in the present chapter, are given in Table 3.2. The values of M_{crit} in Table 3.2 are approximately the same for fixed m_{max} and the values vary much less with α than N_{crit}. Thus the conclusion of Murphy et al (1990), who

[1]SPEDI is a multi-component gas code which was initially based on a formulation by Louis & Spurzem (1991) and was subsequently further developed by Spurzem & Takahashi (1995). Further information regarding SPEDI is available at http://www.ari.uni-heidelberg.de/gaseous-model/.

Table 3.1: Critical value of N (N_{crit}) in units of 10^4. The values of N_{crit} in brackets were obtained using 5-component models, while all other values were obtained using 10-component models. The value of N_{ef} for the case $\alpha = -2.35$ and extreme masses $(3, 0.1)$ could not be obtained with a 10-component model due to numerical difficulties.

$(m_{max}, m_{min})\backslash\alpha$	**0**	**-0.65**	**-1.3**	**-1.65**	**-2.0**	**-2.35**
(3,0.1)	2.0	2.8	5.2	8.0	12.0	–
					(10.0)	(15.7)
(2,0.1)	2.0	2.6	4.5	7.0	8.0	10.0
						(10.0)
(1,0.1)	2.0	2.5	3.5	4.5	6.0	8.0

Table 3.2: Critical value of M (M_{crit}) in units of 10^4

$(m_{max}, m_{min})\backslash\alpha$	**0**	**-0.65**	**-1.3**	**-1.65**	**-2.0**	**-2.35**
(3,0.1)	3.1	3.1	3.4	3.8	4.2	(4.3)
(2,0.1)	2.1	2.0	2.3	2.8	2.5	2.6
(1,0.1)	1.1	1.1	1.2	1.3	1.5	1.8

considered only evolved IMFs with fixed m_{max}, appears also to apply to pure power law IMFs with fixed m_{max}. What has been added in the study in the present chapter is that the value of M_{crit} also has a strong dependence on m_{max}.

We can compare the dependence on m_{max} in Table 3.2 with the results of the two-component models of Chapter 2 (Breen & Heggie, 2012a) if we fix the stellar mass of the light component in that earlier chapter. This is done in Section 3.5 (see Table 3.7). In Table 3.7 there is a clear trend of increasing M_{crit} with increased stellar mass of the heavy component for fixed total mass ratio (i.e. moving up through one column of Table 3.7). Therefore the trend of increasing M_{crit} with increasing stellar mass range (or stellar mass ratio), for fixed m_{min}, seems to be a common feature of multi-component systems. It is also worth noting that for two-component systems with fixed stellar mass ratio (see Section 3.5 Table 3.7 where we consider values along a given row) there is a trend of increasing M_{crit} with decreasing total mass ratio. As decreasing total mass ratio for two-component systems is the analogue of decreasing *alpha*, these systems have the same stability trends as the multi-component systems in Table 3.2. Now we will attempt to extend the interpretation of Breen & Heggie (2012a) from two-component to multi-component models in a way which also accounts for the dependence on m_{max}.

Breen & Heggie (2012a) first argued that for the two-component case, the dynamics of the system were dominated by the heavier component. The reasoning behind this emphasis on N_2 is that the heavier component concentrates within the central region where it behaves like a one-component system deep in the potential well of the low mass stars, and it can exhibit gravothermal instability like the central part of a one-component system[2]. Breen & Heggie (2012a) showed that N_2, the number of heavy stars, does indeed provide an approximate criterion for the onset of instability, and found the critical value of N_2 to be of order 2000. For the case of multi-component models, however, it is unclear if and how the system can be divided into a heavy and a light component. Nonetheless, it may still be expected that the heavier stars may be more important to the dynamics of the system and to the onset of gravothermal oscillations.

Breen & Heggie (2012a) then gave an alternative measure of the importance of the heavy component, in terms of what they called the "effective" number of heavy stars, and this is a concept that is more readily adapted to the case of several components. Breen & Heggie (2012a) argued that, as the light component acts as a kind of container for the heavy component, it was the overall mass of this container (i.e. the total mass in the light component) that was

[2]Note that, in this picture, the gravothermal instability of the system is essentially confined to the massive stars; it is in the centrally concentrated massive stars that the temperature inversions occur which drive the expansion phase of the gravothermal oscillations. Around $N = N_{crit}$, the light stars always exhibit a normal temperature gradient, and if their heat capacity is negative this does not lead to instability.

Table 3.3: Critical value of N_{ef} in units of 10^4.

$(m_{max}, m_{min})\backslash\alpha$	**0**	**-0.65**	**-1.3**	**-1.65**	**-2.0**	**-2.35**
(3,0.1)	1.1	1.0	1.1	1.3	1.4	(1.4)
(2,0.1)	1.1	1.0	1.2	1.4	1.3	1.3
(1,0.1)	1.1	1.1	1.2	1.3	1.5	1.8

the important factor and not the stellar mass of the light component. Therefore it could be replaced by an equal mass of stars of the massive component, giving rise to the idea of the effective number of stars N_{ef}. This was defined as follows

$$N_{ef} = \frac{M_1 + M_2}{m_2}. \tag{3.1}$$

They also defined a modified half-mass relaxation time scale ($t_{ef,rh}$) by using N_{ef} in place of N in the standard formula for the half-mass relaxation time. They used this effective relaxation time to modify and improve upon a stability criterion suggested by Goodman (1993); see Section 3.3.3 of the present chapter. It is worth pointing out that N_{ef} itself can be used as an approximate stability condition for the two-component models of Breen & Heggie (2012a) (see Appendix 3.5). It is this form of condition for the stability of two-component systems which we shall attempt to generalise to multi-component systems.

Again it is not immediately clear what the most appropriate extension of N_{ef} to the multi-component case should be, as the appropriate definition of heavy stars is not clear. However, the result is much less sensitive to our choice than the number of heavy stars, N_2. One simple approximate way to define a heavy star in this context is simply any star with a stellar mass of $\approx m_{max}$. This would lead to the definition of N_{ef} as M_{tot}/m_{max} for the multi-component model and no change in the definition for a two-component model (equation (3.1)). This value is given in Table 3.3, for the multi-component models considered in this chapter. We find that there is much less variation among the critical values of N_{ef} than for M_{crit}, especially for varying m_{max}. Nevertheless, the same trend of increasing M_{crit} with decreasing α as seen in Table 3.2 is still present in Table 3.3 in the form of increasing N_{ef}.

Now we will discuss a possible explanation for the increase in the critical value of N_{ef} with decreasing α in Table 3.3. The idea behind N_{ef} is that a multi-component system behaves in approximately the same way as a single-component system consisting of N_{ef} stars of stellar mass m_{max}. As systems with higher α have more stars with stellar mass $\approx m_{max}$ than systems with lower α, we may expect that the approximation with the one-component system is better for higher α than for lower α. Therefore, it is not surprising that in Table 3.3 it is the systems with $\alpha = 0$ that have the closest critical values of N_{ef} to the critical value of N for a one-component system, i.e. about 7000.

We can take our discussion further by considering systems with fixed N_{ef}. For systems with fixed N_{ef}, as α decreases there is an increasing number of light stars (stars with stellar mass not $\approx m_{max}$). As the number of light stars increases and the number of heavy stars decreases the two-body relaxation time increases, as it becomes increasingly dominated by the light component. According to Hénon's principle (Hénon, 1975) the rate of energy generation in the system is regulated by two-body relaxation, and therefore there is a lower rate of energy generation as α decreases. Regardless of the value of α, the average mass in the core is approximately m_{max}, and the lower rate of energy generation can be met by a core of lower density. Thus for lower alpha there is a smaller density contrast between the core and the mean density in the system. This would imply that the stability would increase with decreasing α, as we indeed see.

3.3.3 Goodman stability parameter

Goodman (1993) suggested the use of the quantity

Table 3.4: Critical value of $\log_{10}\epsilon$

$(m_{max}, m_{min})\backslash\alpha$	**0**	**-0.65**	**-1.3**	**-1.65**	**-2.0**	**-2.35**
(3,0.1)	-2.26	-2.38	-2.54	-2.61	-2.57	(-2.62)
(2,0.1)	-2.26	-2.32	-2.48	-2.53	-2.58	-2.56
(1,0.1)	-2.26	-2.30	-2.39	-2.40	-2.43	-2.42

$$\epsilon \equiv \frac{E_{tot}/t_{rh}}{E_c/t_{rc}} \tag{3.2}$$

as a stability indicator, where $\log_{10}\epsilon \sim -2$ is the stability limit below which the cluster becomes unstable. Here E_{tot} is the total energy, E_c is the energy of the core, t_{rc} is the core relaxation time and t_{rh} is the half mass relaxation time. A condition of this type has been supported for two-component models by Kim, Lee & Goodman (1998) who studied Spitzer stable models using a Fokker-Planck code and by Breen & Heggie (2012a) who studied Spitzer unstable models using a gas code. However, Breen & Heggie (2012a) also introduced a modified definition of ϵ (see below) because the definition given in equation (3.2) was found to yield a critical value which varied with total mass ratio and stellar mass ratio. Also, the critical value at which the instability appears is somewhat different in Breen & Heggie (2012a) from that in Kim, Lee & Goodman (1998).

For the multi-component models studied in the present chapter, the values of $\log_{10}\epsilon$ are given in Table 3.4. The values of $\log_{10}\epsilon$ (based on the original definition, i.e. equation (3.2)) range from -2.26 to -2.56 and there is a decreasing trend with decreasing α.

In equation (3.2), t_{rc} and t_{rh} are defined by

$$t_{rc} = \frac{0.34\bar{\sigma}_c^3}{G^2\bar{m}_c\rho_c \ln\Lambda} \tag{3.3}$$

and

$$t_{rh} = \frac{0.138N^{\frac{1}{2}}r_h^{\frac{3}{2}}}{(G\bar{m})^{\frac{1}{2}}\ln\Lambda}. \tag{3.4}$$

where $\bar{m}_c$ and $\bar{\sigma}_c$ are the mass density weighted averages over all the components in the core. However, the definition of t_{rh} does not take into account the mass spectrum. Breen & Heggie (2012a) have shown that for two-component models, modifying the definition of t_{rh} to take into account the mass spectrum leads to an improved stability condition. As has already been shown in Section 3.3.1, we can construct a value N_{ef} which provides an approximate stability condition. Now we will use this value to define a new half mass relaxation time defined as

$$t_{ef,rh} = \frac{0.138N_{ef}^{\frac{1}{2}}r_h^{\frac{3}{2}}}{(Gm_{max})^{\frac{1}{2}}\ln\Lambda}. \tag{3.5}$$

We use this in place of t_{rh} in equation (3.2) to define the new stability parameter ϵ_2 as in Breen & Heggie (2012a). The values of this parameter are given in Table 3.5. The variation of $\log_{10}\epsilon_2$ in Table 3.5 is of comparable magnitude to the variation of $\log_{10}\epsilon$ in Table 3.4, but the values in Table 3.5 are more consistent with that of a one-component model ($\log_{10}\epsilon = \log_{10}\epsilon_2 = -2$) than those in Table 3.4.

For the one-component model the definitions of ϵ and ϵ_2 are identical. Also, it is worth noting that, for two-component systems with extremely small amounts of the heavy component (relative to M_{tot}), $t_{ef,rh}$ as defined in equation (3.5) is not a suitable approximation to the relaxation time. This is the case for the models considered by Kim, Lee & Goodman (1998), and so the extension to ϵ_2 would not have been necessary or useful in the context of their paper.

The logarithm of the Goodman stability parameter (or our somewhat more consistent modified version) seems to have a particular value approximately -2 at the stability boundary (Kim,

Table 3.5: Critical value of $\log_{10} \epsilon_2$

$(m_{max}, m_{min})\backslash\alpha$	**0**	**-0.65**	**-1.3**	**-1.65**	**-2.0**	**-2.35**
(3,0.1)	-2.06	-2.02	-1.99	-1.94	-1.75	(-1.73)
(2,0.1)	-2.04	-1.99	-2.00	-1.95	-1.75	-1.81
(1,0.1)	-2.05	-2.01	-2.01	-1.96	-1.94	-1.87

Lee & Goodman (1998), Chapter 2 (Breen & Heggie, 2012a) and the present chapter). However, it is not known if ϵ (or ϵ_2) can be predicted for a particular IMF without carrying out numerical simulations, which limits its usefulness. In contrast N_{ef} has the advantage that it can be easily calculated before carrying out numerical simulations, and also provides an approximate indication of the stability boundary.

3.4 Direct N-body Simulations

In order to validate the results obtained from the gas code SPEDI a series of N-body runs were carried out. The direct N-body simulations in the present chapter were conducted using the NBODY6 code (Aarseth, 2003; Nitadori & Aarseth, 2012). As the IMF's with $\alpha = 0$ in Table 3.1 have the lowest values of N_{crit} (2.0×10^4), for this value of α N-body runs were carried out for the mass ranges $(1, 0.1)$ and $(2, 0.1)$. The case with parameters $\alpha = -1.3$ and $(m_{max}, m_{min}) = (1.0, 0.1)$ was also chosen because it has a higher value of N_{crit} (3.5×10^4) than for $\alpha = 0$, although the value is still low enough to make it suitable for direct N-body simulations.

For the case of $\alpha = 0.0$ the values of N_{crit} are the same (see Table 2.2) regardless of the stellar mass range. For the two mass ranges chosen, there were no signs of gravothermal behaviour in the N-body runs with $N = 8k$ or $N = 16k$. The first clear sign of gravothermal behaviour occurs with $N = 32k$ for both chosen mass ranges. For the stellar mass range $(1.0, 0.1)$, the three panels of Fig. 3.1 show, respectively, (i) the evolution of the core radius r_c, (ii) an example of a single cycle of gravothermal oscillation in the post-collapse evolution, and (iii) evidence of the gravothermal nature of the oscillation for the $32k$ run. The same graphs for the $32k$ run with stellar mass range $(2.0, 0.1)$ are given in Fig. 3.2.

For the case $\alpha = -1.3$ and stellar mass range $(1.0, 0.1)$ the value of N_{crit} is 3.5×10^4 (see Table 2.2). No gravothermal behaviour was seen in the N-body runs with $N = 8k$, $12k$ and $32k$ for this set of conditions. The first signs of gravothermal behaviour occurred in the $64k$ run as would be expected from the above value of N_{crit} obtained from SPEDI. The same three graphs shown for both the $\alpha = 0.0$ cases (see previous paragraph) are plotted for the $64k$ run in Fig 3.3.

In the graphs of r_c for all cases (see Fig. 3.1 top, Fig. 3.2 top and Fig. 3.3 top), behaviour can be seen which is qualitatively similar to gravothermal oscillations (see Makino (1996), Takahashi & Inagaki (1995), Heggie & Giersz (2009) and Breen & Heggie (2012a)). For the case of $\alpha = 0.0$ with the mass range $(1.0, 0.1)$ (Fig. 3.1 top) one oscillation can be seen between 3830 and 4570, and another between 5970 and 6560. During each of these oscillations r_c changes by more than a factor of 10. Similarly for the case of $\alpha = 0.0$ with the mass range $(2.0, 0.1)$ (Fig. 3.2 top) an oscillation in r_c can be seen between 6800 and 7950, and part of an oscillation can also be observed after 8610. In this model the change in r_c is about a factor of 10. Finally for the case of $\alpha = -1.3$ with the mass range $(1.0, 0.1)$ (Fig. 3.3 top) an oscillation in r_c can be seen between 4800 and 5600, and part of an oscillation can also be observed after 7400. The change in r_c is about a factor of 10, which is similar to the change in r_c for the $\alpha = -1.3$ runs.

Now we consider the physical nature of these oscillations, which could in principle be driven by sustained binary activity or by gravothermal behaviour. A sign of gravothermal behaviour is that the binding energy of the binaries remains roughly constant during times of expansion (McMillan & Engle, 1996). This is because the expansion phase of a gravothermal oscillation should be driven by the core absorbing heat from the rest of the cluster rather than by energy generation. At core bounce, where ρ_c reaches a local maximum, there is an increase in binary activity, and enough energy is produced to halt and reverse the collapse. This behaviour is

particularly clear in Fig. 3.3 (middle) where there is an initial increase in relative binding energy of the binaries coinciding with core bounce and the initial expansion. A binary escapes, and then there is a period of expansion during which the relative binding energy of the binaries remains nearly constant (from 4850 to 5000). Towards the end of the oscillation there is renewed binary activity corresponding to the next core bounce. There is also binary activity at other times during the oscillation, but it has no discernible effect on the evolution of r_c. Fig. 3.1 (middle) is also a good example of gravothermal behaviour. Mild binary activity continues after core bounce (from $t = 3860$ to $t = 3930$) but expansion continues thereafter for a period. However in Fig. 3.2 evidence of gravothermal behaviour is more ambiguous. We will discuss the case of Fig. 3.2 in detail in the last paragraph of this section.

The cycles of ρ_c vs the core velocity dispersion v_c^2, as seen in Fig. 3.1 (bottom), Fig. 3.2 (bottom) and Fig. 3.3 (bottom), are believed to be a sign of gravothermal behaviour (Makino , 1996). During these cycles, the temperature is lower during the expansion where heat is absorbed and higher during the collapse where heat is released. The velocity dispersion in Fig 3.2 (bottom) and Fig. 3.3 (bottom) has been smoothed to make the cycle clearer. These cycles are similar to the cycles found by Makino (1996) for one-component models and by Breen & Heggie (2012a) for two-component models.

The gravothermal nature of the behaviour is clearer in Fig. 3.1 (where $(m_{max}, m_{min}) = (1.0, 0.1)$) than in Fig. 3.2 (where $(m_{max}, m_{min}) = (2.0, 0.1)$). This is perhaps surprising as both cases have the same value of N_{crit} as found with SPEDI. We will now discuss a number of possible reasons for this apparent difference in behaviour. Firstly, as the values of N_{crit} are only correct to 10%, it is possible that in reality the values could differ by up to 4×10^3. Secondly, another issue is that in the gas model the mass function is discretised, resulting in a difference between the mass of the heavy component (m_{10}) and m_{max}. m_{10} is about 14% percent less than m_{max} for the stellar mass range $(2.0, 0.1)$ and 11% for $(1.0, 0.1)$. It is argued in Appendix 3.5 that the stability of a system will increase if the average stellar mass inside the core is increased (while keeping the stellar masses outside the core approximately the same). This would imply that in both cases the values of N_{crit} found with the 10-component models are underestimates for the onset of instability, and that the true value of N_{crit} for $(2.0, 0.1)$ is slightly higher than for $(1.0, 0.1)$. Finally, the fact that the gravothermal nature of the behaviour is clearer in one run might simply be a stochastic effect.

For the purposes of this thesis, we have not considered the evolution of multi-component systems in the regime $N < N_{crit}$. In Spitzer-unstable cases, there is no reason to doubt that this is characterised by mass-segregation, followed by post-collapse expansion powered by binary evolution as in the much smaller N-body models considered long ago by van Albada (1967), Aarseth (1968) and many more since.

3.5 The two-component case revisited

The purpose of this section is to reconsider the results of Breen & Heggie (2012a) in terms of the effective particle number N_{ef} defined in equation 3.1. Breen & Heggie (2012a) investigated gravothermal oscillation in a range of two-component models, specified by the stellar mass ratio m_2/m_1 and total mass ratio M_2/M_1, where m_2 (m_1) is the stellar mass of the heavy (light) component and M_2 (M_1) is the total mass of the heavy (light) component. For reference the values of N_{crit} for these models are given in Table 3.6, which is similar to Table 2 in Breen & Heggie (2012a). The difference is that the data have been rearranged to compare more closely to the arrangement in the present chapter. Thus the columns in Table 3.6 are arranged in order of decreasing M_2/M_1 as this is the analog for two components of decreasing α.

Following the approach in the present chapter, we will firstly consider the values of M_{crit}. In order to consider M_{crit} we need to specify the mass unit, and to make the results comparable with the multi-component models in the main part of the present chapter m_1 has been fixed at $0.1 M_{sun}$. The values of M_{crit} for the two-component models in Table 3.6 are given in Table 3.7. For comparison the value of M_{crit} for a one-component model would be 0.07×10^4 (using $m = 0.1 Msun$). This is significantly lower than any of the values in Table 3.7[3]. For fixed

[3]In Table 3.7 for fixed m_2/m_1, M_{crit} increases with decreasing M_2/M_1. Given that M_{crit} for $M_2/M_1 = 0$ is significantly lower than any of the values in Table 3.6, one may wonder if that increasing trend observed in

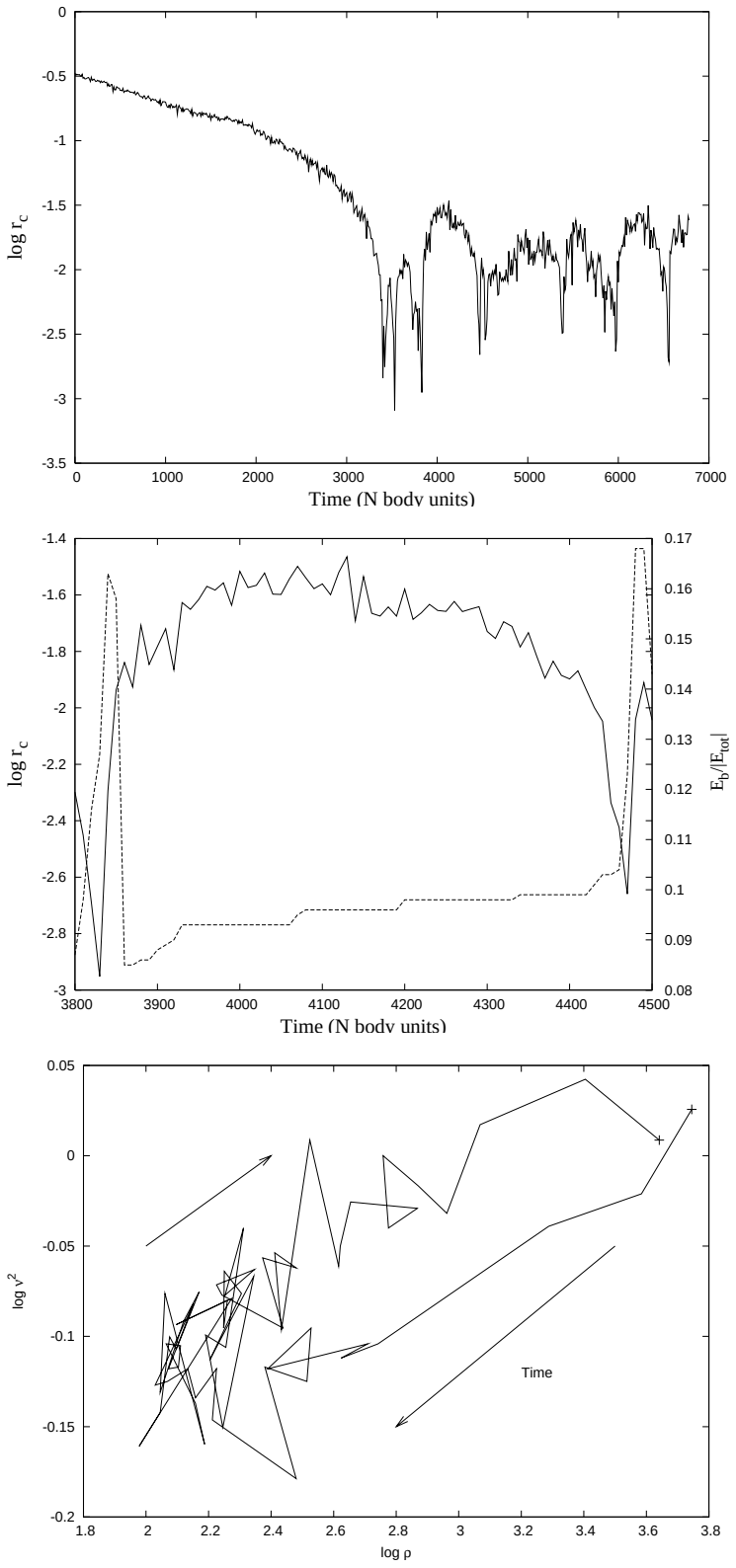

Figure 3.1: N-body run of a multi-component model with $N = 32k$, $\alpha = 0.0$ and $(m_{max}, m_{min}) = (1.0, 0.1)$. **Top**: $\log r_c$ vs time (N body units) over the entire run. **Middle**: $\log r_c$ vs time (N body units) over-plotted with the relative binding energy of binaries. The plot is over the period of a gravothermal oscillation which occurs between 3830 and 4570. **Bottom**: ρ_c vs v_c^2, showing the gravothermal nature of the cycle over the same time period as the middle plot.

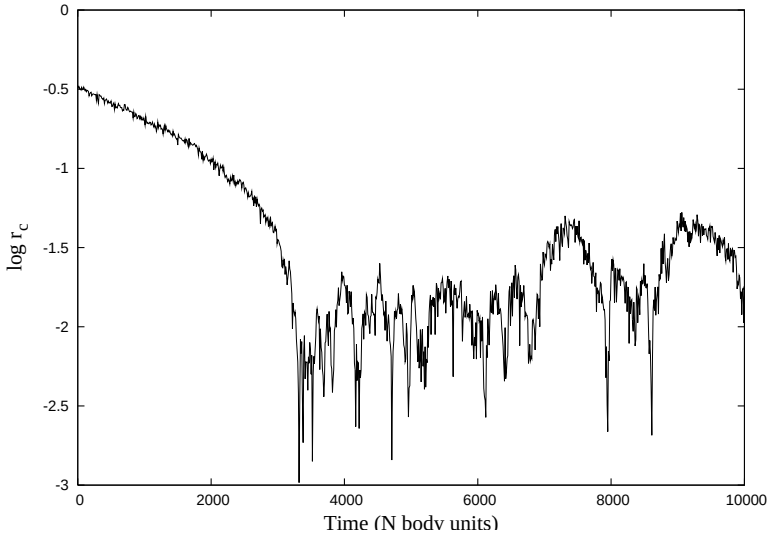

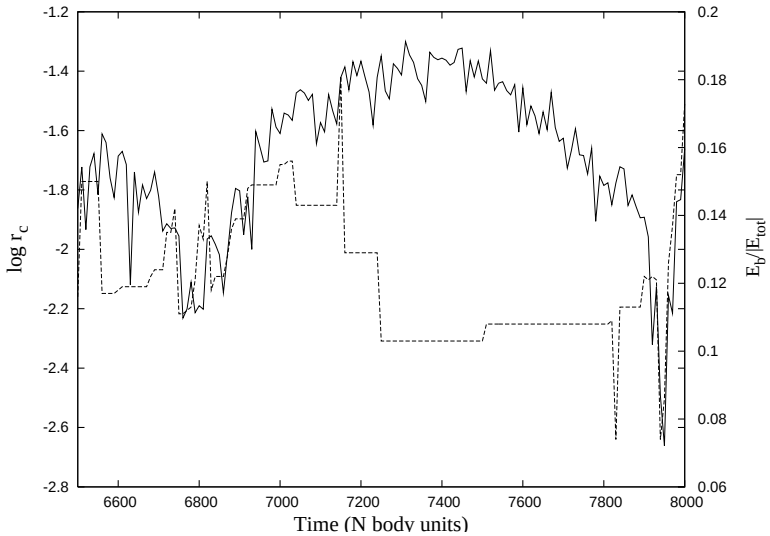

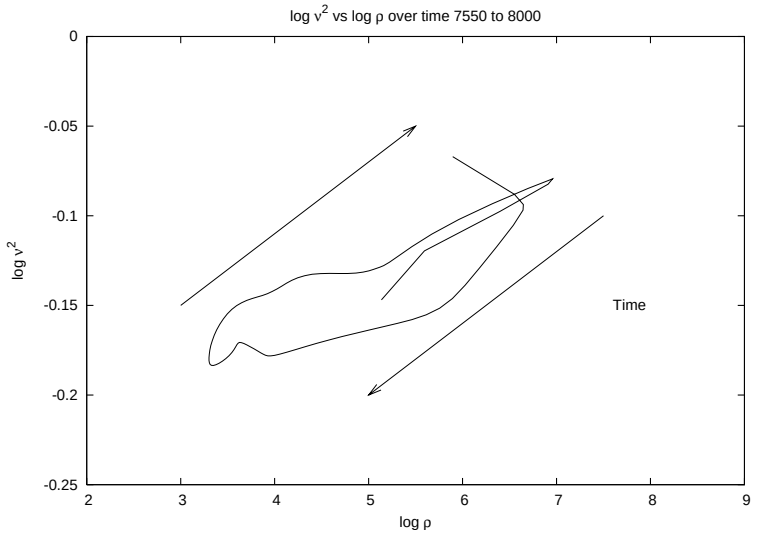

Figure 3.2: As Fig. 3.1, with $N = 32k$ and $\alpha = 0.0$, but $(m_{max}, m_{min}) = (2.0, 0.1)$. The velocity dispersion has been smoothed to make the cycle clearer.

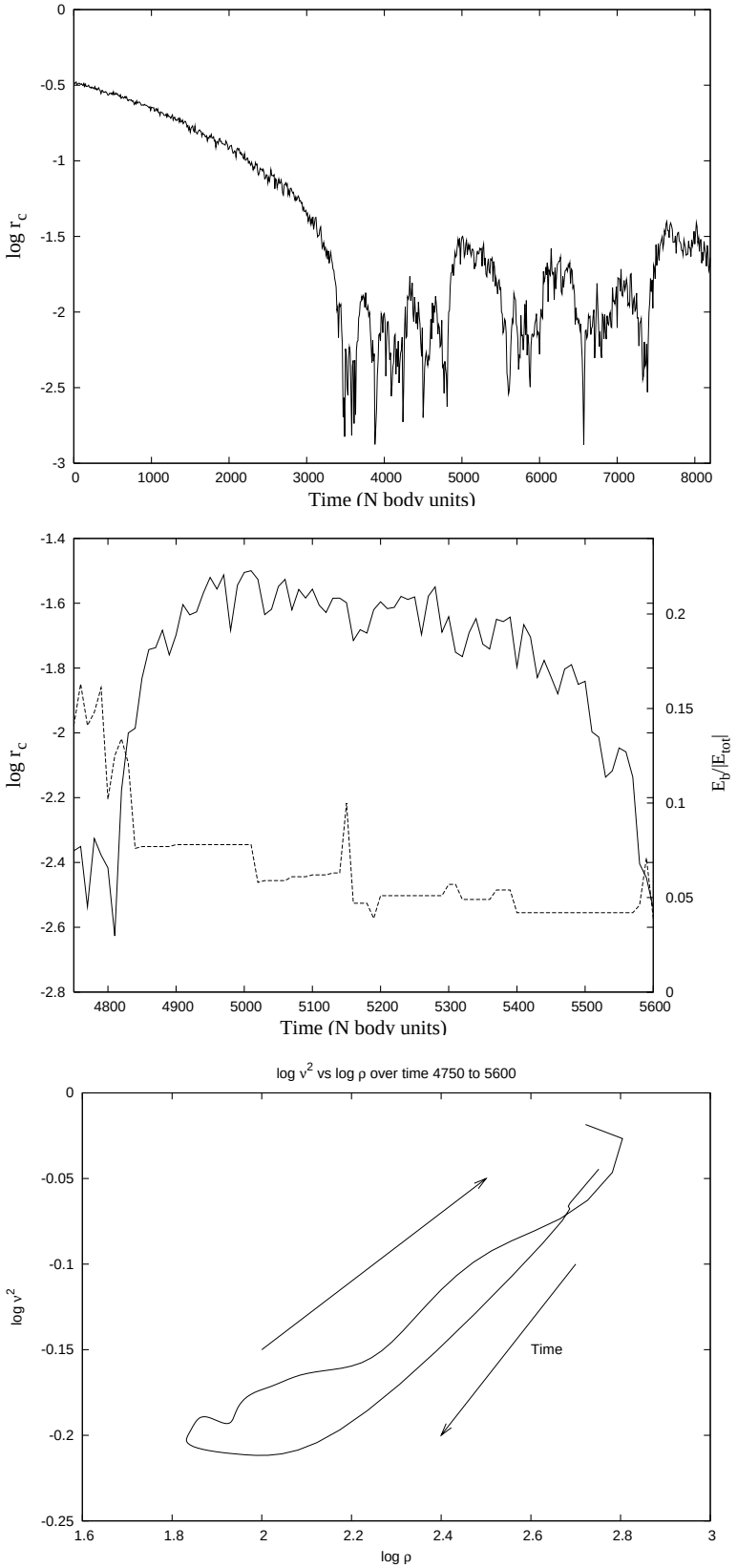

Figure 3.3: As Fig. 3.1, with $(m_{max}, m_{min}) = (1.0, 0.1)$, but $N = 64k$ and $\alpha = -1.3$. The velocity dispersion has been smoothed to make the cycle clearer.

Table 3.6: Critical value of N (N_{crit}) in units of 10^4

$\frac{m_2}{m_1} \backslash \frac{M_2}{M_1}$	**1.0**	**0.5**	**0.4**	**0.3**	**0.2**	**0.1**
50	18	30	33	42	55	100
20	8.5	13	15	18	22	36
10	5.0	7.2	8.2	10	12	22
5	2.8	4.0	4.6	5.4	7.0	10
4	2.4	3.5	3.8	4.6	5.5	8.5
3	2.0	2.8	3.2	3.6	4.4	6.0
2	1.7	2.2	2.3	2.6	3.0	3.8

Table 3.7: Critical value of M_{crit} in units of $10^4 M_{sun}$. The value of m_1 is fixed at $0.1 M_{sun}$. For reference the value of M_{crit} is $0.07 \times 10^4 M_{sun}$ for $M_2/M_1 = 0$, which is obtained from the result of Goodman (1987) for a one-component cluster with $m_1 = 0.1 M_{sun}$.

$\frac{m_2}{m_1} \backslash \frac{M_2}{M_1}$	**1.0**	**0.5**	**0.4**	**0.3**	**0.2**	**0.1**
50	3.529	4.455	4.583	5.427	6.574	10.978
20	1.619	1.902	2.059	2.305	2.614	3.940
10	0.909	1.029	1.104	1.262	1.412	2.396
5	0.467	0.545	0.596	0.662	0.808	1.078
4	0.384	0.467	0.484	0.556	0.629	0.912
3	0.300	0.360	0.395	0.425	0.495	0.639
2	0.227	0.264	0.268	0.294	0.327	0.398

values of m_2/m_1 the value of M_{crit} varies by factors of up to ≈ 3 between $M_2/M_1 = 1$ and 0.1. Therefore for fixed m_2/m_1, M_{crit} does provide a rough stability condition. However for fixed M_2/M_1, the variation in M_{crit} is a factor of $\approx 15 - 30$. The variation of M_{crit} with varying m_2 resembles the variation of M_{crit} with varying m_{max} in Table 3.2.

We will now consider the values of N_{ef} for the two-component systems; these are given in Table 3.8. For comparison the critical value of N_{ef} for a one-component model is the same as its value of N_{crit}, which is 0.7×10^4. The values in Table 3.8 vary much less then those of M_{crit} in Table 3.7, although, as pointed out in Section 3.3.1, N_{ef} can be interpreted as a measure of the total mass of the system in units of m_2. A stability condition of $N_{ef} \sim 10^4$ or slightly more covers, within a factor 2 at most, the values of Table 3.8 and indeed Table 3.3.

All of the trends in Table 3.8 may be understood if we consider the reasoning behind the use of N_{ef} as an approximate stability condition. The basic idea is that the multi-component system in question evolves in a similar way to a one-component system of N_{ef} stars with stellar mass m_2. This requires that the half mass relaxation timescale of the multi-component system is similar to that of the one-component system with which we are comparing it. We assume this to be true if the heavy component amounts to a significant faction of the total mass within the

Table 3.6 continues below $M_2/M_1 = 0.1$. This is a topic considered in Chapter 4.

Table 3.8: Critical value of N_{ef} in units of 10^4

$\frac{m_2}{m_1} \backslash \frac{M_2}{M_1}$	**1.0**	**0.5**	**0.4**	**0.3**	**0.2**	**0.1**
50	0.71	0.89	0.91	1.09	1.31	2.20
20	0.81	0.95	1.02	1.15	1.31	1.97
10	0.91	1.03	1.10	1.26	1.42	2.40
5	0.93	1.09	1.19	1.32	1.62	2.16
4	0.96	1.17	1.21	1.39	1.57	2.28
3	1.00	1.20	1.32	1.42	1.65	2.13
2	1.13	1.32	1.34	1.47	1.64	1.99

half-mass radius r_h, which is certainly not the case as M_2/M_1 tends to 0, i.e. on the extreme right of Table 3.8.

We now consider with more care how the two-component system actually differs from the corresponding one-component system as the parameters M_2/M_1 and m_2/m_1 are varied. For fixed m_2/m_1, as M_2/M_1 decreases the relaxation process is increasingly dominated by the light stars. This leads to the system behaving more like a one-component system of M_{tot}/m_1 stars as opposed to a one-component system of N_{ef} stars, and this increases the half-mass relaxation time. As the rate of two body relaxation becomes slower the core becomes larger (relative to r_h; see the discussion of Hénon's Principle in Section 2.4.2) as it can produce the required energy at a lower mass density (as the average stellar mass in the core remains the same, roughly m_2). Because gravothermal instability depends on a high density contrast within the system, it would be expected that stability would increase as M_2/M_1 decreases, as can be seen in Table 3.8.

Now let us consider the case of fixed M_2/M_1. If we consider the post collapse evolution of series of systems with fixed M_2 and m_2, as m_2/m_1 decreases the tendency towards mass segregation becomes weaker. Therefore the half mass radius of the heavy component ($r_{h,2}$) is smaller compared to r_h for larger m_2/m_1 than for smaller m_2/m_1. It follows that the mass density of the heavy component (within $r_{h,2}$) is smaller for smaller m_2/m_1 than for larger m_2/m_1. The relaxation time of the heavy component within its half-mass radius $r_{h,2}$ ($t_{rh,2}$) decreases with increasing mass density. This leads to the conclusion that the relaxation time within the heavy component increases with decreasing m_2/m_1. The energy flux in the heavy component, which we are assuming regulates the rate of energy generation, is of order $|E_2|/t_{rh,2}$ (where E_2 is the energy of the heavy system). Therefore, as m_2/m_1 decreases so does the energy flux, which results in a lower rate of energy generation. The lower rate of energy generation leads to a larger core (relative to r_h) as the core can produce the required energy at a lower mass density. Thus it would be expected that stability (as measured by N_{ef}) would increase as m_2/m_1 decreases, and this is what is observed in Table 3.8 for most values of M_2/M_1. However, the trend of increasing stability with decreasing m_2/m_1 seems to disappear for small M_2/M_1. Reasons for this will be discussed in the next chapter.

3.6 Summary and Discussion

The focus of this chapter has been on the conditions for the onset of gravothermal oscillations in multi-component systems. We have investigated power law IMFs with different exponents and three different stellar mass ranges $(3.0, 0.1)$, $(2.0, 0.1)$ and $(1.0, 0.1)$. A multi-component gas code has been used to obtain the values of N_{crit}. In order to verify the validity of the results direct N-body runs were carried out on appropriately chosen cases. The values of N_{crit} found ranged from 2×10^4 to 10^5, and varied with α and the stellar mass range.

Motivated by Murphy et al (1990), who found that the total mass of the systems they studied could be used as an approximate stability condition, the value of M_{crit} (the total mass of the system at N_{crit}) for each system was calculated (see Table 3.2). While for a fixed mass range M_{crit} does provide an approximate stability condition, the value of M_{crit} varied by roughly a factor m_{max}. M_{crit} can also be used as an approximate stability condition for the two-component models of Breen & Heggie (2012a) so long as the stellar mass ratio is fixed (see Appendix 3.5).

In order to find a more general stability condition we applied an extension of an idea first employed in Breen & Heggie (2012a). They used a quantity called the effective particle number (N_{ef}). The value was useful because the two-component system that was being considered was expected to behave in roughly the same manner as a one-component system with N_{ef} stars. In the present chapter this idea has been extended to multi-component systems. The values of N_{ef} for the multi-component models in this chapter are given in Table 3.3. The variation in Table 3.3 is significantly less then that in either Table 3.1 or Table 3.2. A stability condition of $N_{ef} \sim 10^4$ covers most of the values of Table 3.3 and indeed the two-component models of Breen & Heggie (2012a) (see Table 3.8).

The Goodman Stability Parameter was also tested for the multi-component case (see Table 3.4). The critical values in Table 3.4 were found to be lower than the value for a one-component

model ($\log_{10}\epsilon = -2$) and also varied with α and, to a much lesser extent, with m_{max}. By modifying the Goodman Stability Parameter using a slightly different definition for the half-mass relaxation time (based on the effective particle number) a critical value was found which was more consistent with the critical value for a one-component model (see Table 3.5).

Goodman (1987) used a gas model to find the value of N_{crit} (= 7000) for a single component system. Technically what he showed was that steady post-collapse expansion was possible in a gas model for all N, but that it was unstable for $N > 7000$. While the gas model used by Goodman (1987) is similar in form to the model used here and in Breen & Heggie (2012a), there are two notable differences. Firstly Goodman (1987) used a larger energy generation rate than the one used here. Secondly, the parameter of the coulomb logarithm that was used was $\lambda = 0.4$. A value of $\lambda = 0.4$ (Spitzer, 1987) was a reasonable choice at the time, but it has since been shown that $\lambda = 0.11$ is a better choice for a single-component model (Giersz & Heggie , 1994). (For multi-component models the value of $\lambda = 0.02$ was found to provide a good fit (Giersz & Heggie , 1996)). These two differences affect the stability in opposite ways: by arguments similar to those given in the last two paragraphs in section 3.5, a larger energy generation rate will increase stability, whereas a larger value of λ tends to reduce stability. For example for $N = 7000$ with $\lambda = 0.4$ the increase in the relaxation rate is 20% compared with $\lambda = 0.11$.

In the present chapter, we have made the assumption that multi-component systems will be depleted in stars with stellar mass greater than $3M_{sun}$. This neglects the possibility of systems containing a population of stellar mass Black Holes, which would require a value of m_{max} about an order of magnitude greater than what is considered here. These systems are outside the parameter space studied by Breen & Heggie (2012a) and Kim, Lee & Goodman (1998), as the total mass ratio is lower than the range considered by Breen & Heggie (2012a) and the stellar mass ratio is higher than the values considered by Kim, Lee & Goodman (1998). The onset of gravothermal oscillations and the more general evolution of systems containing a population of stellar mass black holes are the topics of the next chapter in this series.

To conclude, a stability condition of $N_{ef} \sim 10^4$ does apply to the multi-component systems in this chatper and the two-component systems of Breen & Heggie (2012a). This condition is expected to apply to any multi-component system provided that there is a sufficient number of stars with stellar mass $\sim m_{max}$.

Chapter 4

On the dynamical evolution of stellar-mass black hole subsystems in star clusters

4.1 Section summary

In this chapter, globular star clusters which contain a sub-system of stellar-mass black holes (BH) are investigated. This is done by considering two-component models, as these are the simplest approximation of more realistic multi-mass systems, where one component represents the BH population and the other represents all the other stars. These systems are found to undergo a long phase of evolution where the centre of the system is dominated by a BH sub-system. After mass segregation has driven most of the BH into a compact sub-system, the evolution of the BH sub-system is found to be influenced by the cluster in which it is contained. The BH sub-system evolves in such a way as to satisfy the energy demands of the whole cluster, just as the core of a one component system must satisfies the energy demands of the whole cluster. The BH sub-system is found to exist for a significant amount of time. It takes approximately $10t_{rh,i}$, where $t_{rh,i}$ is the initial half-mass relaxation time, from the formation of the compact BH sub-system up until the time when 90% of the sub-system total mass is lost (which is of order 10^3 times the half-mass relaxation time of the BH sub-system at its time of formation). Based on theoretical arguments the rate of mass loss from the BH sub-system ($\dot{M}_2$) is predicted to be $\frac{M}{t_{rh}}\frac{\beta\zeta}{\alpha}$: where M is the total mass, t_{rh} is the half-mass relaxation time, and α, β, ζ are three dimensionless parameters. (see Section 4.3 for details). An interesting consequence of this is that the rate of mass loss from the BH sub-system is approximately independent of the stellar mass ratio ($\frac{m_2}{m_1}$) and the total mass ratio ($\frac{M_2}{M_1}$) (in the range $\frac{m_2}{m_1} \gtrsim 10$ and $\frac{M_2}{M_1} \approx 10^{-2}$, where m_1, m_2 are the masses of individual low-mass and high-mass particles respectively, and M_1, M_2 are the corresponding total mass). The theory is found to be in reasonable agreement with most of the results of a series of N-body simulations, and all of the models if the value of ζ is suitable adjusted. Predictions based on theoretical arguments are also made about the structure of BH sub-systems. Other aspects of the evolution are also considered such as the conditions for the onset of gravothermal oscillation.

4.2 Introduction

Hundreds of stellar mass black holes (BH) can form within a massive globular cluster (see Kulkarni, Hut & McMillan (1993), Sigurdsson & Hernquist (1993) and Portegies Zwart & McMillan (2000)). Some of the BH might escape at the time of their formation due to large natal kicks. However the subject of natal kicks for BH is still under debate (Repetto, 2012) and it is possible that the largest BH may form without any supernova explosion (Fryer, 1999). Uncertainty in the natal kicks leads to uncertainty in the initial size of the BH population. As the BH are more massive than the other stars in the system, any retained BH will undergo

mass segregation and almost all are likely to become concentrated in the centre of the system, eventually forming a compact sub-system.

The mass of the BH sub-system decreases over time because BH binaries form in the dense core of the BH sub-system, causing the ejection of single BH and ultimately the binaries themselves through super-elastic encounters (see Kulkarni, Hut & McMillan (1993), Sigurdsson & Hernquist (1993), Portegies Zwart & McMillan (2000), Banerjee et al (2010), Downing et al (2010), Aarseth (2012)). Early work by Kulkarni, Hut & McMillan (1993) and Sigurdsson & Hernquist (1993) seemed to indicate that the BH population will become depleted over a relatively short timescale. This conclusion was reached in part by treating the BH sub-system as if it were an independent system once most of the BH had segregated to the centre of the cluster.

Merritt et al (2004) and Mackey et al (2008) found that heating by a retained population of BH causes large-scale core expansion in massive star clusters. They suggest this may partly explain the core radius-age trend observed for such objects in the Magellanic Clouds. The BH binaries that are formed in the core of the BH sub-system are an interesting class of objects in their own right, especially as the merger of two BH may be detectable as a source of gravitational waves (Portegies Zwart & McMillan (2000) and Banerjee et al (2010)). It has even been suggested that star clusters consisting almost entirely of BH, known as dark star clusters, could exist (Banerjee & Kropua, 2011). Dark star clusters could be created if the stars in the outer parts of a larger system were stripped away by a strong tidal field, leaving behind the BH sub-system. If one were to observe the few remaining stars in these systems they would appear to be super virial, as the velocity dispersion of the remaining stars would be enhanced by the unseen BH.

Breen & Heggie (2012a) investigated the evolution of two-component models and found that, within the parameter space they considered, the stability of the two-component system against gravothermal oscillations was dominated by the heavy component. They only considered systems with a total mass ratio of order $M_2/M_1 \gtrsim 10^{-1}$, where M_2 (M_1) is the total mass of the heavy (light) component. However the mass ratio of a system containing a BH sub-system would only be expected to be $M_2/M_1 \sim 10^{-2}$ (Portegies Zwart & McMillan, 2000), where M_2 is the total mass of the BH sub-system, which is smaller by an order of magnitude than any of the systems studied by Breen & Heggie (2012a). As Hénon's Principle (Hénon, 1975) states that the energy generating rate of the core is regulated by the bulk of the system, it seems unlikely that the approach of Breen & Heggie (2012a) is appropriate in this case due to the small value of M_2/M_1.

This chapter is structured as follows. In Section 4.3, some theoretical results are derived and discussed. This is followed by Section 4.4, where the theoretical results regarding the size of the BH sub-system are tested using both gas models and direct N-body runs. Section 4.5 contains empirical results regarding the mass loss rates from BH sub-systems and a comparison between the empirical results and the theory of Section 4.3. The qualitative behaviour of these systems is also discussed in this section. Section 4.6 is concerned with gravothermal oscillations in systems containing a BH sub-system. Finally Section 4.7 consists of the conclusions and a discussion.

4.3 Theoretical Understanding

4.3.1 BH sub-system: half-mass radius

Here we will consider aspects of the dynamics of a system containing a BH sub-system. We will assume that the system is Spitzer unstable (Spitzer, 1987) and that the total mass of the BH sub-system (M_2) is very small compared to the total mass of the system (M). (Since the Spitzer stability criterion is $(M_2/M_1)(m_2/m_1)^{\frac{3}{2}} < 0.16$, these assumptions are consistent provided the stellar mass ratio m_2/m_1 is large enough). We will also assume that the initial state of the system has a constant mass density ratio between the two components throughout and that the velocity dispersions of both components are equal at all locations. If this is the case then the system would first experience a mass segregation-dominated phase of evolution which lasts of order $(m_1/m_2)t_{\rm cc}$ (Fregeau et al, 2002, and references therein), where m_2 (m_1) is the stellar mass of the BH (other stars), and $t_{\rm cc}$ is the core collapse time in a single component

system, although technically for the outermost BH mass segregation can last much longer than $(m_1/m_2)t_{\rm cc}$ (see Appendix E for details).

If we consider the 50% Lagrangian shell of the heavy component, initially it will be approximately the same size as the 50% Lagrangian shell of the entire system. As the BH lose energy to the other stars in the system the 50% Lagrangian shell of the BH component contracts. The shell will continue to contract until the energy loss to the light component is balanced by the energy the shell receives from the inner parts of the BH component. As we have assumed that the system is Spitzer unstable, it follows that a temperature difference must remain between the two components and thus there is still a transfer of energy between the two components. As the total mass of BH is small, the contraction of the 50% Lagrangian shell of the heavy component continues until the system is concentrated in a small region in the centre of the system. This is what we call the BH sub-system. The BH sub-system is very compact and therefore rapidly undergoes core collapse. The subsequent generation of energy by the formation of BH binaries, and interactions of BH binaries with single BH, support the 50% Lagrangian shell of the heavy component.

In the present chapter, we will assume that the main pathway for the transport of thermal energy throughout the system is as follows: energy is generated in the core of the BH sub-system (we are assuming that the BH core radius is much smaller than $r_{\rm h,2}$, the half mass radius of the BH sub-system), then the energy is conducted throughout the BH sub-system via two-body relaxation just as in the conventional picture of post-collapse evolution; but in the standard one-component setting this flux causes expansion and, ultimately, dispersal of the system. In a two-component system, however, the coupling to the lighter component changes the picture dramatically. We will assume that at a radius comparable with $r_{\rm h,2}$ most of the energy flux is transferred into the light component, where it then spreads throughout the bulk of the light system. These assumptions will hold if most of the heating, either direct (heating by reaction products which remain in the cluster) or indirect, initially occurs within the BH sub-system rather than within the regions dominated by the light component (see Appendix D for a discussion on this issue). A similar assumption is made in one-component gas models (Goodman, 1987; Heggie & Ramamani , 1989) which have been shown to be in good agreement with direct N-body models (Bettwieser & Sugimoto, 1985).

From Hénon's Principle (Hénon, 1975) we argue that the rate of energy generation is regulated by the energy demands of the bulk of the system. For the systems we are considering here the bulk of the system is in the light component as $M_1 \approx 0.99M$ for $M_2/M_1 = 10^{-2}$. The energy demands of a system are normally thought of as the energy flux at the half-mass radius, which is of order $|E|/t_{\rm rh}$, where E is the total energy of the system and $t_{\rm rh}$ is the half mass relaxation time. Under our assumptions the energy flux must be supplied by the BH sub-system, which ultimately must be generated by binaries in the core of the BH sub-system. However, we can ignore the details of how the energy is actually generated and consider the BH sub-system itself as the energy source for the cluster as a whole. In this picture, the energy exchange ($\dot{E}_{\rm ex}$) between the BH sub-system and the light component must balance the flux at the half mass radius of the light component i.e.

$$\frac{|E|}{t_{\rm rh}} \sim |\dot{E}_{\rm ex}|.$$

The BH sub-system is concentrated in the centre of the cluster, and therefore the half-mass relaxation time in the BH sub-system ($t_{\rm rh,2}$) is quite short. It follows that the flux at the half-mass radius of the BH sub-system is quite high. The flux at the half-mass radius of the BH sub-system ($r_{\rm h,2}$) is of order $|E_2|/t_{\rm rh,2}$, where E_2 is the energy of the BH sub-system. Most of the energy that passes $r_{\rm h,2}$ must be transferred to the light component or else the BH sub-system would rapidly expand until the flux around $r_{\rm h,2}$ is comparable to the rate of energy exchange. Therefore the energy exchange rate between the two components must be approximately equal to the flux at the half mass radius of the heavy sub-system i.e.

$$\frac{|E_2|}{t_{\rm rh,2}} \approx |\dot{E}_{\rm ex}|.$$

All this leads to the conclusion that the flux at $r_{\rm h}$ must be balanced by the flux at $r_{\rm h,2}$ i.e.

$$\frac{|E|}{t_{\rm rh}} \sim \frac{|E_2|}{t_{\rm rh,2}},$$

which can be rearranged as

$$\frac{|E|}{|E_2|} \sim \frac{t_{\rm rh}}{t_{\rm rh,2}}. \tag{4.1}$$

Using the definition of $t_{\rm rh}$ as given in Spitzer (1987) (and an equivalent definition for $t_{\rm rh,2}$), the right hand side of equation 4.1 becomes

$$\frac{t_{\rm rh}}{t_{\rm rh,2}} \approx \frac{N^{\frac{1}{2}} r_{\rm h}^{\frac{3}{2}} m_2^{\frac{1}{2}} \ln\Lambda_2}{N_2^{\frac{1}{2}} r_{\rm h,2}^{\frac{3}{2}} m^{\frac{1}{2}} \ln\Lambda} = \frac{M^{\frac{1}{2}} r_{\rm h}^{\frac{3}{2}} m_2 \ln\Lambda_2}{M_2^{\frac{1}{2}} r_{\rm h,2}^{\frac{3}{2}} m \ln\Lambda}, \tag{4.2}$$

where m is the mean mass, and $\ln\Lambda$, $\ln\Lambda_2$ are the coulomb logarithms of the entirely system and the BH sub-system respectively.

Using equation 4.1, the left hand side of equation 4.2 becomes

$$\frac{|E|}{|E_2|} \approx \frac{M\sigma^2}{M_2\sigma_2^2} \approx \frac{M^2 r_{\rm h,2}}{M_2^2 r_{\rm h}}. \tag{4.3}$$

where we have estimated the squared one dimensional velocity dispersions, σ_2^2 and σ^2, by assuming that both the system and the sub-system are in virial equilibrium, so that $\sigma^2 \simeq 0.2GM/r_{\rm h}$ and $\sigma_2^2 \simeq 0.2GM_2/r_{\rm h,2}$. Putting the above equations together we have

$$\frac{M^2 r_{\rm h,2}}{M_2^2 r_{\rm h}} \sim \frac{M^{\frac{1}{2}} m_2 r_{\rm h}^{\frac{3}{2}} \ln\Lambda_2}{M_2^{\frac{1}{2}} m r_{\rm h,2}^{\frac{3}{2}} \ln\Lambda}$$

and then by rearranging this we have

$$\frac{r_{\rm h,2}^{\frac{5}{2}}}{r_{\rm h}^{\frac{5}{2}}} \sim \frac{M_2^{\frac{3}{2}}}{M^{\frac{3}{2}}} \frac{m_2}{m} \frac{\ln\Lambda_2}{\ln\Lambda}. \tag{4.4}$$

This result implies that for a fixed total mass ratio M_2/M_1 ($\approx M_2/M$) and ignoring the variation of the coulomb logarithms, the ratio of $r_{\rm h,2}/r_{\rm h}$ grows with increasing stellar mass ratio m_2/m.

4.3.2 BH sub-system: core radius

In Section 4.3.1 $r_{\rm h,2}/r_{\rm h}$ was estimated by assuming that the energy flow in the BH sub-system balances the energy flow in the bulk of the system (i.e. the other stars). In order for equation 4.4 to hold it is assumed that the BH core radius $r_{\rm c,2}$ must be significantly smaller than $r_{\rm h,2}$ and that the BH sub-system is actually capable of producing and supplying the energy required by the system. Usually it is assumed that the core (in this case the core of the BH sub-system) adjusts to provide the energy required. In this section we estimate the size of the core, and use the estimate to place a condition on the validity of our assumptions.

As most of the mass within $r_{\rm h,2}$ is BH, we may treat the BH sub-system as a one-component system and we can make use of the standard treatments of one-component systems. In balanced

evolution (i.e. a situation in which energy is produced at the rate at which it flows over the half-mass radius), the rate of energy production is given by $\dot{E} = (|E_2|/t_{\rm rh,2})\zeta_2$, where ζ_2 is a constant (for a one-component model $\zeta_2 \approx 0.0926$, see Hénon (1965)). We will follow the derivation in Heggie & Hut (2003, page 265) of the dependence of $r_{\rm c}/r_{\rm h}$ on N for a one component model, although here it will be necessary to keep track of the numerical constants and account for the fact that the properties correspond to those of the BH sub-system. In order to derive a condition on $r_{\rm c,2}/r_{\rm h,2}$ it is necessary to express $\dot{E}$, E_2 and $t_{\rm rh,2}$ in terms of the other properties of the BH sub-system. $\dot{E} \approx M_{\rm c,2}\epsilon$ where $M_{\rm c,2}$ is the BH core mass and ϵ is the energy generating rate per unit mass (Heggie & Hut, 2003). $M_{\rm c,2}$ and ϵ can be expressed in terms of $\rho_{\rm c,2}$ (the central mass density of BH), $r_{\rm c,2}$ and $\sigma_{\rm c,2}$ (the central one-dimensional velocity dispersion of the BH), which results in

$$\dot{E} = 85\frac{G^5 m_2^3 \rho_{\rm c,2}^3 r_{\rm c,2}^3}{\sigma_{\rm c,2}^7}.$$

As in the previous section we shall use

$$|E_2| \approx 0.2\frac{GM_2^2}{r_{\rm h,2}}.$$

It will be convenient to use a different but equivalent definition of $t_{\rm rh,2}$ (Spitzer, 1987) rather than the one used in the previous section, i.e.

$$t_{\rm rh,2} = \frac{0.195\sigma_2^3}{Gm_2\rho_{\rm h,2}\ln\Lambda_2},$$

where σ_2 is the one-dimensional velocity dispersion of the BH inside $r_{\rm h,2}$ and $\rho_{\rm h,2}$ is the mean mass density of the BH inside $r_{\rm h,2}$.

Using $\dot{E} = (|E_2|/t_{\rm rh,2})\zeta_2$ all of the above equations can be combined into

$$83G^2 m_2^2 \rho_{\rm c,2}^3 \sigma_2^3 r_{\rm c,2}^3 r_{\rm h,2} \approx M_2^2 \sigma_{\rm c,2}^7 \rho_{\rm h,2}\zeta_2 \ln\Lambda_2.$$

This can be simplified by using $4\pi G\rho_{\rm c,2}r_{\rm c,2}^2 = 9\sigma_{\rm c,2}^2$. Also the BH sub-system is expected to be nearly isothermal inside $r_{\rm h,2}$; therefore $\sigma_2 \approx \sigma_{\rm c,2}$ and furthermore it follows that $\rho_2 \propto r^{-2}$ inside $r_{\rm h,2}$. Taking all of this into account and by rearranging the above we have

$$\frac{r_{\rm c,2}}{r_{\rm h,2}} \approx N_2^{-\frac{2}{3}}\left(\frac{104}{\zeta_2\ln\Lambda_2}\right)^{\frac{1}{3}}. \tag{4.5}$$

4.3.3 Limitations of the theory

One of our assumptions was that $r_{\rm c,2} \ll r_{\rm h,2}$ and now we can derive an approximate condition for the validity of the theory. As N_2 is small we shall take $\ln\Lambda_2 \approx 1$. As the entire system is in balanced evolution it is also true that $(|E_2|/t_{\rm rh,2})\zeta_2 = (|E|/t_{\rm rh})\zeta$, where ζ is a dimensionless parameter defined implicitly by the equation $\dot{E} = (|E|/t_{\rm rh})\zeta$; we expect $|E_2|/t_{\rm rh,2} \sim |E|/t_{\rm rh}$ (equation 4.1) and so for the purposes of our estimate we can assume that $\zeta_2 \approx \zeta$. Therefore $r_{\rm c,2} \lesssim r_{\rm h,2}$ provided $N_2 \gtrsim 40$. This value is only a rough guide, and what is important to take from this result is that for sufficiently small N_2 the theory in Section 4.3.1 breaks down.

As M_2 decreases the BH sub-system will ultimately reach a point where it can no longer solely power the expansion of the system by the mechanism we have considered (i.e. formation, hardening and ejection of BH binaries by interaction amongst the BH sub-system). After this point it may be possible for BH binaries to generate the required energy through strong interaction with the light stars. However this will probably require a much higher central mass density of the light component than at the time of formation of the BH sub-system, as at this central mass density interactions between the light stars and the BH binaries are expected to be much less efficient at generating energy than interactions between single BH and BH binaries. This implies a potentially significant adjustment phase towards the end of the life of the BH sub-system, as is illustrated by an N-body model in Section 4.5 (see Fig. 4.7).

In Section 4.3.1 we made the assumption that the BH sub-system was Spitzer stable. How-

ever, as pointed out to us by Sambaran Banerjee (private communication), it is also possible that as M_2 decreases a point may be reached were the sub-system becomes Spitzer stable. If so, the two components could reach equipartition at the centre, i.e. $m_2\sigma_2^2 = m_1\sigma_1^2$, and in that case our assumption that heat flows from the heavy component to the light component is false. The temperature ratio of the two component may be estimated by

$$\frac{m_2\sigma_2^2}{m_1\sigma_1^2} \sim \frac{m_2}{m_1}\frac{M_2}{M_1}\frac{r_{\rm h}}{r_{\rm h,2}} \sim \big(\frac{m_2}{m_1}\big)^{\frac{3}{5}}\big(\frac{M_2}{M_1}\big)^{\frac{2}{5}}\big(\frac{\ln\Lambda_2}{\ln\Lambda}\big)^{-\frac{2}{5}},$$

were we have made use of equation 4.4 and the assumptions made in Section 4.3.1. Initially $(m_2\sigma_2^2)/(m_1\sigma_1^2) > 1$ but for fixed m_2/m_1 it decreases towards equipartition ($(m_2\sigma_2^2)/(m_1\sigma_1^2) = 1$) as BH escape and M_2 decreases. By setting $(m_2\sigma_2^2)/(m_1\sigma_1^2) = 1$, ignoring the variation of coulomb logarithms and taking each side to the power 2/5 we arrive at

$$\frac{M_2}{M_1} \sim C\big(\frac{m_2}{m_1}\big)^{-\frac{3}{2}}$$

where C is a constant. This is exactly the same form as the Spitzer stability criterion (Spitzer, 1987), the only difference being that we have not specified the constant C. Again it follows that the theory of Sections 4.3.1 and 4.3.2 will fail when M_2 becomes too small, and that the limiting value of M_2 is smaller for larger m_2/m_1.

We will now briefly consider the case of a Spitzer stable BH sub-system. As the BH move more slowly than the other stars they still concentrate in the centre of the system. If the heavy component still dominates within $r_{\rm h,2}$ then the BH sub-system is self-gravitating and

$$\sigma_2^2 \sim \frac{GM_2}{r_{\rm h,2}}$$

still holds. From equipartition of kinetic energy we have

$$\frac{m_1}{m_2}\sigma_1^2 \sim \frac{m_1}{m_2}\frac{GM}{r_{\rm h}} \sim \frac{GM_2}{r_{\rm h,2}}.$$

This result can be rearranged as

$$\frac{r_{\rm h,2}}{r_{\rm h}} \sim \frac{m_2}{m_1}\frac{M_2}{M}. \tag{4.6}$$

In equation 4.6 there is a different dependence of $r_{\rm h,2}/r_{\rm h}$ on m_2/m_1 and M_2/M than in equation 4.5.

4.3.4 Evaporation rate

We will now consider the evaporation rate as a result of two-body encounters for the BH sub-system. It is important to note that evaporation is only one of the mechanisms by which BH are removed from the system. Another important mechanism as already discussed is ejection via encounters involving BH binaries and single BH. In this section we will ignore this effect although it will be considered in detail in the next section.

The one dimensional velocity dispersion of the BH sub-system has the following dependence on M_2 and $r_{\rm h,2}$ (assuming it is nearly self gravitating):

$$\sigma_2^2 \sim \frac{GM_2}{r_{\rm h,2}}.$$

From the previous section we know that $\big(\frac{r_{\rm h,2}}{r_{\rm h}}\big)^{\frac{5}{2}} \sim \frac{M_2^{\frac{3}{2}}}{M^{\frac{3}{2}}}\frac{m_2}{m}\frac{\ln\Lambda_2}{\ln\Lambda}$. Therefore, if we consider the post collapse evolution of a series of models with different values of m_2/m, at the same values of $r_{\rm h}$, M_2 and M, as m_2/m increases so does $r_{\rm h,2}$ and therefore σ_2^2 decreases. Here we have ignored the variation of the coulomb logarithms; for a system with $N = 10^6$ and $M_2/M_1 = 10^{-2}$, the

variation of $\ln\Lambda_2/\ln\Lambda$ is a factor of 2.2 between $m_2/m_1 = 10$ and 50 if $\Lambda_2 = 0.02N_2$ and $\Lambda = 0.02N$. **The source of the value** 0.02 **is Giersz & Heggie (1996).**

The mean-square escape velocity is related to the mean-square velocity of the system (see Spitzer (1987) and Binney & Tremaine (2008)) by $v_{\rm e}^2 = 4v^2$. The mean-square velocity of the system is dominated by the light component and remains approximately fixed with varying m_2/m. Therefore, as m_2/m increases the mean-square velocity of the BH sub-system decreases relative to the mean-square escape velocity. This implies that systems with higher m_2/m lose a lower fraction of their stars by evaporation per $t_{\rm rh,2}$; in fact we will show in the next paragraph that escape via evaporation is negligible.

A rough estimate of the fraction of stars lost by evaporation each $t_{\rm rh}$ can be calculated from the Maxwellian velocity distribution (Spitzer, 1987; Binney & Tremaine, 2008). This is done by assuming that the fraction of stars with v greater than $v_{\rm e}$ in a Maxwellian velocity distribution is removed each $t_{\rm rh}$, i.e.

$$\frac{dN}{dt} = -\frac{N}{t_{\rm rh}}\gamma,$$

where γ denotes the fraction of stars removed. Its value for a one component model is $\gamma = 7.38\times10^{-3}$. In order to estimate the value of γ for a two component model we need to know the relationship between v_2^2 and v_1^2, where v_2^2 (v_1^2) is the mean-square velocity of the heavy (light) component. If the system was Spitzer stable then $m_2v_2^2 = m_1v_1^2$; however the systems we are considering are not Spitzer stable because of the large stellar mass ratios, and therefore it is expected that $m_2v_2^2 > m_1v_1^2$. Over a period of time where M_2 and $r_{\rm h}$ remain roughly constant then v_2^2 and v_1^2 will be approximately constant. Therefore over the same time period we have $m_2v_2^2 \approx km_1v_1^2$, where k is a constant. Using a two-component gas model (see Heggie & Aarseth (1992) and Breen & Heggie (2012a)), for the range of parameters in Section 4.4, k was found to be ≤ 2. Assuming a stellar mass ratio of 10 and letting $k = 2$ to insure the highest possible value of γ leads to $\gamma = 5.87\times10^{-13}$. This exceedingly small value of γ is a result of the fact that the Maxwellian velocity distribution drops exponentially with increasing velocity, so that even a slight increase in escape velocity leads to a much smaller value of γ.

Based on this approximate theory we can conclude that mass loss from evaporation due to two body encounters is not significant for the case of BH sub-systems. It is worth noting (based on the arguments in this section) that constraints based on evaporation timescales (for example see Maoz, 1998) which only take into consideration the potential of the BH sub-system are not generally valid if the sub-system is embedded in a much more massive system. BH which escape the sub-system in two-body encounters generally cannot escape from the deep potential well of the surrounding system. Instead, they return to the sub-system on the mass segregation/dynamical friction timescale.

4.3.5 Ejection rate

Dynamical evolution of BH binaries and ejection of BH is an energy source which is assumed in the present chapter to comply with Hénon's Principle. As has been stated in Section 4.3.1, Hénon's Principle states that $\dot{E}$ is regulated by the energy demands of the bulk of the system, i.e.

$$\dot{E} \simeq \frac{|E|}{t_{\rm rh}}\zeta, \tag{4.7}$$

where ζ is a constant. For systems with $M_2 \ll M$, $(|E|/t_{\rm rh})\zeta$ is determined mainly by the properties of the light component and is approximately independent of M_2 and m_2. Therefore the energy generation rate is also approximately independent of M_2 and m_2.

The encounters which generate energy (either by formation of binaries or their subsequent harding) happen where the density is highest, in the core of the BH sub-system. As the BH are concentrated in the centre of the system, through mass segregation, we may assume that encounters which generate energy predominantly occur between BH binaries and single BH. The BH sub-systems considered in this chapter consist of BH with identical stellar mass, therefore

the mechanism by which energy is generated in the BH sub-systems is similar to that for a one-component system. The two key differences for the BH sub-system are that the escape potential is elevated and the size of the system is regulated by the much more massive system of light stars (see equation 4.4).

In a one-component system each hard binary formed in the core on average contributes a fixed amount of energy $\propto m\phi_c$ (where ϕ_c is the central potential) before being ejected from the system (see for example Heggie & Hut, 2003). Typical estimates of the average energy each hard binary contributes in a one component system are $\approx 7.5m\phi_c$ (Goodman, 1984) and $\approx 8.27m\phi_c$ (Heggie & Hut, 2003)[1]. Also on average each hard binary causes the ejection of a fixed number of stars. Goodman (1984) estimated this to be approximately 6 stars (including the binary itself) and Heggie & Hut (2003) estimated this to be approximately 3 stars (excluding the binary itself). The situation is similar for a BH sub-system and we can assume that the mass ejected and the average contribution per hard BH binary is the same as for the one-component case. Furthermore as mass loss due to evaporation is negligible for a BH sub-system (see Section 4.3.4), the loss of mass from the sub-system is always associated with energy generation. Therefore we can express the rate of energy generation in the core in terms of mass loss,

$$\dot{E} \approx \beta \dot{M}_2 \phi_c, \tag{4.8}$$

where β is a constant; $\beta \approx 2.2$ in the one component case, where we have used the values of energy generated and mass lost given in Heggie & Hut (2003), adjusted to account for the energy generated and mass lost in the escape of the binary itself, $\approx 10.6m_2\phi_c$ and $\approx 4.7m_2$ receptively. Since $\dot{E}$ is regulated by the light component (equation 4.7), we can use equation 4.8 to estimate the rate of mass loss. Note that the estimates in this paragraph are entirely theoretical, without detailed numerical support especially for the value of β. Note also that the estimate ignores the heating effect of encounters which do not lead to ejection once the binary has reached a sufficient binding energy for ejection to be likely.

We will now show that ϕ_c is approximately independent of the properties of the BH sub-system. This will be done by showing that the main contribution to the central potential is from the light component. We can estimate the contribution of the lights to ϕ_c to be $\phi_1 \approx -GM/r_h$ and the contribution of the BH to be $\phi_2 \approx -GM_2/r_{h,2}$. In the regime of interest $M_2/M = 10^{-2}$ and $r_{h,2}/r_h = 10^{-1}$ (for typical values of $r_{h,2}/r_h$: see Table 4.1). Therefore,

$$\frac{\phi_2}{\phi_1} \approx \frac{M_2}{M}\frac{r_h}{r_{h,2}} \approx 10^{-1},$$

and we can approximate ϕ_c by ϕ_1 (see also Section 4.4.3).

We can now use $\dot{E} \approx \beta \dot{M}_2 \phi_c$ to make an estimate of the mass loss rate: from equations 4.7 and 4.8 we have

$$\beta \dot{M}_2 \phi_c \simeq \frac{|E|}{t_{rh}}\zeta,$$

and so

$$\dot{M}_2 \simeq M\frac{|E|}{M\phi_c}\frac{1}{t_{rh}}\frac{\zeta}{\beta}.$$

The term $E/(M\phi_c)$ is dimensionless and approximately independent of the properties of the BH sub-system; we will use α to represent its value. For a Plummer model $\alpha \approx 0.15$, however during core collapse $|\phi_c|$ increases while E and M remain approximately constant, resulting in smaller values of α. The two-component gas models used in Section 4.4 indicate a value of $\alpha \approx 0.13$. We now have

$$\dot{M}_2 \simeq -\frac{M}{t_{rh}}\frac{\alpha\zeta}{\beta} \tag{4.9}$$

[1]Note there is an error in Heggie & Hut (2003) p. 225: the constant is stated incorrectly but the correct value can be obtained by evaluating the formula given on the same page.

Scaling to the values of α, ζ and β, we have

$$\dot{M}_2 \simeq -0.0061 \frac{M}{t_{\rm rh}} \frac{\alpha}{0.15} \frac{\zeta}{0.09} \frac{2.2}{\beta}. \tag{4.10}$$

By this estimate the sub-system should last $\sim 1.6 t_{\rm rh}$ to $3.3 t_{\rm rh}$, for $M_2/M_1 = 0.01$ to 0.02 and canonical values of α, β and ζ. The important point to take from this result is that the rate of mass loss from the BH sub-system depends on the half-mass relaxation time of the whole system and not on any property of the BH sub-system.

While a system is in balanced evolution, the only parameter that varies significantly (over a timescale where $\dot{M}$ is negligible) in the right hand side of the above equation is $t_{\rm rh}$, due to the increase in $r_{\rm h}$ (Here we assume that the system is isolated; the case of a tidally limited system is considered in the following section.). Therefore, for a particular system equation 4.10 can be expressed in the form $\dot{M}_2 \simeq -C r_{\rm h}^{-\frac{3}{2}}$, where C is a constant ($C = \frac{\alpha\zeta}{\beta} \frac{M r_{\rm h,i}^{\frac{3}{2}}}{t_{\rm rh,i}}$ where $\alpha\zeta/\beta \approx 6.1 \times 10^{-3}$ for canonical values of α, β, and ζ and i denotes values at the start of the balanced evolution). $r_{\rm h}$ itself is a function of time which can be derived from the relation $\dot{r}_{\rm h}/r_{\rm h} = \zeta/t_{\rm rh}$, which follows in turn from equation 4.7 if we assume $E \propto GM^2/r_{\rm h}$ and we assume mass loss from the entire system is negligible. Since $t_{\rm rh} \propto r_{\rm h}^{\frac{3}{2}}$ it follows that $r_{\rm h} \simeq r_{\rm h,i}\big(1 + \frac{3\zeta}{2t_{\rm rh,i}}(t - t_{\rm cc})\big)^{\frac{3}{2}}$, where powered expansion starts at time $t_{\rm cc}$ (the reason for this notation will become clear in Section 4.5). Therefore $\dot{M}_2$ can be expressed as

$$\dot{M}_2 \simeq -\frac{C r_{\rm h,i}^{-\frac{3}{2}}}{1 + \frac{3\zeta}{2t_{\rm rh,i}}(t - t_{\rm cc})} \tag{4.11}$$

and if we integrate the above equation we get

$$M_2 \simeq M_{2,\rm i} - \frac{2}{3}\frac{\alpha}{\beta} M \ln\big(1 + \frac{3\zeta}{2t_{\rm rh,i}}(t - t_{\rm cc})\big). \tag{4.12}$$

Throughout this section it has been assumed that ζ is a constant. However, as discussed in Section 4.5, ζ has been found to vary with time in situations where the BH sub-system cannot provide enough energy for balanced evolution. Even if ζ is time-dependent equation 4.9 and the equation

$$\frac{1}{r_{\rm h}}\dot{r}_{\rm h} = \frac{1}{t_{\rm rh}}\zeta,$$

are still expected to hold (under the other assumptions made in this section). These two equations can be combined into a single equation which relates $\dot{M}_2$ to $\dot{r}_{\rm h}$ and has no explicit ζ dependence (i.e. $\dot{M}_2 = -M\frac{\alpha}{\beta}\frac{1}{r_{\rm h}}\dot{r}_{\rm h}$). The resulting equation can be easily solved (assuming that the variation of M and α/β are neglected) and its solution is

$$M_2 = M_{2,\rm i} - M\frac{\alpha}{\beta}\ln\frac{r_{\rm h}}{r_{\rm h,i}}. \tag{4.13}$$

This result implies that, regardless of ζ, systems with the same $M_{2,\rm i}$ and $r_{\rm h,i}$ should evolves along the same curve in M_2, $r_{\rm h}$ space.

4.3.6 Tidally limited systems

In this section we will briefly consider the theory of tidally limited systems containing BH sub-systems. In Hénon's tidally limited model (Hénon, 1961), the rate of mass loss is

$$\dot{M} = -\frac{M}{t_{\rm rh}}\xi \tag{4.14}$$

where ξ is a constant ($\xi = 0.045$). In Section 4.3.5 an equation of the same form was found for $\dot{M}_2$, i.e.

$$\dot{M}_2 = -\frac{M}{t_{\rm rh}}\frac{\alpha\zeta}{\beta}.$$

The relation between $\dot{M}$ and $\dot{M}_2$ can be found by simply dividing these two equations, which results in

$$\frac{\dot{M}_2}{\dot{M}} = \frac{\alpha\zeta}{\beta\xi} = 0.11\frac{\alpha}{0.15}\frac{\zeta}{0.0725}\frac{2.2}{\beta}\frac{0.045}{\xi}.$$

Therefore $\dot{M}_2/\dot{M}$ is a constant. For canonical values of the constants in the above equation $\dot{M}_2/\dot{M} \approx 0.11$. Note that the tidally limited model has a different value of ζ ($\zeta = 0.0725$, see Hénon 1961) than for an isolated model ($\zeta = 0.0926$, see Hénon 1965). The constant value of $\dot{M}_2/\dot{M}$ implies that for two-component systems there is a threshold value of M_2/M_1 at $\sim 10^{-1}$ above which M_2/M (and hence M_2/M_1) is expected to grow with time and below which M_2/M decreases with time. In other words if $M_2/M_1 \gtrsim 10^{-1}$ then the system is expected to become more BH dominated, ultimately becoming a so-called dark star cluster (Banerjee & Kropua, 2011). Alternatively if $M_2/M_1 \lesssim 10^{-1}$ then the BH sub-system is expected to dissolve. In Section 4.7.3, where two-component parameter space is classified into different regions (see Fig. 4.16), there is already a distinction at roughly $M_2/M_1 \sim 10^{-1}$ (between region II & III systems), based on other reasons discussed in that section. The theory in this section can be viewed as another reason for the distinction.

It is important to note that this result has yet to be rigorously tested because tidally limited systems are not considered further in this chapter and the exact threshold value is likely to depend on a number of astrophysical issues (e.g. initial mass function, tidal shocks etc). Indeed while equation 4.14 is a reasonable approximation, Baumgardt (2001) showed that the time scale of escape depends on both $t_{\rm rh}$ and the crossing time. Nevertheless it seem likely that a threshold value of M_2/M_1 exists even for more realistic systems, although it may have some dependence on the other properties of the system (e.g. m_2/m_1).

4.4 Dependence of $r_{\rm h,2}/r_{\rm h}$ on cluster parameters

4.4.1 Gas models

The aims of Sections 4.4.1 and 4.4.2 are to test the dependence of $r_{\rm h,2}/r_{\rm h}$ on the cluster parameters and compare the results with the theory presented in Section 4.3.1. The simulations in this section (4.4.1) were run using a two-component gas code (see Heggie & Aarseth (1992) and Breen & Heggie (2012a)). In all cases, the initial conditions used were realisations of the Plummer model (Plummer, 1911; Heggie & Hut, 2003). The initial velocity dispersion of both components and the initial ratio of density of both components were equal at all locations. The choices for the ratio of stellar masses (m_2/m_1) are 2, 5, 10, 20, 50 and 100. The values of the total mass ratio (M_2/M_1) used in this section are 0.5, 0.1, 0.05, 0.02 and 0.01, though the first two values are outside the parameter space of interest in most of the present chapter. The value of $r_2/r_{\rm h}$, which was found to be approximately constant during the post collapse phase of evolution (see Fig. 4.1), was measured for the series of models and is given in Table 4.1.

The results in Table 4.1 are plotted in Fig. 4.2. As can be seen in Fig. 4.2 (and Table 4.1) the results are in qualitative agreement with the theory in Section 4.3.1, in the sense that for $M_2/M_1 < 0.1$ there is an increase in the values of $r_{\rm h,2}/r_{\rm h}$ with increasing m_2/m_1. For $M_2/M_1 = 0.5$ the trend is qualitatively different than for $M_2/M_1 < 0.1$; there is an increase in the values of $r_{\rm h,2}/r_{\rm h}$ with decreasing m_2/m_1. The theory in Section 4.3.1 cannot be expected to apply in this regime, as the light component does not dominate. In this regime the decrease of $r_{\rm h,2}/r_{\rm h}$ with m_2/m_1 can be explained qualitatively by the fact that if the BH have larger stellar masses then there is a stronger tendency towards mass segregation (see Breen & Heggie (2012a) for a discussion of this topic).

We now consider the comparison with theory more quantitatively in the regime $M_2/M_1 \lesssim 0.1$. In Fig. 4.2 we can see that values of $r_{\rm h,2}/r_{\rm h}$ are also in *quantitative* agreement with

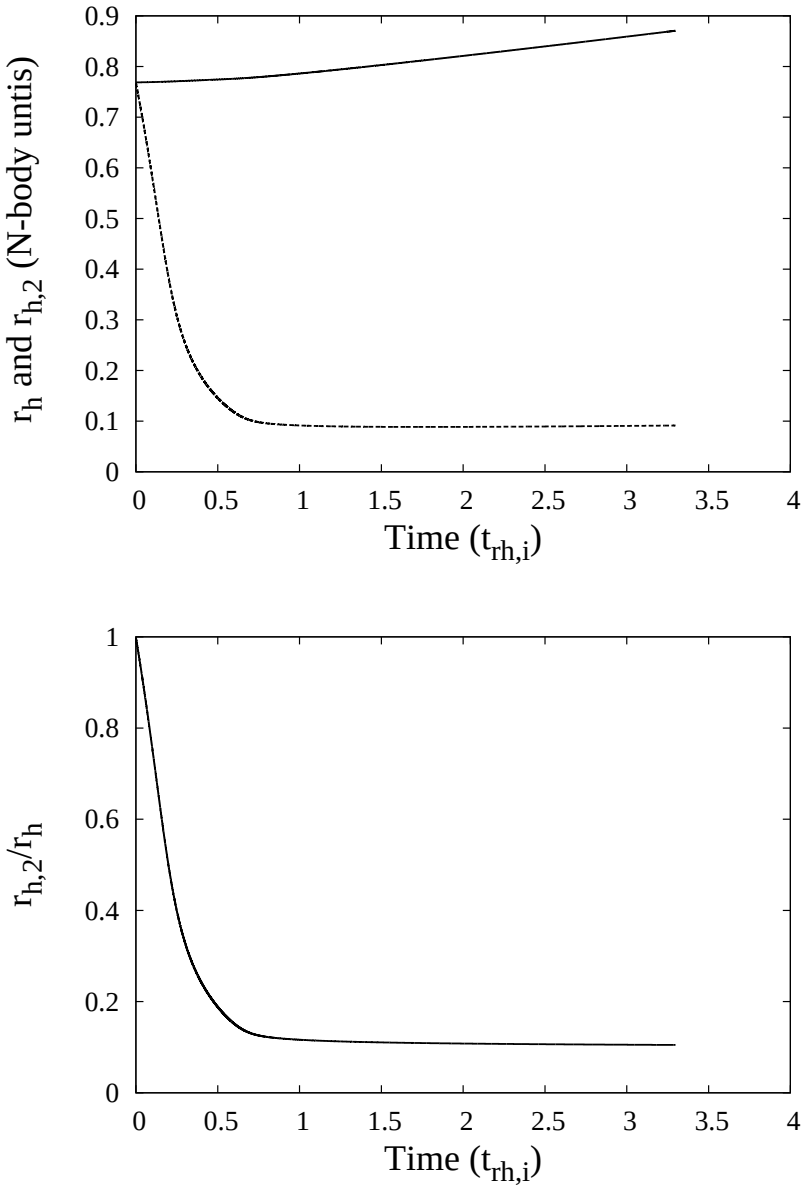

Figure 4.1: Top: $r_{\rm h}$ (top line) and $r_{\rm h,2}$ (bottom line) vs time (units $t_{\rm rh,i}$) of gas models with $N = 32k$, $m_2/m_1 = 10$ and $M_2/M_1 = 0.02$. $r_{\rm h}$ and $r_{\rm h,2}$ are given in N-body units. Initially $r_{\rm h}$ and $r_{\rm h,2}$ have the same value, but mass segregation quickly decreases $r_{\rm h,2}$, after which it reaches an approximately steady value. Bottom: $r_{\rm h,2}/r_{\rm h}$ vs time (units $t_{\rm rh,i}$). Core collapse (see Section 4.3.1) occurs at $\approx 1 t_{\rm rh,i}$; shortly before this $r_{\rm h,2}/r_{\rm h}$ reaches a nearly constant value.

Table 4.1: Values of $r_{\rm h,2}/r_{\rm h}$ in post collapse evolution ($N = 32k$). These values where measured over $1t_{\rm rh,i}$ after a time of at least $2t_{\rm cc}$, where $t_{\rm cc}$ is the time of core collapse. For low M_2/M_1 (< 0.1) there is a clear trend of increasing $r_{\rm h,2}/r_{\rm h}$ with increasing m_2/m_1. The total mass ratios of 0.5 and 0.1 have also been included to demonstrate that there is an inverse dependence of $r_{\rm h,2}/r_{\rm h}$ on m_2/m_1 for the largest value of M_2/M_1 considered. See text for more details.

$\frac{m_2}{m_1} \backslash \frac{M_2}{M_1}$	**0.5**	**0.1**	**0.05**	**0.02**	**0.01**
100	0.37	0.34	0.29	0.24	0.21
50	0.38	0.27	0.24	0.19	0.18
20	0.40	0.21	0.18	0.15	0.13
10	0.42	0.18	0.14	0.11	0.09
5	0.44	0.18	0.11	0.07	0.04
2	0.50	0.20	0.10	0.03	0.02

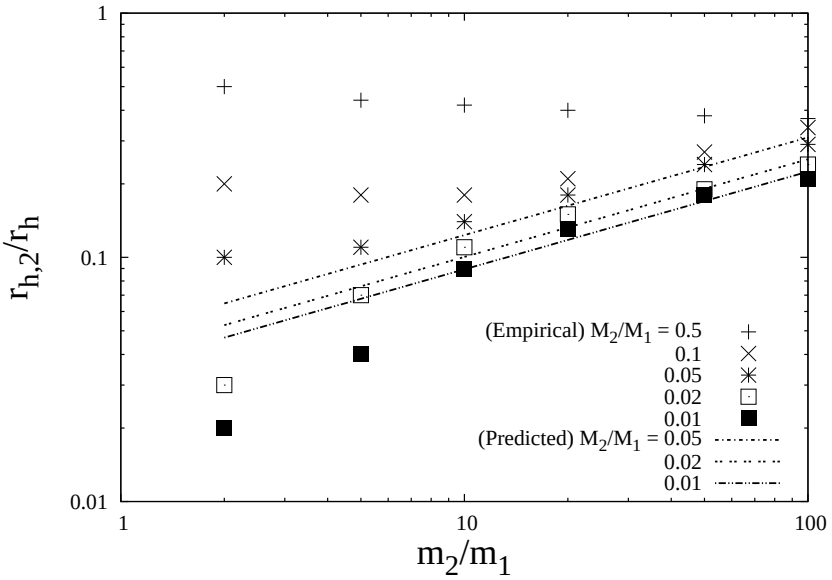

Figure 4.2: The variation of $r_{\rm h,2}/r_{\rm h}$ with m_2/m_1. The points represent the values of $r_{\rm h,2}/r_{\rm h}$ given in Table 4.1. The lines represent the expected variation of $r_{\rm h,2}/r_{\rm h}$ with m_2/m_1 (fitted curves of the form $b(m_2/m_1)^{0.4}$) as given by the theory in Section 4.3.1. The lines have only been included for $M_2/M_1 < 0.1$ as this is where the theory is expected to apply. The empirical measured variation of $r_{\rm h,2}/r_{\rm h}$ with m_2/m_1 is in good agreement with theory in Section 4.3.1, when $m_2/m_1 \gtrsim 10$ and $M_2/M_1 < 0.1$. See text for further details.

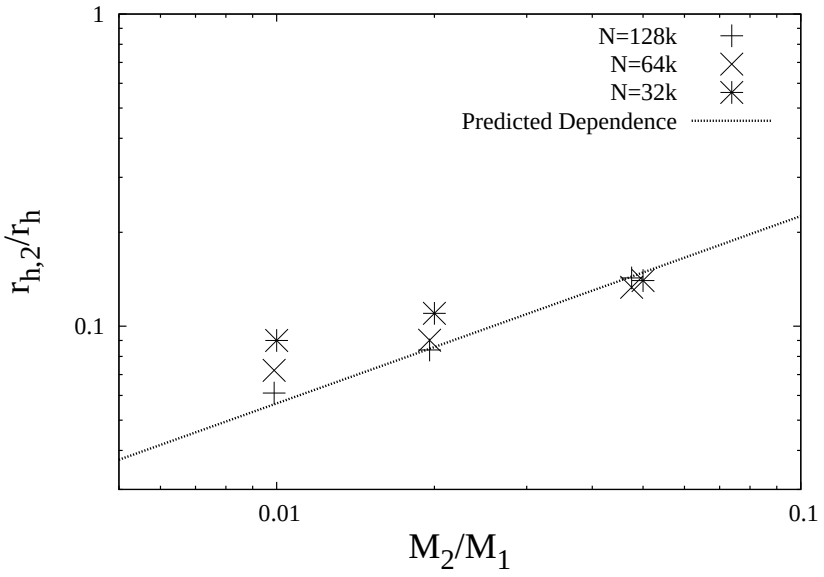

Figure 4.3: The variation of $r_{\rm h,2}/r_{\rm h}$ with M_2/M_1. The points represent the values of $r_{\rm h,2}/r_{\rm h}$ for the case $m_2/m_1 = 10$ with $N = 32k$, $N = 64k$ and $N = 128k$. The line represents the expected variation of $r_{\rm h,2}/r_{\rm h}$ with M_2/M_1 as given by the theory in Section 4.3.1.

equation 4.4 for $m_2/m_1 \gtrsim 10$ in the sense that the power law index is approximately confirmed. However $r_{\rm h,2}/r_{\rm h}$ increases more rapidly then is expected by equation 4.4 for $m_2/m_1 < 10$ and $M_2/M_1 < 0.05$. This behaviour is possibly explained by equation 4.6, which predicts a different power law index for Spitzer stable systems than in equation 4.4. Indeed for the lowest values of M_2/M_1 the slope is approximately consistent with equation 4.6. Nevertheless the stellar mass ratios of interest are $m_2/m_1 \gtrsim 10$ as realistic ratios for systems containing BH sub-systems would be in this range.

The variation of $r_{\rm h,2}/r_{\rm h}$ with M_2/M_1 over a range of different N is shown in Fig. 4.3, for the case of $m_2/m_1 = 10$. For the case of $N = 32k$ the variation is less than expected from equation 4.4 (see Section 4.3.1). The variation is approximately of the same form, i.e. $r_{\rm h,2}/r_{\rm h} \propto (M_2/M_1)^a$, but $a \approx 0.3$ for the case of $m_2/m_1 = 10$ and $N = 32K$, which is less than the expected value of $a \simeq 0.6$. (Here we ignore the dependence on the Coulomb logarithms). The variation of $r_{\rm h,2}/r_{\rm h}$ with M_2/M_1 comes into better agreement with equation 4.4 with increasing N, with the case of $N = 128k$ being in good agreement with the theory in Section 4.3.1. This seems to indicate that the disagreement is caused by small values of N_2. One of the assumptions under which equation 4.4 is derived is that $r_{\rm c} \ll r_{\rm h,2}$, but it is possible that $r_{\rm c,2} \approx r_{\rm h,2}$ for small N_2 as shown in equation 4.5. In this case one of the assumptions underlying the theory is not satisfied.

4.4.2 $r_{\rm h,2}/r_{\rm h}$ in N-body runs

In Section 4.3.1 it was predicted that $r_{\rm h,2}/r_{\rm h}$ would increase with increasing m_2/m_1 in a system with fixed M_2/M_1 and N. This prediction will now be tested with direct N-body runs (see Section 4.5). The initial conditions are realisations of the Plummer Model with $N = 64k$, $M_2/M_1 = 0.02$ and two different values of m_2/m_1 (10 and 20). We have compared the values of $r_{\rm h,2}/r_{\rm h}$ in Fig. 4.4. The value of $r_{\rm h,2}/r_{\rm h}$ is indeed larger for $m_2/m_1 = 20$ than for $m_2/m_1 = 10$ as expected. This effect was confirmed using a two-component gas code in the previous subsection. However mass is conserved in the gas models whereas in the more realistic N-body systems mass is lost over time. Therefore we need to ensure that we are comparing the values of $r_{\rm h,2}/r_{\rm h}$ for both the runs at constant M_2/M_1. For the two runs in Fig. 4.4 mass is lost from the BH sub-system at approximately the same rate (see Fig.4.11, bottom), as predicted by the theory in Section 4.3.5. The mass loss from the light component is negligible over the length of these

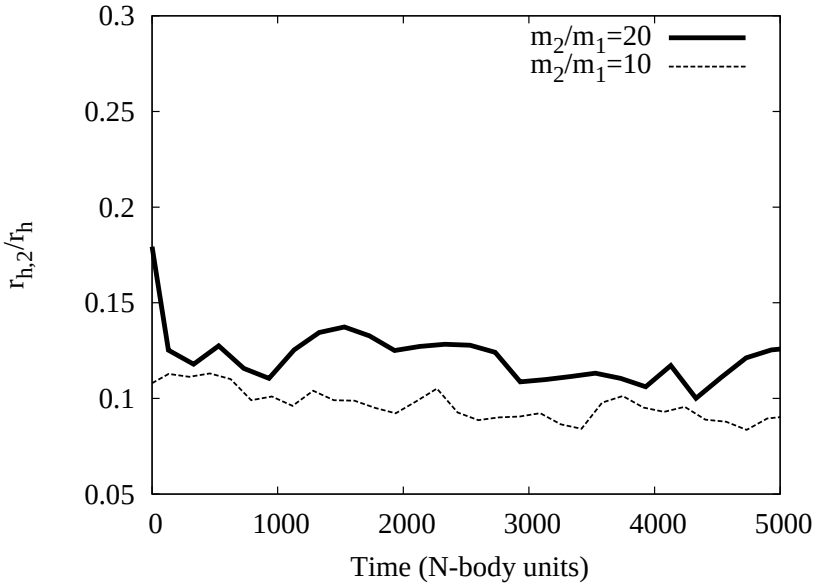

Figure 4.4: $r_{\rm h,2}/r_{\rm h}$ vs time (in N-body units). N-body runs with initial values $N = 64k$, $M_2/M_1 = 0.02$, $m_2/m_1 = 20$ (thick line) and $m_2/m_1 = 10$ (thin line). Time is set so that core collapse occurs at $t = 0$ for both systems. $r_{\rm h,2}/r_{\rm h}$ has been smoothed to make the plot clearer. The values of $r_{\rm h,2}/r_{\rm h}$ in the graph are in approximate agreement with the results from the two-component gas model given in Table 4.1.

N-body runs: less than 5% of the light component is lost during the entire run. Therefore while M_2/M_1 does decrease with time over the runs in Fig. 4.4, the values of M_2/M_1 for both runs are approximately the same at any given time.

The variation of $r_{\rm h,2}/r_{\rm h}$ with M_2/M_1 is shown in Fig. 4.5 for the N-body run with $N = 64k$, $m_2/m_1 = 10$ and $M_2/M_1 = 0.02$. Initially $r_{\rm h,2}/r_{\rm h} = 1$ before being quickly reduced due to mass segregation. The BH sub-system starts producing energy when $r_{\rm h,2}/r_{\rm h}$ reaches ≈ 0.1 and M_2/M_1 begins to decrease at this point. The variation of $r_{\rm h,2}/r_{\rm h}$ with M_2/M_1 is again less then expected from equation 4.4, with the result indicating a dependence of $r_{\rm h,2}/r_{\rm h} \propto (M_2/M_1)^{0.28}$. Although this is not in agreement with equation 4.4 if we neglect the coulomb logarithm, the results are in good agreement with the gas model.

4.4.3 Central potential

In section 4.3.5 we made the assumption that the main contribution to the central potential is from the light component. In order to test this assumption the central potential and the relative contribution of each component to the central potential (ϕ_2/ϕ_1), have been measured in a series of two-component gas models with $M_2/M_1 = 0.02$. These results are presented in Table 4.2. The values in Table 4.2 were measured once the systems had reached a certain value of $r_{\rm h}$ ($r_{\rm h} = 0.83$). This was done in order to insure the systems had reached a similar point in their evolution (see Fig. 4.6). The variation in $\phi_{\rm c}$ in Table 4.2 is only about a factor of 1.2 for fixed N even though m_2/m_1 varies by a factor of 5. The variation in ϕ_2/ϕ_1 is higher, but the values are of the same order of magnitude as the estimate in Section 4.3.5 and indeed in satisfactory agreement, considering that M_2/M_1 is higher here. As the energy generation rate per unit mass is $\propto m_2^3\rho_2^2/\sigma_2^7$ (Heggie & Hut, 2003), for systems with the same value of N, M_2/M_1 and m_1, as m_2 increases the system can produce the required energy at a lower central density, thus the central potential is expected to becomes shallower with increasing m_2/m_1 as seen in Table 4.2. This is also why two-component systems with larger m_2/m_1 are stable against gravothermal oscillation to higher values of N then for lower m_2/m_1 (Breen & Heggie, 2012a).

These values serve as a rough guide to how the variation of m_2/m_1 will affect the system.

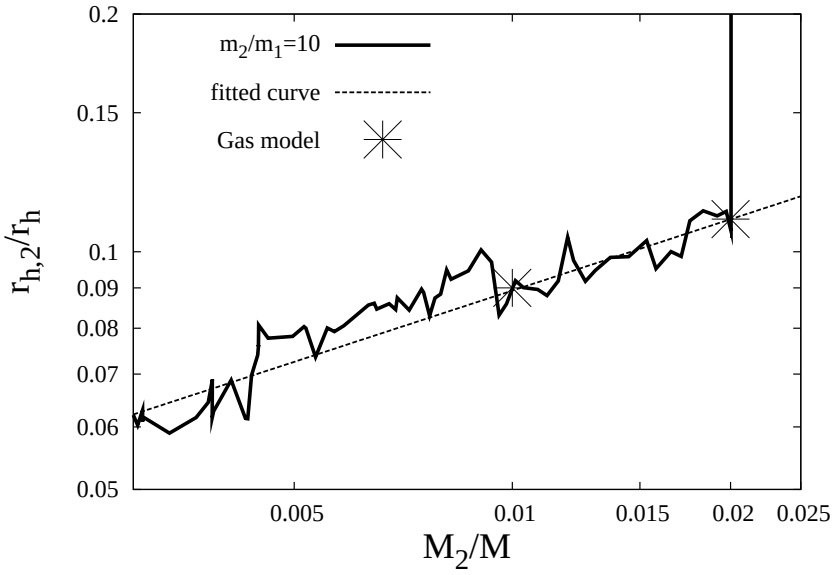

Figure 4.5: $r_{\rm h,2}/r_{\rm h}$ vs M_2/M_1. The solid line represents results from an N-body run with initial values $N = 64k$, $M_2/M_1 = 0.02$ and $m_2/m_1 = 10$. The results are smoothed to make the value of $r_{\rm h,2}/r_{\rm h}$ clearer. The dotted line is the best matching curve of the form $b\big(M_2/M_1\big)^a$ (where a and b are constants, the best match values being $b \approx 0.33$ and $a \approx 0.28$). The points are results from the two-component gas model (see Table 4.1), where M_2/M_1 is fixed. At the beginning of the run $r_{\rm h,2}/r_{\rm h} = 1$ before mass segregation rapidly reduces its value, whence the vertical line segment in the top right corner.

Table 4.2: Variation of $|\phi_{\rm c}|$ and ϕ_2/ϕ_1 with m_2/m_1 for systems with $M_2/M_1 = 0.02$. The values are measured in the post-collapse phase of evolution when the systems have reached a certain size ($r_{\rm h} \approx 0.83$).

m_2/m_1	$N = 32k$		$N = 128k$	
	$\lvert\phi_{\rm c}\rvert$	ϕ_2/ϕ_1	$\lvert\phi_{\rm c}\rvert$	ϕ_2/ϕ_1
50	1.55	0.10	1.62	0.15
20	1.67	0.14	1.80	0.22
10	1.85	0.18	2.00	0.28

If we consider systems with fixed N, M_2 and M_2/M_1 and use similar reasoning as in Section 4.3.5, we would expect systems with lower m_2/m_1 to last slightly longer than systems with higher m_2/m_1. This is because the average energy contribution per binary is dependent on the depth of the central potential. The deeper the central potential the greater the average energy contribution per binary will be, and therefore it is expected that for fixed M_2/M_1 a two-component system with $m_2/m_1 = 20$ will lose mass slightly faster than a system with $m_2/m_1 = 10$.

4.5 Evolution of the BH sub-system: Direct N-body Simulations

4.5.1 Overview

In order to study BH sub-systems we carried out a number of N-body simulations using the NBODY6 code (Nitadori & Aarseth, 2012). Because of the computational cost of large N simulations we have mostly limited ourselves to runs with $N = 32k$ and $64k$. The total mass

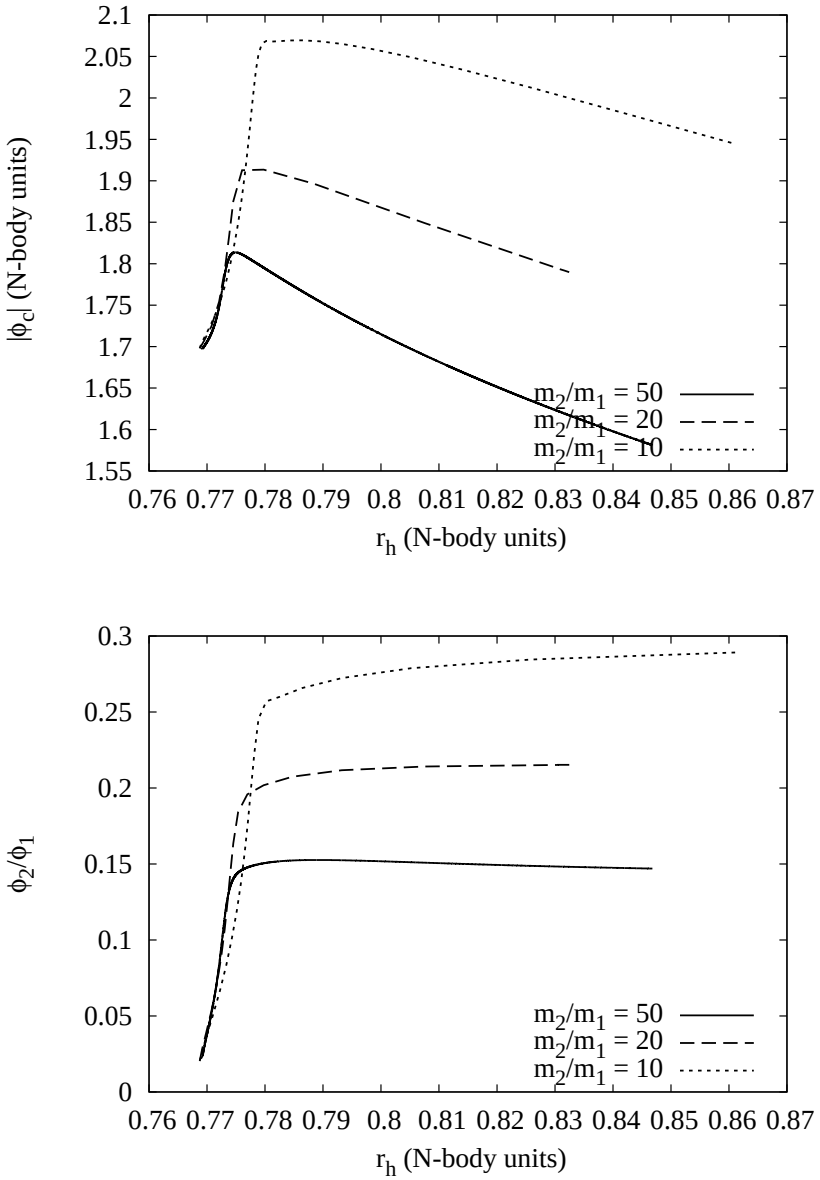

Figure 4.6: Top: $|\phi_{\rm c}|$ vs $r_{\rm h}$ for gaseous systems with fixed N ($128k$) and $M_2/M_1 = 0.02$; the different values of m_2/m_1 are 10, 20 and 50. Bottom: ϕ_2/ϕ_1 vs $r_{\rm h}$ for the same systems as in the top figure. This plot shows that the contribution of the light component to the central potential is dominant.

Table 4.3: Parameters used for N-body runs. In all cases the initial conditions were realisations of the Plummer Model (Plummer, 1911). The values of $t_{\rm rh,i}$ (the initial half-mass relaxation time) are calculated using $\Lambda = 0.02N$ for the coulomb logarithm.

N	m_2/m_1	M_2/M_1	$t_{\rm rh,i}$ (N-body units)
$32k$	10, 20	0.01, 0.02	471
$64k$	10, 20	0.01, 0.02	851
$128k$	20	0.02	1552

ratios used were $M_2/M_1 = 0.01$ and 0.02. The stellar mass ratios used were $m_2/m_1 = 10$ and 20. An additional run with $N = 128k$, $M_2/M_1 = 0.02$ and $m_2/m_1 = 20$ was also carried out to increase the number of systems with $N_2 > 10^2$. These parameters are summarised in Table 4.3 and the results of these runs are given in Table 4.4. The evolution of the fraction of mass remaining in BH ($M_2/M_{2,\rm i}$) in all runs is shown in Figs 4.10, 4.11 and 4.12.

First we will discuss the qualitative behaviour of systems containing a BH sub-system. We do this by considering the case $m_2/m_1 = 20$, $M_2/M_1 = 0.02$ and $N = 64k$, which we refer to henceforth as (20,0.02,64k). The graphs of $r_{\rm h}$ and $r_{\rm c}$ against time for this run are shown in Fig. 4.7. The BH population quickly segregates to the centre of the system causing core collapse to occur in the BH sub-system. For the parameters of this model, this takes approximately $0.3t_{\rm rh,i}$ (where $t_{\rm rh,i}$ is the initial half-mass relaxation time) to occur. The collapse time for other parameter choices is discussed at length in Breen & Heggie (2012a). In Fig. 4.7 this occurs at 270 N-body units. We will refer to this as the first collapse. This is followed by a phase of powered expansion. This can be seen in Fig. 4.7 where, after the first collapse, both $r_{\rm c}$ and $r_{\rm h}$ increase up until ~ 5000 N-body units. As BH escape, the BH sub-system becomes less efficient at producing energy (see Section 4.3.3) and the rate of expansion decreases. The core stops expanding and begins to contract again at ≈ 7500 N-body units; at this stage there is only 15% of the BH sub-system remaining (see Fig. 4.11, bottom, solid line). Most of the remaining BH escape before ≈ 9500 N-body units leaving the system with a single remaining BH binary from ~ 11500 N-body units. The contraction of the core that begins after ≈ 7500 N-body units shall be referred to as the second core collapse or recollapse. As with the first core collapse the core is contracting because there is not enough energy being produced to meet the energy demands of the cluster. As the core (which is dominated by the low mass stars as most of the BH have escaped) becomes smaller towards the end of the run the remaining BH binary starts to interact strongly with the light stars, producing energy more efficiently. This causes the more rapid increase in $r_{\rm h}$ seen towards the end of the plot. The contraction of the core was still ongoing at the end of the run. The core will presumably continue to contract until balanced evolution is restored. If the last remaining BH binary is providing most of the energy, then how long that binary persists in the system depends on the hardness of that binary. Assuming the last BH binary is only slightly hard it is possible that the core contracts sufficiently for a single BH binary to produce the required energy to power the expansion of the system. Ultimately the BH binary will become hard enough to cause its ejection from the system. However if it is extremely hard it is likely that the binary gets ejected from the system during the second core collapse. If this happens the collapse of the core will continue until light binaries are produced as in a one-component model.

4.5.2 The rate of loss of BH

Now we compare the values of $\dot{M}_2$ with the theory of Section 4.3.5 (equation 4.10). $\dot{M}_2$ is estimated by calculating the average mass loss rate over the time taken (from the start of mass loss) for the BH sub-system to lose 50% of its initial mass (i.e. $0.5M_{2,\rm i}/T_{50\%}$; where $T_{50\%}$ is the time taken from $t_{\rm cc}$ until 50% of the BH sub-system has escaped, see Table 4.4 for details). Note that there is a small systematic error introduced by measuring mass loss from the point at which it first occurs. The values of $\dot{M}_2$ (in units of $10^{-3}t_{\rm rh,i}^{-1}$) are plotted in Fig. 4.8. The error bars (estimated as stated in the caption of Table 4.4) are large because N_2 is relatively small, and most data points are consistent with a value of approximately $3\times10^{-3}t_{\rm rh,i}^{-1}$. Equation

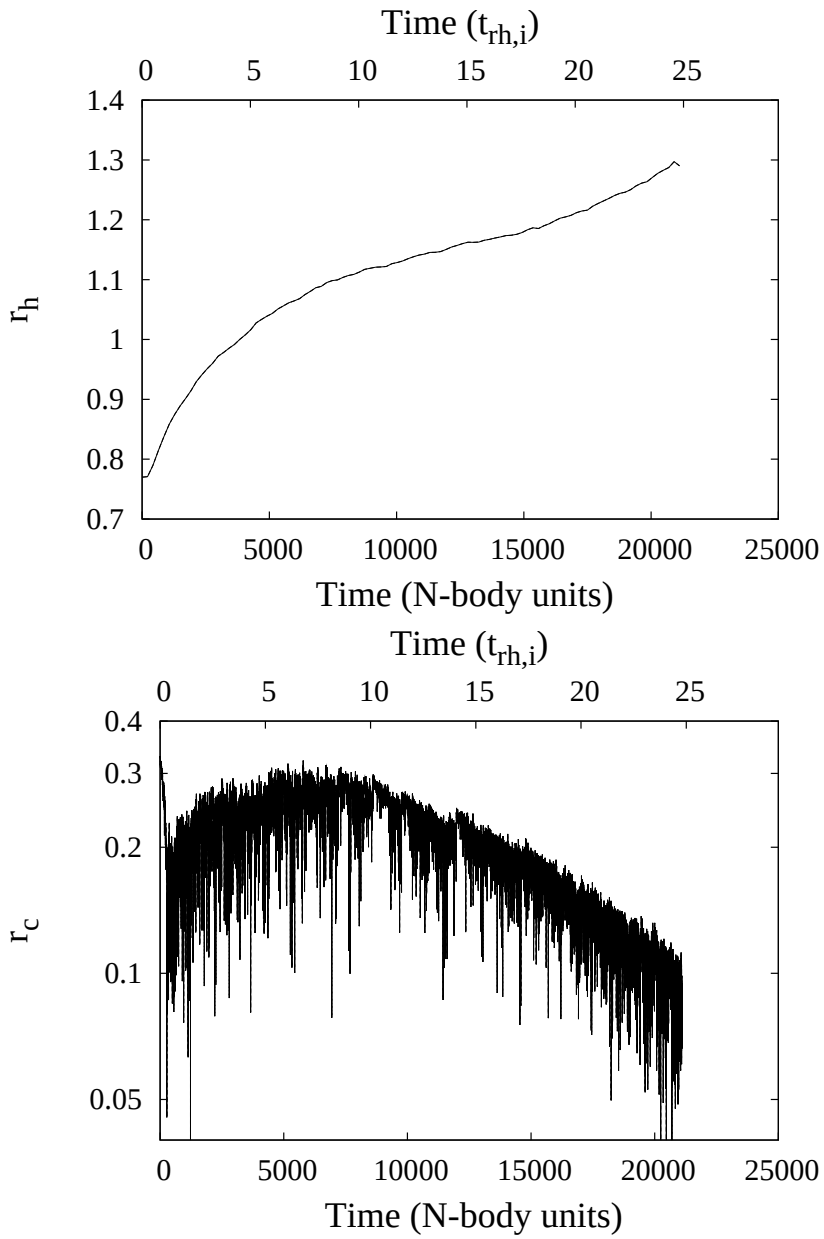

Figure 4.7: N-body run (20,0.02,64k), i.e. with $N = 64k$, $m_2/m_1 = 20$ and $M_2/M_1 = 0.02$. Bottom: r_c vs time (N-body units). At $t = 270$ N-body units core collapse occurs. After most of the BH have escaped ($t \approx 7500$) the core starts to re-collapse. Top: r_h vs time (N-body units). r_h initially expands rapidly before gradually slowing down as the BH sub-system dissolves. From $t \approx 10000$ to ≈ 15000 there is little change in r_h as the system is no longer in a balanced energy generating phase of evolution. The expansion after $t \approx 15000$ results from a single remaining BH binary which becomes more active as the core collapses.

Table 4.4: Results from N-body runs with parameters given in Table 4.3. The values given are (m_2/m_1,M_2/M_1,N), (triple containing stellar mass ratio (m_2/m_1), initial total mass ratio (M_2/M_1), initial total particle number (N)), initial number of BH (N_2), core collapse time ($t_{\rm cc}$), the time at which 50% ($T_{50\%}$) and 90% ($T_{90\%}$) of the initial BH total mass has escaped, the recollapse time of the system, the rate of mass loss from the sub-system $-\dot{M}_2$, ζ (see Section 4.3) and the number of the figure which plots the fraction of remaining BH mass ($M_2/M_{2,\rm i}$) with time. Times for $T_{50\%}$, $T_{90\%}$ and the recollapse are given in N-body units and given in brackets in units of $t_{\rm rh,i}$. Times for $T_{50\%}$, $T_{90\%}$ and the recollapse are measured from the time at which core collapse finishes. The value of $T_{90\%}$ for the case $m_2/m_1 = 20$, $M_2/M_1 = 0.01$ and $N = 32k$ (marked with $*$) is actually the point where 88% mass loss occurs; after this point all that remains in the system is a single binary BH. The values of $\dot{M}_2$ are given in units of 10^{-6} N-body units, (or 10^{-3} $t_{\rm rh,i}^{-1}$ for the values in brackets); these are measured between the loss of the first BH and 50% of the BH, by $\dot{M}_2 = -0.5 M_{2,\rm i}/T_{50\%}$. The values given in the subscript and superscript are the upper and lower 90% confidence limits assuming that BH escape is a Poisson process. The values of ζ were measured by assuming $\dot{E}/|E| \approx \dot{r}_{\rm h}/r_{\rm h}$ (which holds if $|E| \propto GM^2/r_{\rm h}$ and $\dot{M}$ is small) and evaluating $\frac{0.138N}{\ln\Lambda}\frac{2}{3}\frac{d(r_{\rm h}^{\frac{3}{2}})}{dt}$($\approx t_{\rm rh}\frac{\dot{r}_{\rm h}}{r_{\rm h}}$ N-body units) between $2t_{\rm cc}$ and $t_{\rm cc} + T_{50\%}$. $\frac{d(r_{\rm h}^{\frac{3}{2}})}{dt}$ was evaluated by taking the slope of the best fit line to $r_{\rm h}^{\frac{3}{2}}$; the typical errors with the fitted lines were small, $< 3\%$.

($\frac{m_2}{m_1}$,$\frac{M_2}{M_1}$,N)	N_2	$t_{\rm cc}$	$T_{50\%}$[a]	$T_{90\%}$[a]	recollapse time[a]	$-\dot{M}_2$[b]	ζ	Figures[c]
(10,0.01,32k)	34	530	2070 (4.4)	5610 (11.9)	8748 (18.6)	$2.4^{3.6}_{1.5}$ ($1.1^{1.7}_{0.7}$)	0.03	4.10 (T)
(20,0.01,32k)	17	380	850 (1.8)	3000* (6.3*)	$>$ 8000 (17.0)	$5.9^{10.6}_{2.9}$ ($2.8^{5.0}_{1.4}$)	0.06	4.10 (T)
(10,0.02,32k)	66	492	1658 (3.5)	5702 (12.1)	$>$ 11876 (25.2)	$6.0^{8.1}_{4.4}$ ($2.8^{3.8}_{2.1}$)	0.06	4.10 (B)
(20,0.02,32k)	33	419	940 (1.9)	3816 (8.1)	$>$ 9902 (21.0)	$10.6^{16.0}_{6.8}$ ($5.0^{7.5}_{3.2}$)	0.10	4.10 (B)
(10,0.01,64k)	66	920	3650 (4.2)	12950 (15.2)	$>$ 13000 (15.3)	$1.4^{1.8}_{1.0}$ ($1.2^{1.6}_{0.9}$)	0.03	4.11 (T)
(20,0.01,64k)	33	404	1750 (2.1)	5400 (6.8)	$>$ 7844 (9.2)	$2.9^{4.3}_{1.8}$ ($2.4^{3.6}_{1.5}$)	0.05	4.11 (T)
(10,0.02,64k)	131	690	3230 (3.7)	12740 (14.6)	$>$ 15580 (17.9)	$3.5^{4.3}_{2.9}$ ($2.6^{3.2}_{2.1}$)	0.05	4.11 (B)
(20,0.02,64k)	66	270	2680 (3.2)	9495 (11.3)	$>$ 19600 (23.4)	$3.7^{5.0}_{2.7}$ ($3.2^{4.2}_{2.3}$)	0.08	4.11 (B)
(20,0.02,128k)	131	650	4120 (2.7)	$>$ 7076 (4.6)	$>$ 7076 (4.6)	$2.4^{3.0}_{2.0}$ ($3.8^{4.6}_{3.0}$)	0.08	4.12

[a] Units: N-body units ($t_{\rm rh,i}$)
[b] Units: 10^{-6} N-body units (10^{-3} $t_{\rm rh,i}^{-1}$)
[c] (T) Top figiure; (B) Bottom figure

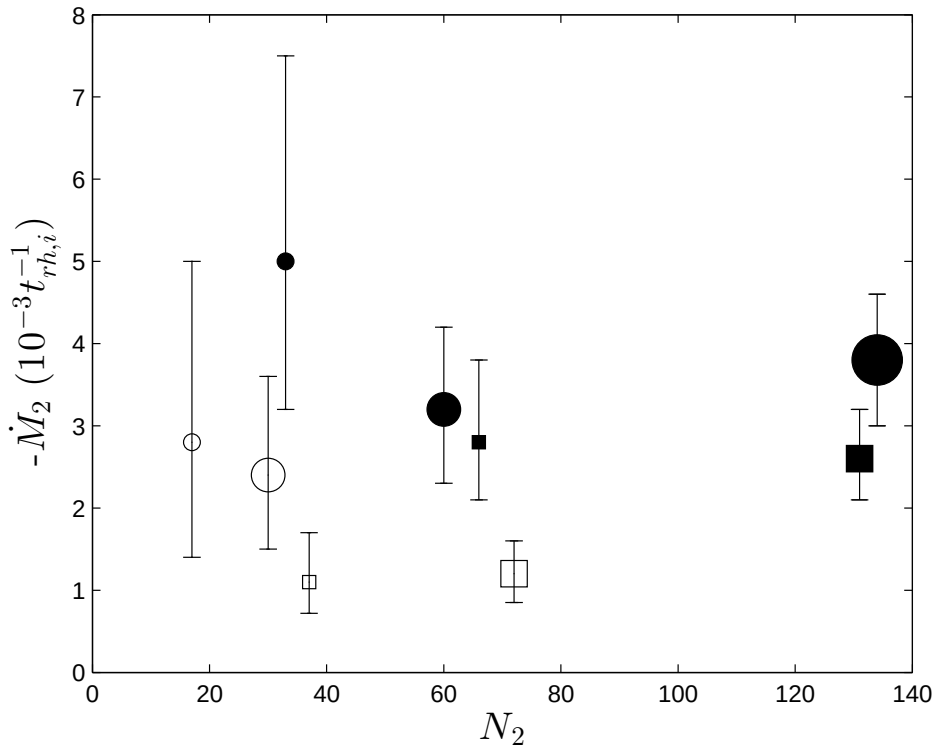

Figure 4.8: $\dot{M}_2$ (units of $10^{-3}t_{\rm rh,i}^{-1}$) versus initial value of N_2. Error bars indicate confidence limits (see Table 4.4 for details). Circles represent $(20, M_2/M_1, N)$, squares represent $(10, M_2/M_1, N)$, filled symbols represent $(m_2/m_1, 0.02, N)$, unfilled symbols represent $(m_2/m_1, 0.01, N)$, larger symbols $(m_2/m_1, M_2/M_1, 64k)$ (with the exception of the largest circle on the right which corresponds to $(20, 0.02, 128k)$) and smaller symbols $(m_2/m_1, M_2/M_1, 32k)$. For cases with the same or similar initial values of N_2 some of the values were adjusted by $\lesssim 10\%$ to stop the symbols from overlapping. To a first approximation $\dot{M}_2$ is independent of m_2/m_1, M_2/M_1 and N.

4.10, with canonical values of α, β and ζ implies that the values in Fig. 4.8 should be nearly $6.1 \times 10^{-3}t_{\rm rh,i}^{-1}$ and we will now consider reasons for the discrepancy.

First, this estimate can be improved upon by taking into account the fact that the system expands as energy is being generated, increasing the relaxation time and in turn decreasing the mass loss rate. The improved estimate can be calculated by using equation 4.12 to estimate the time taken for half the BH to be lost and evaluating $\dot{M}_2$ as was done in Table 4.4. This results in a slightly smaller estimate of $5.4 \times 10^{-3}t_{\rm rh,i}^{-1}$, which is still significantly larger than most of the values in Table 4.4.

Another factor is that the values of ζ for most of the runs are smaller than the canonical value used for the estimate (i.e. $\zeta \approx 0.09$). Equation 4.12 predicts an approximately linear dependence of $\dot{M}_2$ on ζ, and this is clearly confirmed in Fig. 4.9. The solid line, which represents the predicted values of $\dot{M}_2$ with varying ζ, nevertheless lies above all the numerical results and outside the confidence intervals for all but a few of the runs. However by adjusting the value of α/β (in equations 4.10 and 4.12 α and β only appear in the form α/β) from $\alpha/\beta \approx 0.068$ (the value estimated on the basis of theoretical arguments) to $\alpha/\beta \approx 0.051$ the theory comes into very good agreement with the values of $\dot{M}_2$. This can be seen in Fig. 4.9 where the dashed line represents the predicted values of $\dot{M}_2$ based on a value of $\alpha/\beta \approx 0.051$. The discussion of Section 4.3.5 makes it clear that the canonical values of α and, especially, β are subject to uncertainty, the latter resting entirely on approximate theoretical arguments. The suggested revision of α/β cannot be ruled out on these grounds.

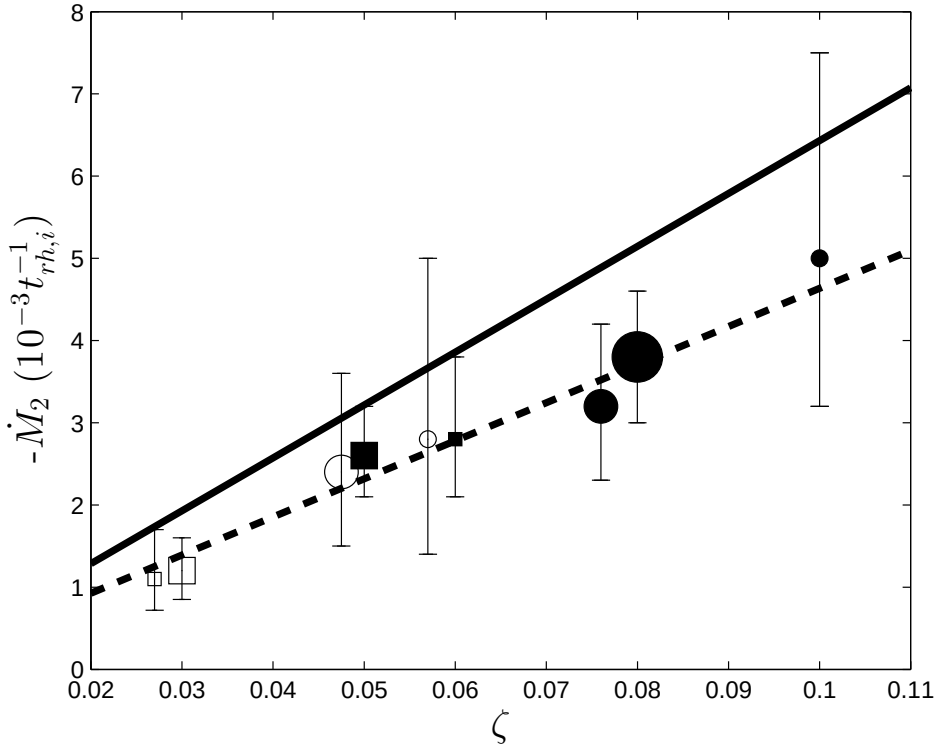

Figure 4.9: $\dot{M}_2$ (units of $10^{-3}t_{\rm rh,i}^{-1}$) versus value of ζ; error bars indicate 90% confidence limits (see Table 4.4 for details). The symbols represent the same runs as in Fig. 4.8, the solid line represents the predicted values of $\dot{M}_2$ using the value of $\alpha/\beta = 0.068$ (based on theoretical arguments), and the dashed line represents the predicted values of $\dot{M}_2$ using the value of $\alpha/\beta = 0.051$ (the empirical value). For cases with the same or similar values of ζ some of the values of ζ were adjusted by $\pm 5\%$ to stop the symbols from overlapping. See text for details.

Equation 4.13 allows us to test the theory constructed in Section 4.3.5, in a ζ-independent way. In Fig. 4.13 the observed dependence of M_2 on $r_{\rm h}$ is in satisfactory agreement with the predictions based on equation 4.13.

The lower values of ζ in Table 4.4 may result from systems in which the BH sub-system is incapable of producing the required energy for the system to achieve balanced evolution. This could possibly be due to the small values of N_2; most of these models reach values of N_2 (at time $T_{50\%}$) below the point at which the theory of Section 4.3.5 is expected to apply (see Section 4.3.3). If a system is not in balanced evolution it is expected to undergo contraction of the inner Lagrangian radii relative to $r_{\rm h}$, qualitatively as in conventional core collapse. This is illustrated in Fig. 4.14 for three of the N-body runs in Table 4.4. The systems with smaller values of ζ show greater contraction. Note that the values ζ are only evaluated over the period to $T_{50\%}$ and appear to decrease after $T_{50\%}$ (~ 3000). Indeed this is what would be expected as the expansion is affected by the weakening energy generation (see also Fig. 4.7).

In this section we have assumed that mass segregation concentrates the BH in the centre of the system by the time of the first core collapse. Though this prevents further contraction of the central BH sub-system, this is not true of all the BH, as discussed in Appendix E and Morscher et al (2012). The outermost BH can continue contracting after core collapse has occurred, indicating that mass segregation can continue in the outermost parts of a system for a while after core collapse. This results in additional heating which is not associated with energy production. The effect of this heating is expected to be small for the models in Table 4.3 due to the small particle number, although the effect may be more significant in larger systems and may be enhanced by the presence of a mass spectrum.

4.5.3 Lifetime of BH sub-systems

Now that the dependence of $\dot{M}_2$ on cluster properties has been discussed, it is natural to move on to considering how long the BH sub-system lasts. For this purpose we shall define the life time of the BH sub-system as the time taken from the core collapse of the BH sub-system (which occurs at $t_{\rm cc}$) until the BH sub-system has lost 90% of its initial mass ($T_{90\%}$). These values are given in Table 4.4, where it can be seen that $T_{90\%} \sim 10 t_{\rm rh,i}$. Equation 4.12 in Section 4.3.5 can be used to estimate the life time of the sub-system (using $\alpha/\beta = 0.051$). For $M_2/M_1 = 0.01$ the theory predicts $T_{90\%} \sim 2.2 t_{\rm rh,i}$ and $T_{90\%} \sim 5.2 t_{\rm rh,i}$ for $M_2/M_1 = 0.02$. These values are significantly smaller than the values seen in Table 4.4. As stated in the previous subsection most of the values of ζ in Table 4.4 are below the value used in Section 4.3.5. Adjusting ζ to 0.05 in equation 4.12 increases the predicted values of $T_{90\%}$ to $4.0 t_{\rm rh,i}$ for $M_2/M_1 = 0.01$ and $9.3 t_{\rm rh,i}$ for $M_2/M_1 = 0.02$. These values are still significantly smaller than those given in Table 4.4 with the corresponding value of ζ. The difference between the empirically found values and the theoretical estimates might be accounted for by the fact that the theory assumes a constant value of ζ; however ζ is expected to decrease as the BH sub-system evaporates (see Section 4.5.1). This behaviour is illustrated by the behaviour of $r_{\rm h}$ in Fig. 4.7. There is a hint that the same decrease of ζ with decreasing N may also be present in one-component models (Alexander & Gieles, 2012). Also as can be seen from the values of ζ in Table 4.4 some systems appear to be incapable of achieving balanced evolution at any time throughout the loss of the BH sub-system.

The expected evolution of a BH sub-system can be illustrated using Fig. 4.9. If we assume that the BH sub-system is capable of achieving balanced evolution, after the formation of the BH sub-system ζ and $-\dot{M}_2$ are predicted to rapidly reach the balanced evolution values of $\zeta \approx 0.09$ and $-\dot{M}_2 \approx 4 \times 10^{-3} t_{\rm rh,i}^{-1}$ (just to upper right of the large filled circle). As the BH sub-system loses mass it will eventually reach the point where it is no longer capable of generating the energy needed for balanced evolution. After this the system will move down the dashed line towards the origin. As it does so the rate of mass loss decreases, prolonging the life of the BH sub-system. This picture may explain the longer lifetimes given in Table 4.4 and is consistent with the evolution of $r_{\rm h}$ in Fig. 4.7.

Finally we briefly consider the recollapse time of these systems (see Table 4.4). This is the time between the first and second core collapse. It can be interpreted as approximately the time it takes for the system to achieve balanced evolution once the BH sub-system has been exhausted. Most of the N-body runs do not reach the second core collapse, and therefore mostly

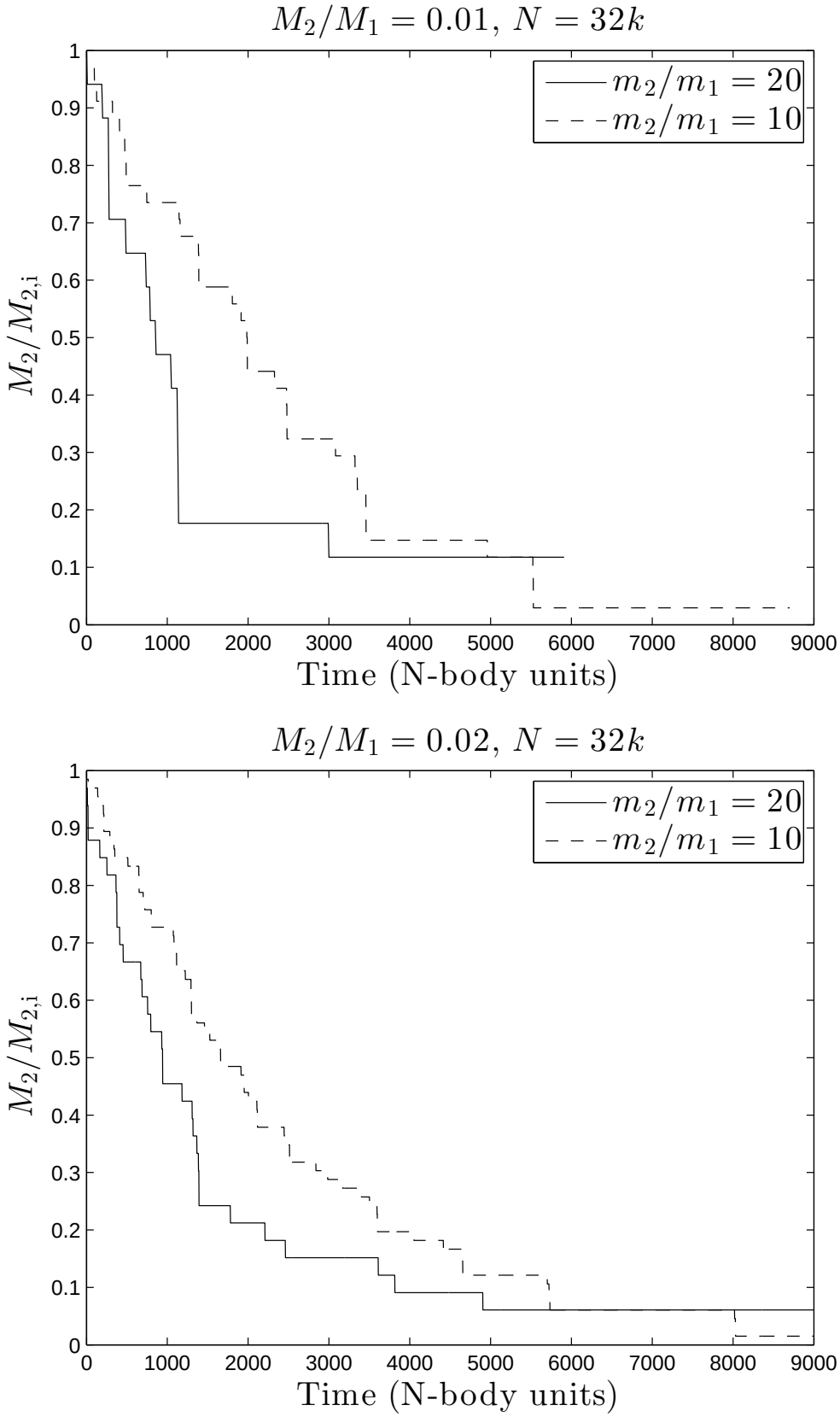

Figure 4.10: Fraction of initial mass remaining ($M_2/M_{2,\mathrm{i}}$, where $M_{2,\mathrm{i}}$ is the initial mass of the heavy component) vs time (in N-body units) for the cases $N = 32k$ with $M_2/M_1 = 0.01$ (Top) and $M_2/M_1 = 0.02$ (Bottom). In both figures the dashed line represents $m_2/m_1 = 10$ and the solid line represents $m_2/m_1 = 20$. $T = 0$ is set as the time when first mass loss occurs, which is at approximately the same time as the first core collapse.

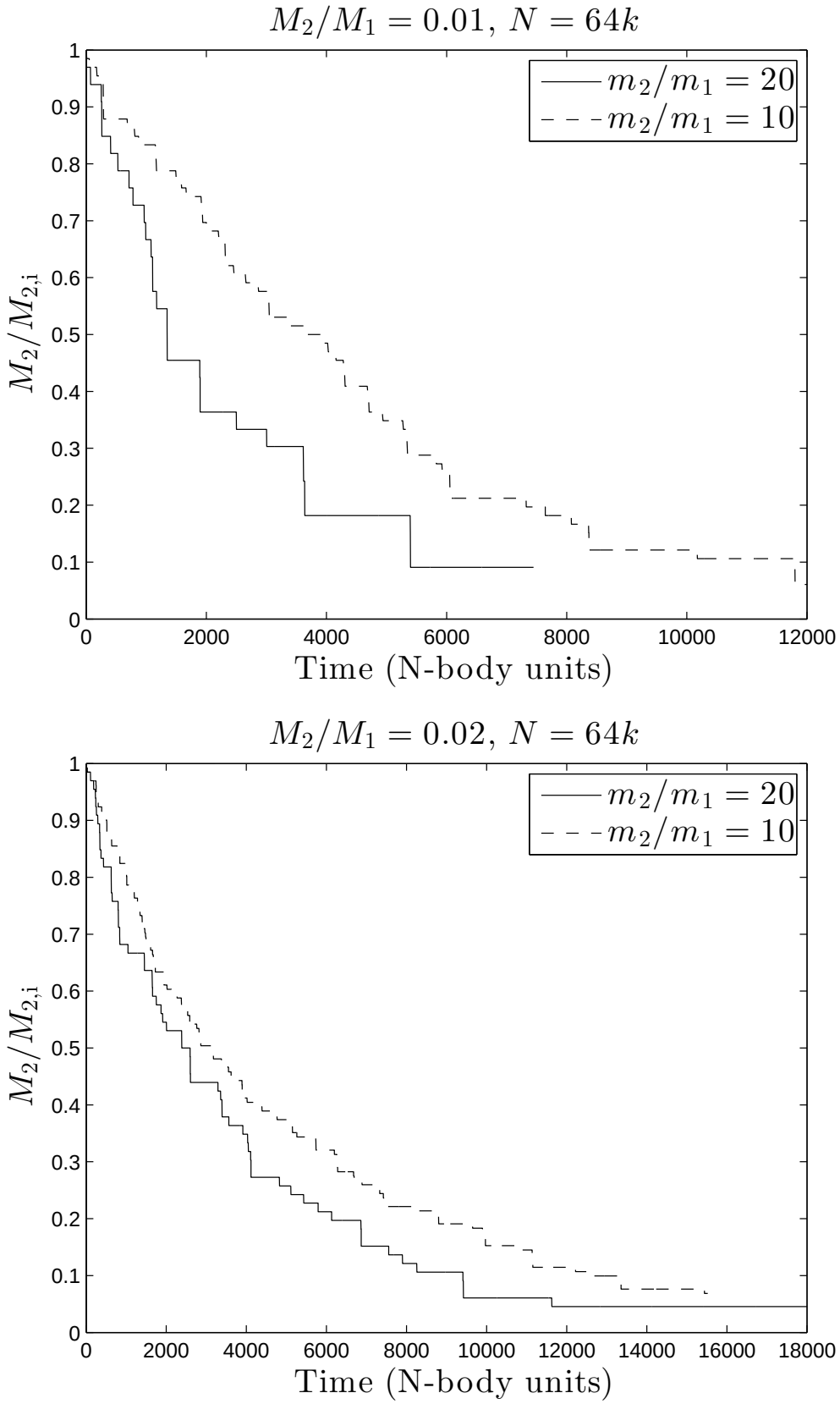

Figure 4.11: Fraction of initial mass remaining ($M_2/M_{2,\mathrm{i}}$, where $M_{2,\mathrm{i}}$ is the initial mass of the heavy component) vs time (in N-body units) for the cases $N = 64k$ with $M_2/M_1 = 0.01$ (Top) and $M_2/M_1 = 0.02$ (Bottom). In both figures the dashed line represents $m_2/m_1 = 10$ and the solid line represents $m_2/m_1 = 20$. $T = 0$ is set at the time when the first mass loss occurs, which is at approximately the same time as the first core collapse.

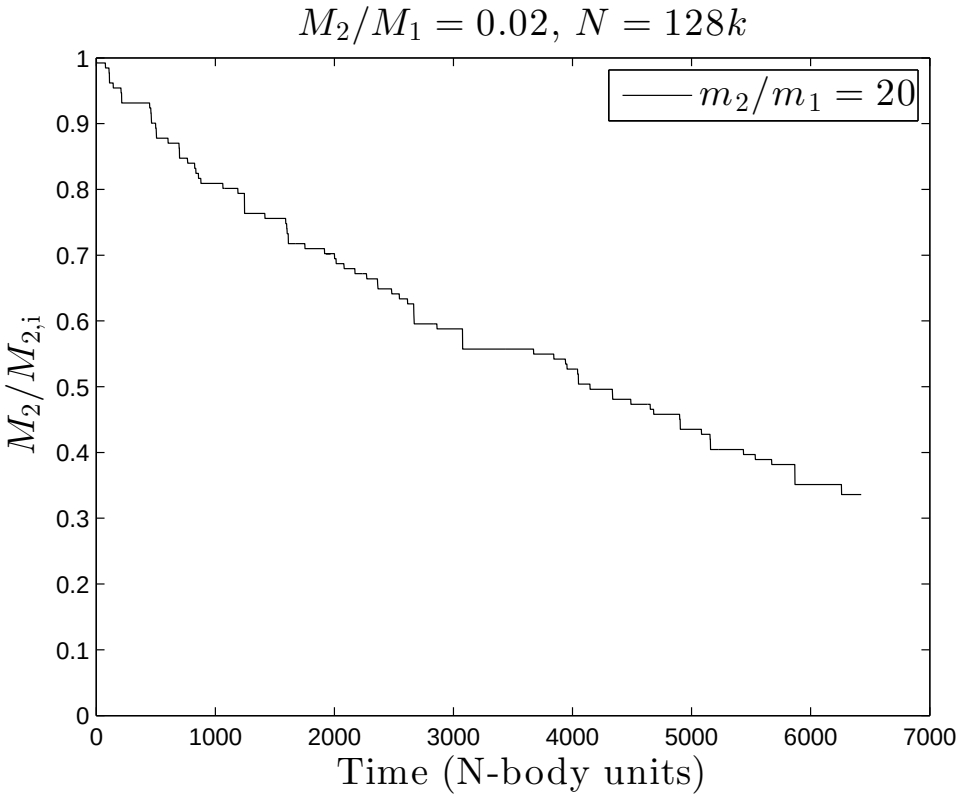

Figure 4.12: Fraction of initial mass remaining ($M_2/M_{2,\mathrm{i}}$, where $M_{2,\mathrm{i}}$ is the initial mass of the heavy component) vs time (in N-body units) for the case $N = 128k$ with $M_2/M_1 = 0.02$ and $m_2/m_1 = 20$. $T = 0$ is set at the time when the first mass loss occurs, which is at approximately the same time as the first core collapse.

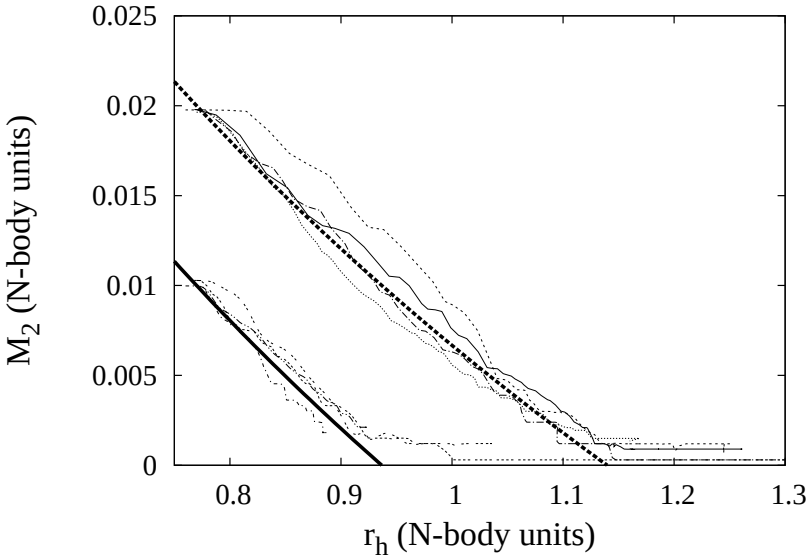

Figure 4.13: Evolution of M_2 vs $r_{\rm h}$ for the $N = 32k$ and $64k$ models in Table 4.4. The thick dashed line is the theoretical prediction (see equation 4.13) for the initial value of $M_2/M_1 = 0.02$ and the thick solid line is the theoretical prediction for the initial value of $M_2/M_1 = 0.01$. The value of $r_{\rm h,i}$ used in equation 4.13 was 0.77 and the empirical value of $\alpha/\beta \approx 0.051$ was used for all models. In all cases the behaviour of the N-body runs is in approximate quantitative agreement with the predicted behaviour until there are only a few BH remaining.

lower limits on the recollapse time are given in Table 4.4. From the results in Table 4.4 this time is at least roughly the same time as the core collapse time of a one component Plummer model ($\approx 15 t_{\rm rh,i}$ see Heggie & Hut, 2003) but can be longer because of the offsetting effect of BH heating.

4.6 Gravothermal Oscillations

The conditions for the onset of gravothermal oscillations in two-component models have been studied by Breen & Heggie (2012a), who found that the value of N_2 (the number of heavy stars) could be used as an approximate stability condition (where the stability boundary is at $N_2 \sim 3000$) for a wide range of stellar and total mass ratios ($2 \leq m_2/m_1 \leq 50$ and $0.1 \leq M_2/M_1 \leq 1.0$). Breen & Heggie (2012b), who researched the onset of gravothermal oscillation in multi-component systems, found that the parameter called the effective particle number $N_{\rm ef}$ (defined as $M/m_{\rm max}$) could be used as an approximate stability condition for both the multi-component systems they studied and the two-component models of Breen & Heggie (2012a). The stability boundary they found was at $N_{\rm ef} \sim 10^4$, which is also consistent with the stability boundary of the one-component model at $N = 7000$ (Goodman, 1987). However both those stability conditions relied on the assumption that the heavy component (or heavier stars for the multi-component case) dominated the evolution of the system, in the sense that the heavy component determined the rate of energy generation. This is not the case for the systems considered in the present chapter as the total mass in the heavy component is so small, and so $N_{\rm ef}$ will not be considered further. (In the systems considered in this chapter the heavy component dominates the production of energy, but the light component controls how much energy is created.) We will now investigate the onset of gravothermal oscillation for the systems of interest in the present chapter (where $M_2/M_1 \ll 1.0$ and $m_2/m_1 \gtrsim 5$).

The critical number of stars ($N_{\rm crit}$) at which gravothermal oscillations first manifest was found for the gas models with $M_2/M_1 = 0.05, 0.01$ and, $m_2/m_1 = 5$, 10, 20, and 50 (see Section 4.4). The results are given in Table 4.5. The values of N_2 at $N_{\rm crit}$ for the runs in Table 4.5

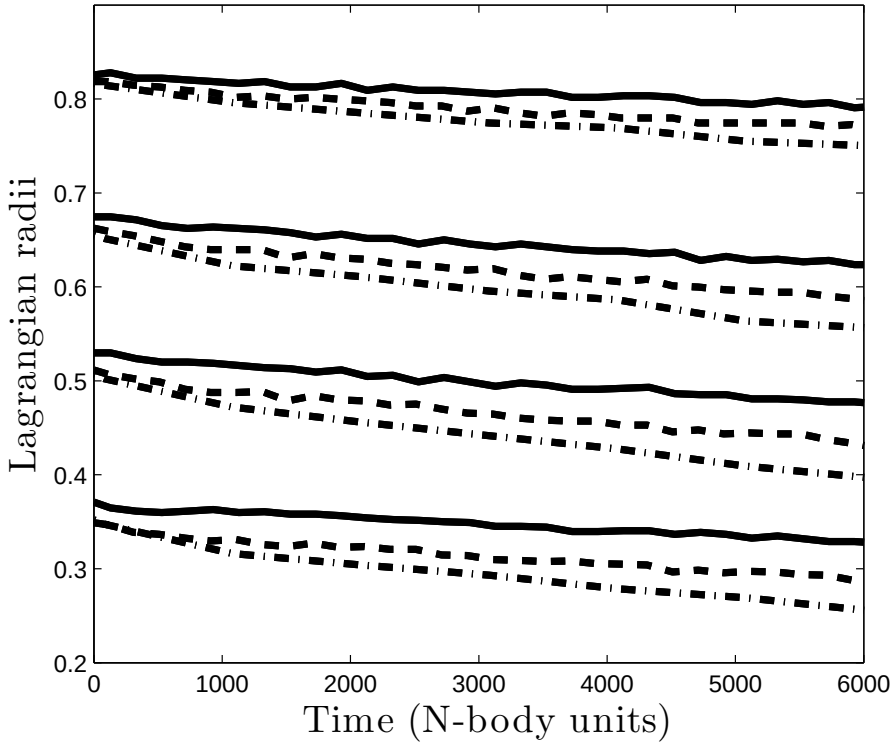

Figure 4.14: Relative contraction in Lagrangian radii (40%, 30%, 20% and 10%) over time (N-body units) for (20,0.02,64k) solid line, (10,0.02,64k) dashed line and (10,0.01,64k) dot dash line. $T = 0$ in all models is set at the time mass loss starts from the BH sub-system. Radii are measured in units of the half-mass radius. The values of ζ for the three runs are 0.08, 0.05 and 0.03, respectively. The parameter ζ measures the dimensionless expansion rate of the half-mass radius and the figure shows that slow expansion is associated with relative contraction of the inner Lagrangian radii.

Table 4.5: Critical values of N in units of 10^4

$\frac{m_2}{m_1} \backslash \frac{M_2}{M_1}$	**0.5**	**0.1**	**0.05**	**0.01**
50	30	100	130	450
20	13	36	63	180
10	7.2	22	32	90
5	4.0	10	17	40

Table 4.6: Values of N_2 at $N_{\rm crit}$ in units of 10^3

$\frac{m_2}{m_1} \backslash \frac{M_2}{M_1}$	**0.5**	**0.1**	**0.05**	**0.01**
50	3.0	2.0	1.3	0.9
20	3.2	1.8	1.6	0.9
10	3.4	2.2	1.6	0.9
5	3.6	2.0	1.7	0.8

are given in Table 4.6. The values for $M_2/M_1 = 0.5$ and 0.1 from Breen & Heggie (2012a) have also been included in Tables 4.5 and 4.6 for reference. For fixed m_2/m_1, the system becomes unstable at a roughly fixed value of N_2 ($N_2 \approx 1500$ for $M_2/M_1 = 0.05$ and $N_2 \approx 900$ for $M_2/M_1 = 0.01$). These results suggest that N_2 still provides an approximate stability condition (for fixed M_2/M_1) even for models in which the heavy component only makes up a tiny fraction of the system.

Given that the theory in the present chapter is built around the assumption that the light component determines the evolution of the BH sub-system, it may be surprising that the appearance of gravothermal oscillations seems solely determined (for fixed M_2/M_1) by the number of stars in the heavy component. However this may be explained if one considers the unique structure of systems containing a BH sub-system. The presence of a BH sub-system tends to produce a system with two cores, one small BH core and another much larger light core, which is larger than the half mass radius of the BH sub-system (Merritt et al 2004; Mackey et al 2008; also see Fig. 4.15 in the present chapter). As gravothermal oscillation in a one-component system requires a small core to half mass ratio (Goodman, 1987), the light system itself is expected to be highly stable against gravothermal oscillations. However as the BH sub-system has to meet the energy generation requirements of the entire system, the BH sub-system can have a very small ratio of core radius to half mass radius (see Section 4.3). If the onset of gravothermal oscillation is a result of the BH sub-system itself becoming unstable then it would be expected that the BH sub-systems would have similar structure at the stability boundary. This is indeed the case as can be seen in Fig. 4.15 which shows the post collapse density profile of two systems (with $m_2/m_1 = 50$ and $m_2/m_1 = 10$) near the stability boundary (i.e. N is slightly smaller than $N_{\rm crit}$): the profiles of the heavy component are almost identical (in terms of density contrast, i.e. $\rho_2/\rho_{\rm h,2}$) whereas the profiles of the light component are significantly different. In fact if one were to plot the BH sub-systems in units of $\rho_{\rm c,2}$ vs $r_{\rm c,2}$ the BH sub-systems would be nearly indistinguishable. We study this more quantitatively below.

The Goodman stability parameter (Goodman, 1993) (or a somewhat modified version (Breen & Heggie, 2012a,b)) has been found to provide a stability criterion. The Goodman stability parameter is defined as

$$\epsilon \equiv \frac{E_{\rm tot}/t_{\rm rh}}{E_{\rm c}/t_{\rm rc}},$$

where $E_{\rm c}$ is the energy of the core. The critical value for the one-component model is $\log_{10}\epsilon \approx -2$. This condition was also found to apply for the Spitzer stable two-component models studied by Kim, Lee & Goodman (1998). However, Breen & Heggie (2012a) found the critical value of ϵ to vary for the Spitzer unstable models they studied. They found that by slightly modifying the definition of ϵ (ϵ_2) a much improved stability criterion could be found, with a critical value $\log_{10}\epsilon_2 \approx -1.5$. We can test a version of these parameters for the BH sub-systems by suitably

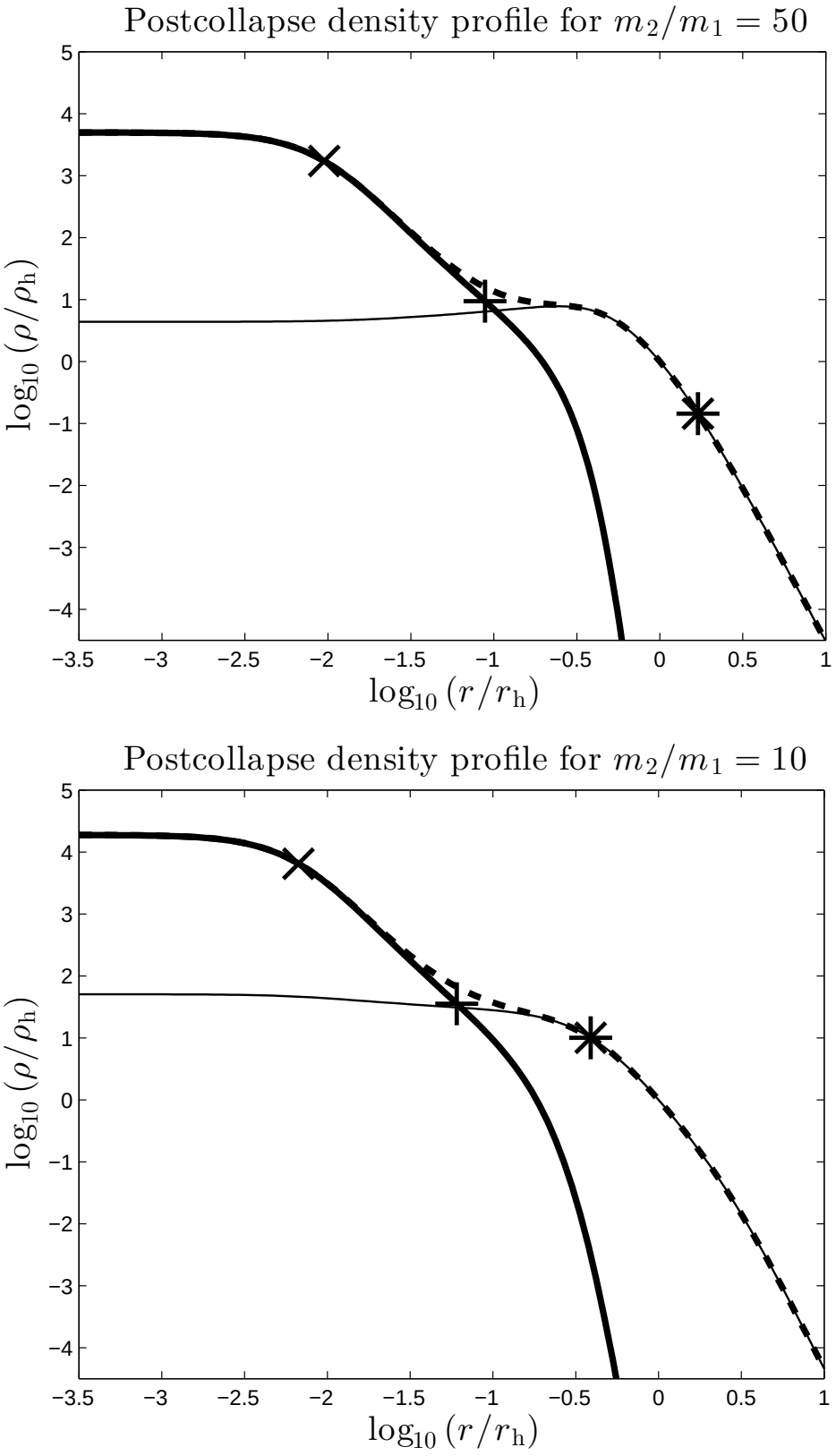

Figure 4.15: Postcollapse density profile in gas models of two-component systems with $M_2/M_1 = 0.01$ near the onset of gravothermal oscillations for $m_2/m_1 = 50$ ($N = 4.3\times10^6$, top) and $m_2/m_1 = 10$ ($N = 8.5\times10^5$, bottom). The following is shown in the plot: ρ_1 (thin line), ρ_2 (thick line), $\rho_{\rm tot}$ (dashed line), core radius of heavy component $r_{\rm c,2}$ ($\times$), core radius of light component $r_{\rm c,1}$ ($*$) and $r_{\rm h,2}$ ($+$). The core radii have been defined as $r_{{\rm c},i} = \sqrt{9\sigma^2_{{\rm c},i}/(4\pi\rho_{{\rm c},i})}$. For the case of $m_2/m_1 = 50$, the BH sub-system creates a density hole in the light component: the density of lights in the centre is approximately a factor of 2 less then its highest value (which occurs at $\log r/r_{\rm h} \simeq -0.5$). The remarkably large value of $r_{\rm c,1}$ for this case results from the low value of $\rho_{\rm c,1}$ and a high value of $\sigma^2_{\rm c,1}$ caused by the presence of the BH sub-system.

Table 4.7: Values of $\log_{10}\epsilon_{\rm BH}$ and $r_{\rm c,2}/r_{\rm h,2}$ near $N_{\rm crit}$ for systems with $M_2/M_1 = 0.01$. For the corresponding values of $N_{\rm crit}$ see Table 4.5. The results in this table indicate that gravothermal oscillation manifests once a certain value of $r_{\rm c,2}/r_{\rm h,2}$ (or $\log_{10}\epsilon$) is reached. See text for details.

m_2/m_1	5	10	20	50
$r_{\rm c,2}/r_{\rm h,2}$	0.14	0.12	0.12	0.11
$\log_{10}\epsilon_{\rm BH}$	−0.21	−0.30	−0.31	−0.32

modifying ϵ to

$$\epsilon_{\rm BH} \equiv \frac{E_{\rm BH}/t_{\rm rh,2}}{E_{\rm c,2}/t_{\rm rc,2}}$$

where $E_{\rm c,2}$ and $E_{\rm BH}$ are the energy of the BH core and the total energy of the BH sub-system respectively. $\epsilon_{\rm BH}$ was measured for a range of systems with $M_2/M_1 = 0.01$ and the results are presented in Table 4.7 along with the values of $r_{\rm c,2}/r_{\rm h,2}$ (following the discussion of the previous paragraph). As can be seen in Table 4.7 all the systems with large enough m_2/m_1 have similar values of $\log_{10}\epsilon_{\rm BH}$ and $r_{\rm c,2}/r_{\rm h,2}$ at their corresponding value of $N_{\rm crit}$ which supports the assertion that the onset of gravothermal oscillation depends on the structure of the BH sub-system.

The critical values of $\log_{10}\epsilon_{\rm BH}$ are larger than the values of $\log_{10}\epsilon$ found for two-component models by Kim, Lee & Goodman (1998) and Breen & Heggie (2012a), and that found for the one-component model by Goodman (1993) by approximately 1.7 dex. Also the critical values of $r_{\rm c,2}/r_{\rm h,2}$ are larger than the corresponding critical value for a single-component system (Goodman, 1987), i.e. $r_{\rm c}/r_{\rm h} \approx 0.02$. This may be because the maximum radius of the isothermal region in the BH sub-system is larger than $r_{\rm h,2}$, as was hinted by Breen & Heggie (2012a). If the condition for gravothermal instability is that the density contrast across the isothermal region exceeds some critical value, and if the edge of this region is well outside $r_{\rm h,2}$, then it can be understood why the critical value of $r_{\rm c,2}/r_{\rm h,2}$ is larger than Goodman's value. To investigate this, the size of the isothermal region was measured for $(50, 0.01, 4.3\times10^6)$, which is shown in Fig. 4.15 (Top). The edge of the isothermal region ($r_{\rm iso}$) was defined as the radius at which σ_2^2 reaches 80% of it central value. This gives $r_{\rm c,2}/r_{\rm iso} \approx 0.022$ which is consistent with the value of $r_{\rm c}/r_{\rm h}$ found by Goodman (1987) for the one-component model. (For a one-component gas model, $r_{\rm c}/r_{\rm iso} \simeq 0.016$ near the stability boundary.)

4.7 Conclusion and Discussion

4.7.1 Summary

In this chapter we have studied systems intended to resemble those containing a significant population of black holes (BH), i.e. two-component systems with one component being the BH and the other the rest of the stars in the system. It was argued in Section 4.3.4 that mass loss by evaporation due to two body relaxation in the BH sub-system does not cause significant mass loss of BH and can be neglected. The principal mechanism for removing BH, for the models considered in the present chapter, is superelastic encounters involving BH binaries and single BH in the core of the BH sub-system. By considering these systems to be in balanced evolution, predictions were made regarding the BH sub-system, for example the escape rate of BH (see Section 4.3.5). Some of the potential limitations of the theory were also discussed in Section 4.3.3.

The theory in Sections 4.3.1 and 4.3.2 makes predictions about the structure of the BH sub-system, particular regarding the variation of $r_{\rm c,2}/r_{\rm h,2}$ with m_2/m_1 and M_2/M_1 (see equation 4.5). (Here the subscripts 2 and 1 refer to the BH and the other stars, M, m denoted the total and individual masses, and $r_{\rm c}$, $r_{\rm h}$ the core and half-mass radii, respectively). The theory was tested in Section 4.4.1 with gas models and was found to be in good agreement with theory under the condition that $m_2/m_1 \gtrsim 10$ and that $N \gtrsim 128k$ (see Figs 4.2 and 4.3). The disagreement with the theory outside of those conditions may be attributable to small N_2 and the fact that the systems become Spitzer stable at low m_2/m_1. One of the assumptions of the

theory was that the BH sub-system only made a small contribution to the central potential (see Section 4.3.5), which was tested in Section 4.4.3 by measuring the contribution to the central potential of each component in a series of simulations.

It was argued in Section 4.3.5 that the rate of mass loss from the BH sub-system should be approximately independent of the properties of the BH sub-system (i.e. M_2/M_1 and m_2/m_1). This theory only requires that the light component regulates the rate of energy production and does not rely on the stronger assumption that energy is transported through the BH sub-system as outlined in Section 4.3.1. In Section 4.5.2 the results of a number of N-body runs were presented (see Table 4.3 and Table 4.4) and the results were used to test the predicted mass loss rates from Section 4.3.5. With the exception of systems with $m_2/m_1 = 10$ and $M_2/M_1 = 0.01$, the mass loss rates for the BH sub-system were all consistent with a value of $\dot{M}_2 \sim 3.0 \times 10^{-3} t_{\rm rh}^{-1}$, where $t_{\rm rh}$ is the half-mass relaxation time of the entire system. However most of the runs had a lower value of the dimensionless expansion rate ζ than expected and $\dot{M}_2$ was found to vary approximately linearly with ζ (see Fig. 4.9). Once the variation of ζ was taken into account and the value of α/β (where α, β are dimensionless parameters determining the energy and central potential) was adjusted to 0.051 (see Sections 4.3.5 and 4.5.2), there was good agreement between the empirical values of $\dot{M}_2$ in Table 4.4 and the predicted values of $\dot{M}_2$ made using equation 4.12. The low values of ζ seen in Table 4.4 may result from the small number of BH in these systems which possibly results in the inability of the BH sub-system to maintain balanced evolution. Larger simulations will be required before this explanation can be confirmed.

In Section 4.6 we considered gravothermal oscillations in systems containing a BH sub-system. This extends the parameter space of two-component clusters studied by Breen & Heggie (2012a) to lower values of M_2/M_1 for $m_2/m_1 \geq 5$. The results in this section imply that the gravothermal instability manifests when the BH sub-system reaches a certain profile (see Fig. 4.15 and Table 4.7). A version of the Goodman stability parameter was also tested for systems with $M_2/M_1 = 0.01$ and was found to provide an approximate stability condition, although the critical value was significantly larger than the value measured for one-component models. The difference between the critical values for the BH sub-systems and the one-component models may result from the fact that the BH sub-system is approximately isothermal to larger radii than $r_{\rm h,2}$. The ratio between $r_{\rm c,2}$ and the radius of the isothermal region ($r_{\rm iso}$) was measured for a selected model and was found to be consistent with the critical value of $r_{\rm c}/r_{\rm iso}$ found for a one-component system. These results indicate that the onset of gravothermal oscillation for systems containing a BH sub-system is determined by the properties of the BH sub-system.

4.7.2 Astrophyical issues

In the present chapter we have made several simplifying assumptions. Importantly we have ignored stellar evolution and the effect of a mass spectrum. A mass spectrum can increase the rate of evolution of a system (Gieles et al, 2010), which by the theory in Section 4.3.5 would lead to a faster escape rate of BH. On the other hand mass loss via stellar evolution from the formation of the BH can cause the system to expand (Mackey et al, 2008) increasing the relaxation time in the system. This in turn would reduce the rate of energy generation in the system, which by the theory in Section 4.3.5 would prolong the life of the BH sub-system.

Another simplifying assumption was not to consider the removal of BH by natal kicks, which if large could significantly reduce the retained BH population. The topic of natal kicks for black holes is still under debate, so here we will only give the topic very general consideration. The ejection of BH by natal kicks is itself an energy source, which heats the system in qualitatively the same way as a BH ejected by superelectic encounters with binaries. Also if a natal kick is not significant enough to remove a BH from the system the BH would shed much of the kinetic energy gained from the kick to the other stars in the system. This is analogous to the results of Fregeau et al (2009), who found that adding natal kicks to white dwarfs was an additional energy source.

Another topic we have ignored is the presence of more than one stellar population in many globular clusters. In the typical scenario for the formation of the second generation stars in a globular cluster (Ventura et al, 2001) ejecta from asymptotic giant branch stars cools and collects in the centre of the cluster. If a BH sub-system is already present at the centre this

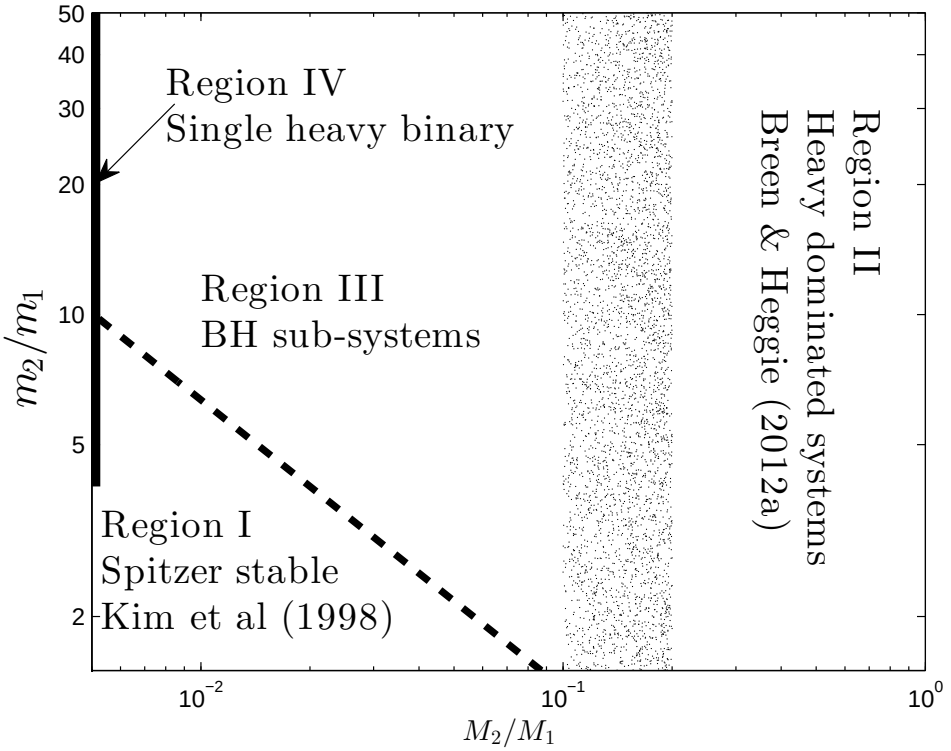

Figure 4.16: The parameter space of two component systems divided up into different regions depending on their structure and the conditions for the onset of gravothermal oscillations. See text and Table 4.8 for details

could lead to a significant increase in the stellar mass of the BH (Krause et al 2012, 2012; Leigh et al, 2012) and by the theory in Section 4.3 an increase in the total mass of the BH sub-system would increase its life time. Even in a single population scenario physical collisions can occur between BH and other stars in the system (Giersz et al, 2012), and this also would increase the total mass in the BH sub-system.

We have not considered systems which contain an intermediate mass black hole (IMBH) alongside a BH sub-system. A recent radio survey by Strader et al (2012) found no evidence of IMBH in the three globular clusters M15, M19, and M22. However, there could be other clusters which contain both an IMBH and a BH sub-system and this would be an interesting topic for future work.

4.7.3 Classification of two-component systems

In Section 4.6 we considered gravothermal oscillations in systems containing a BH sub-system. This extends the parameter space of two-component clusters studied by Breen & Heggie (2012a) to lower values of M_2/M_1 for $m_2/m_1 \geq 5$. But there are rather distinct physical characteristics of the systems studied in the two papers, as we have already seen in the study of gravothermal oscillations (Section 4.6). Here we attempt to summarise these ideas.

In order to differentiate between two-component systems a classification scheme has been devised that divides the two-component system parameter space into four regions (see Fig. 4.16). The criteria used to divide the parameter space are, (a) whether or not the isothermal region which becomes gravothermally unstable is associated with the heavy component (regions II & III) or the light component (regions I & IV), (b) whether or not the system is Spitzer stable (region I) or Spitzer unstable (regions II & III) and (c) whether or not the two-body relaxation process within $r_{\rm h}$ is dominated by the heavy component (region II) or the light component (regions I, III & IV). The differences between the regions are summarised in Table 4.8. We

Table 4.8: Summary of the different regions in the parameter space of two-component systems. The table states whether a given dynamical process is dominated by the light or heavy component of the system. $t_{\rm rh}$ represents the two-body relaxation time within $r_{\rm h}$, $t_{\rm rc}$ represents the two-body relaxation time within $r_{\rm c}$, GTO stands for gravothermal oscillations, with reference to which component contains the large isothermal region which becomes unstable, and the final column represents whether or not the system is Spitzer stable; (for Region IV, since $N_2 \sim 2$, Spitzer instability is not an appropriate concept). See text for further details.

Region	$t_{\rm rh}$	$t_{\rm rc}$	GTO	Spitzer stable
I	light	heavy	light	Y
II	heavy	heavy	heavy	N
III	light	heavy	heavy	N
IV	light	light	light	–

shall now justify the classification by considering each of the criteria used more closely.

The simplest distinction to make is between systems which are Spitzer stable and these which are Spitzer unstable, that is systems which achieve equipartition of kinetic energy by mass segregation and those which cannot. Spitzer (1987) constructed the following stability condition

$$\frac{M_2}{M_1} < 0.16\Big(\frac{m_2}{m_1}\Big)^{-\frac{3}{2}}$$

based on theoretical arguments and some simplifying assumptions. However a study by Watters, Joshi & Rasio (2000), using Monte Carlo simulations, found Spitzer's condition to be too strong and suggested a different condition of similar form with a different constant and power, for the range of stellar mass ratios they studied ($m_2/m_1 < 7$). For simplicity the Spitzer (1987) condition is used in Fig. 4.16 to divide the parameter space. The important differences between Spitzer stable and Spitzer unstable systems are, first, that equipartition of kinetic energy holds after mass segregation (i.e. $m_2\sigma_2^2 = m_1\sigma_1^2$) and, second, that for any appreciable value of m_2/m_1 the value of M_2/M_1 has to be significantly small. Both the systems in the present chapter and the systems studied by Breen & Heggie (2012a) fall into the more general class of Spitzer unstable systems. Region I consists of Spitzer stable two-component systems, and occupies the lower left part of Fig. 4.16.

Gravothermal oscillations in Spitzer stable systems were studied by Kim, Lee & Goodman (1998). They argued that because of the small values of M_2/M_1 (and the high values of m_2/m_1) the heavy component was confined to the centre of the system. They showed that the systems they studied became gravothermally unstable once a certain ratio of energy flux at $r_{\rm h}$ and $r_{\rm c}$ (i.e. ϵ) was reached, and that this value was the same as that for a one-component system. As the bulk of the system is in the light component this implies that the instability results from a large isothermal region in the light component. These remarks justify the entries in line 1 of Table 4.8.

One situation where the concept of Spitzer stability is inappropriate is where the number of heavy particles is small ($N \sim 2$). As the heavy particles tend to find their way to the core of the system and form a binary, the role of the heavy component is still significant, because this binary becomes the power source for the system lying inside the core of the light system. That is why these systems have been given their own classification, although they may be regarded as the extreme of low M_2/M_1 for both Spitzer stable and Spitzer unstable systems. Clearly in this case if gravothermal oscillations are found, they will result from a large isothermal region in the light component, hence the entries in line 4 of Table 4.8.

Finally the last division in Fig. 4.16 is between Regions II & III. The space occupied by Regions II & III consists entirely of Spitzer unstable models. The difference between these two models depends on the value of M_2/M_1. The case where $M_2 \ll M_1$, includes the topic of interest in the present chapter (i.e. systems containing BH sub-systems). Due to small M_2/M_1 in these systems the light component dominates at $r_{\rm h}$ and thus the rate of energy generation is regulated by the light component. In the case where $M_2 \gtrsim 0.1M_1$ the heavy component has a significant effect on the relaxation process within $r_{\rm h}$, particularly when $M_2 \sim M_1$ (Breen & Heggie, 2012a). The distinction between the two cases is clear when considering extreme values

of M_2/M_1, but the exact division between the two is unclear and may have some dependence on m_2/m_1. This is why a shaded area separates the two regions in Fig. 4.16. In both cases the onset of gravothermal instability is associated with a large isothermal region in the heavy component (see Section 4.6 in the present chapter and Breen & Heggie (2012a)). Another reason for the distinction between regions II & III is the theoretical arguments given in Section 4.3.6: if we consider tidally limited systems, M_2/M_1 is expected to grow with time for region II systems and decrease with time for region III systems.

Chapter 5

Conclusion and future work

5.1 Highlights

As Chapters 2, 3 & 4 in the present thesis contain a chapter summary, in the present chapter only the main conclusions and concepts will be discussed. A number of possible future projects are also discussed in Section 5.2, which build upon the research in the present thesis.

The two main topics of interest in the present thesis are gravothermal oscillations (Chapters 2 & 3, Section 4.6) and the dynamical evolution of black hole sub-systems (Chapter 4). The results form the research on gravothermal oscillations in the present thesis seems to suggest that the instability depends on the properties of the heavy component (or heavier stars for the multi-component case). A potential explanation for this is discussion in Section 2.4.2. In Chapter 2 it was found that N_2 (the number of heavy stars) acted as an approximate stability condition (for the two-component models studied in that chapter). For the pure power law IMFs considered in Chapter 3, the parameter N_{ef} (M/m_{max}) was found to act as an approximate stability condition with the stability boundary at $N_{ef} \sim 10^4$ (see Section 3.3.2). The parameter N_{ef} was also found to act as an approximate stability condition, with the same stability boundary, for the two-component models studied in Chapter 2 (see Section 3.5).

Also of interest in Section 2.4.3 was the discussion of the cycles of oscillation, where it was shown that there was a collapse in the outer part of the system to compensate for the reduction in energy generation by the expanding core. The nature of cycles discussed should be a common feature of any system undergoing gravothermal oscillations.

The most significant result in Chapter 4 is most likely that the rate of escape of BH is predicted to be independent of the properties of the BH sub-system, and is regulated by the flux of kinetic energy at r_h (Hénon's Principle). This leads to the conclusion that BH sub-systems evaporate on the t_{rh} time scale and if natal kicks are such that a globular cluster retains a significant amount of BH then it is possible that many BH exist within globular star clusters today. Another important issue discussed in Chapter 4 was that if the BH sub-system is too small balanced evolution may not be achievable. However the models considered in the present thesis were idealised and it would be interesting extending the theory developed in Chapter 4 to more realistic systems.

5.2 Future projects

5.2.1 Globular cluster containing a single massive binary

In all of the N-body runs in Chapter 4 at least a single BH - BH binary remained in the system after the BH sub-system dissolved. Alternatively if there were only two BH initially within a system, they would segregate to the centre and form a binary (as the most massive objects in the system tend to form a binary (Aarseth, 1968)). Therefore globular clusters may undergo a phase of evolution where the core is dominated by a single BH - BH binary. In a recent large N-body simulation ($N = 2 \times 10^5$), Hurley & Shara (2012) found that a BH - BH binary was found to reside in the core of the cluster for a period of $\sim 1Gyr$.

This project could be investigated initially by studying the idealised case of a single massive black hole binary in a cluster of equal mass stars. The stellar masses of the black holes in the binary could be varied and the effect that this has on the core of the cluster measured. The aim of the study could be to gain a better understanding of the effect the BH-BH binary has on the core and the time scale for the ejection of the BH-BH binary. How the time scale for the binary's ejection varies with the cluster parameters would be of particular interest.

5.2.2 Black hole sub-systems in nuclear star clusters

Nuclear star clusters are very frequent with around 75% of galaxies containing them (Côte et al, 2006). It would be interesting to see how the results of Chapter 4 apply to nuclear star clusters and how the presence of a super massive black hole (or intermediate mass black hole) affects the dynamical evolution of a black hole subsystem. Miller & Davies (2012) argued that it would not be possible for binaries to provide the energy necessary to prevent core collapse if the central velocity dispersion exceeded $\sim 40 kms^{-1}$. It would be interesting to see if any insight can be gained by treating a super massive black hole as an energy source and assuming that the nuclear star cluster is in balanced evolution (i.e. using the same approach as in Chapter 4).

5.2.3 Modelling Omega Centauri with a BH sub-system

There have been suggestions that the globular star cluster Omega Centauri might host an Intermediate Mass Black Hole (Noyola et al, 2008). Some scaled N-body simulations also indicate that this may be the case (Jalali et al, 2012). However the alternative possibility that Omega Centauri may contain a BH sub-system has never been seriously investigated. In fact Noyola et al (2008) found that the observed velocity dispersion of the centre of Omega Centauri implied the existences of a compact isothermal dark component (see Fig 6. in Noyola et al (2008)). This is exactly what one would expect to find in the core of a system containing a BH sub-system. However Noyola et al (2008) disregarded this possibility on the grounds that such a sub-system could only survive for a relatively short period of time. This is not supported by the arguments of Chapter 4, which predicted long times for BH sub-system.

To investigate the possibility of the existence of a BH sub-system in Omega Centauri, one could use scaled models in a similar way to research conducted by Jalali et al (2012). Some initial work on this project has already been done using the Monte Carlo Code (Giersz, 1998, 2001, 2006) which is part of the Astrophysical Multipurpose Software Environment (AMUSE) which is publicly available at http://amusecode.org.

Bibliography

Aarseth S.J., 1968, Bull. Astr., 3, 150

Aarseth S.J., 2003, Gravitational N-body simulations. Cambridge Univ. Press, Cambridge

Aarseth S.J., 2012, MNRAS, 422, 841

Alexander P., Gieles M., 2012, MNRAS, 422, 3415

Antonov V.A., 1962, Vest. Leningrad Univ., 7, 135 (English Transl. in IAU Symp. 113, Dynamics of Star Clusters, ed. J. Goodman & P. Hut [Dordrecht: Reidel], 525 [1985])

Banerjee S., Baumgardt H., Kroupa P., 2010, MNRAS, 402, 371B.

Banerjee S., Kroupa P., 2011, ApJ, 741, L12

Baumgardt H., 2001, MNRAS, 325, 1323

Baumgardt H., Hut P., Heggie D. C., 2002, MNRAS, 336, 1069

Baumgardt H., Makino J., Hut P. 2005, ApJ, 620, 238

Belczynski K., Kalogera V., Bulik T., 2002, ApJ, 572, 407

Bettwieser E., Sugimoto. D. 1984, MNRAS, 208, 493

Bettwieser E., Sugimoto D., 1985, MNRAS, 212, 189

Binney J., Tremaine S., 2008, Galactic Dynamics Second Edition (Princeton: Princeton University Press)

Breen P.G., Heggie D.C., 2012a, MNRAS, 420, 309

Breen P.G., Heggie D.C., 2012b, MNRAS, 425, 2493

Chernoff D.F., Weinberg M.D., 1990, ApJ, 351, 121

Cohn H., Hut P., Wise M., 1989, ApJ, 342, 814

Cohn, H. N. 1979, ApJ, 234, 1036

Côte, P., Piatek, S., Ferrarese, L., Jordan, A., Merritt, D., Peng, E. W., Hasegan, M., Blakeslee, J. P., Mei, S., West, M. J., Milosavljevic, M., Tonry, J. L. 2006, ApJS, 165, 57

Downing J.M.B., Benacquista M.J., Giersz M. & Spurzem R., MNRAS, 407, 1946

Fregeau J. M., Joshi K. J., Portegies Zwart S. F., Rasio F. A., 2002, ApJ, 570, 171

Fregeau, J. M., Richer, H. B., Rasio, F. A., Hurley, J. R. 2009, ApJ, 695, L20

Fryer, C. L., 1999, ApJ, 522, 41

Fukushige T., Heggie D. C., 2000, MNRAS, 318, 753

Giersz M., Heggie D. C., 1994, MNRAS, 268, 257

Giersz M., Heggie D. C., 1996, MNRAS, 279, 1037

Giersz, M. 1998, MNRAS, 298, 1239

Giersz, M. 2001, MNRAS, 324, 218

Giersz, M. 2006, MNRAS, 371, 484

Giersz M., Heggie D. C., 2009, MNRAS, 395, 1173

Giersz M., Heggie D.C., Hurley J., Hypki A., 2012, (arXiv:1112.6246)

Giersz M., Spurzem R., 1994, MNRAS, 269, 241

Gieles M., 2012, proceedings of the conference "370 years of Astronomy in Utrecht", eds. G. Pugliese, A. de Koter and M. Wijburg

Gieles, M., Heggie, D. C., Zhao, H. 2011, MNRAS, 413, 2509

Gürkan M. A., Freitag M., Rasio F. A., 2004, ApJ, 604, 632

Goodman J., 1984, ApJ, 280, 298

Goodman J., 1987, ApJ, 313, 576

Goodman J., 1993, in Djorgovski S.G., Meylan G., eds, ASP Conf. Ser. Vol. 50, Structure and Dynamics of Globular Clusters, Astron. Soc. Pac., San Francisco. p. 87

Gieles M., Baumgardt H., Heggie D. C., Lamers H. J. G. L. M., 2010, MNRAS, 408, L16

Harris, W.E. 1996, AJ, 112, 1487

Heggie D. C., 1975, MNRAS, 173, 729

Heggie, D.C., Aarseth S. J., 1992, MNRAS, 257, 513

Heggie D.C., Giersz M., 2009, MNRAS, 397, 46

Heggie D.C., Hut P., 2003, The Gravitational Million Body Problem. Cambridge Univ. Press, Cambridge

Heggie, D. C., Mathieu, R. D., 1986 in The Use of Supercomputers in Stellar Dynamics, ed. Hut, P., McMillan, S. L. W., p.233

Heggie, D.C., Ramamani, N., 1989, MNRAS, 237, 757

Hénon, M. 1961, AnAp, 24, 369

Hénon, M. 1965, Ann. Astr., 28, 499

Hénon, M. H. 1971, Ap&SS, 14, 151

Hénon M., 1975, in Hayli A., ed., Proc. IAU Symp 69, Dynamics of Stellar Systems. Reidel, Dordrecht, p. 133

Hurley J.R., Shara M.M., 2012, MNRAS, 425, 2872

Jalali B., Baumgardt H., Kissler-Patig M., Gebhardt K., Noyola E., L tzgendorf N., de Zeeuw P.T., 2012, A&A, 538, A19

Khalisi E., Amaro-Seoane P., Spurzem R., 2007, MNRAS, 374, 703

Kim S.S., Lee H.M. 1997, Publ, Korean Astron. Soc., 30(2), 115

Kim, S. S., Lee, H. M., Goodman, J. 1998. ApJ, 495, 786

Krause M., Charbonnel C., Decressin T., Meynet G., Prantzos N., Diehl R., 2012, A&A 546, L5

Kulkarni S.R., Hut P., McMillan S.J., 1993., Nature, 364, 421

Küpper A. H. W., Kroupa P., Baumgardt H., Heggie D. C., 2010, MNRAS, 401, 105

Lamers, H. J. G. L. M., Gieles M., Bastian N., Baumgardt H., Kharchenko N. V., Portegies Zwart S., 2005, A&A, 441, 117

Leigh N.W.C., Böker T, Maccarone T.J., Perets H.B., 2012, MNRAS, in press, (arXiv:1212.1461)

Louis P.D., Spurzem R., 1991, MNRAS, 251, 408

Lynden-Bell D., Eggleton P.P., 1980, MNRAS, 191, 483

Lynden-Bell D., Wood R., 1968, MNRAS, 138, 495

Mackey A. D., Wilkinson M. L., Davies M. B., Gilmore G. F., 2008, MNRAS, 386, 65

Makino, J. 1996, ApJ, 471, 796

Maoz E., 1998, ApJ Lett., 494, 181

McMillan S.L.W., Engle E.A., 1996, in Hut P., Makino J., eds, IAU Symp. 174, Dynamical Evolution of Star Clusters. Kluwer, Boston, p. 379

McMillan S.L.W., Hut P., Makino J., 1990, ApJ, 362, 522

Merritt D., Piatek S., Portegies Zwart S., Hemsendorf M., 2004, ApJ, 608, L25

Miller M. C., Davies, 2012, ApJ, 755, 81

Morscher M., Umbreit S., Farr W. M., Rasio F. A., 2012, ApJ, in press, (arXiv:1211.3372)

Murphy B.W., Cohn H.N., Hut P., 1990, MNRAS, 245, 335

Nitadori K., Aarseth S.J., 2012, MNRAS, 424, 545

Noyola E., Gebhardt K., Bergmann M., 2008, ApJ, 676, 1008

Takahashi K., 1995, PASJ, 47, 561

Takahashi K., Inagaki S., 1991, PASJ, 43, 589

Plummer H.C., 1911, MNRAS, 71, 460

Portegies Zwart S. F., McMillan S. L. W., 2000, ApJ, 528, L17

Repetto S, Davies M.B., Sigurdsson S., MNRAS, (subbmitted to)

Sigurdsson S., Hernquist L., 1993, Nature, 364, 423

Strader J., Chomiuk L., Maccarone T. J., Miller-Jones J.C.A., Seth A.C., Heinke C.O., Sivakoff G.R., 2012, ApJ, 750, L27

Spitzer L., 1987, Dynamical Evolution of Globular Clusters. Princeton Univ. Press, Princeton, NJ

Spurzem R., Takahashi K., 1995, MNRAS, 272, 772

van Albada T.S., 1967, Bull. Astr., 2, 59

Ventura, P., DAntona, F., Mazzitelli, I., Gratton, R., 2001, ApJ,550, L65

Vesperini E., McMillan S.L,. D'Ercole A., D'Antona F., 2010, ApJ, 713, L41

Watters W. A., Joshi K. J., Rasio F. A. 2000, ApJ, 539, 331

Appendix A

Table of Notation

Table A.1: Table of Notation. For the case of multi-component models a subscript is used to show that the term corresponds to a particular component (e.g. ρ_2 is the density of the 2nd component). Where a bar appears over a quantity in the thesis it signifies the quantity is an average (e.g. $\bar{m}$ is the average stellar mass). The subscript i is sometimes used to signify the initial value of a quantity (e.g. $t_{rh,i}$ is the initial value of t_{rh}).

α	value of dimensionless parameter $\frac{E}{M\phi_c}$
β	coefficient of energy generation by BH binary heating (equation 4.8)
BH	black hole(s)
C	various constants
G	Newton's constant
$\frac{D}{Dt}$	Lagrangian derivative (at fixed M)
$\frac{\partial}{\partial r}$	radial derivative (at fixed t)
ϵ	Goodman stability parameter (also used as energy generation rate per unit mass)
E	total energy
E_c	total energy of the core
L	energy flux
L_h	energy flux at r_h
$\ln\Lambda$	coulomb logarithm ($\Lambda = \lambda N$)
λ	coefficient in coulomb logarithm ($\lambda = 0.02$ or $\lambda = 0.11$ depending on system)
m	stellar mass
m_2/m_1	stellar mass ratio
M	total mass (sometime used as total mass within radius r)
M_{sun}	solar mass
M_2/M_1	total mass ratio
$\dot{M}_2$	rate of mass loss from BH sub-system
N	number of stars
N_{crit}	number of stars at which gravothermal oscillation first appears
N_{ef}	effective number of stars (M_{tot}/m_{max})
NBU	N-body units
p	pressure ($\rho\sigma^2$)
σ	one dimensional velocity dispersion
r	radius
r_c	core radius
r_h	half mass radius
r_t	tidal radius
ρ	mass density
t_{rh}	half-mass relaxation time
$t_{rh,ef}$	effective relaxation time based on N_{ef}
t_{rc}	core relaxation time
t_{cr}	crossing time
$T_{50\%}$ ($T_{90\%}$)	time taken for 50% (90%) of the initial mass to be lost in a BH sub-system
v	three dimensional velocity dispersion
ξ	fraction of mass lost per t_{rh}
ζ	fraction of energy conducted per t_{rh}

Appendix B

Relaxation driven evolution in multicomponent systems

B.1 Introduction

In this appendix some aspects of the dynamical evolution of multicomponent systems are considered. The two topics considered are the expansion rate and the core collapse times of multi-component systems. The main aim of the appendix is to test the use of the effective relaxation time ($t_{rh,ef}$) as a timescale for expansion and for core collapse.

B.2 Expansion rate in two-component systems

The half-mass relaxation time t_{rh} is normally defined as

$$t_{rh} = \frac{0.138 N^{\frac{1}{2}} r_h^{\frac{3}{2}}}{(G\bar{m})^{\frac{1}{2}} \ln \Lambda} \tag{B.1}$$

where $\bar{m}$ is the average stellar mass (i.e. $1/N$ in N-body units). However, as argued in Chapter 2, systems with large M_2/M_1 behave in a similar way to one-component clusters with N_{ef} stars, where N_{ef} is defined by M/m_2. In this appendix we consider the evolution of the systems in terms of the relaxation time of the equivalent one-component system, i.e. the one-component system with N_{ef} stars. This relaxation time will be referred to as the effective relaxation time ($t_{rh,ef}$) (which has been used in Chapters 2 & 3) and is defined as follows

$$t_{rh,ef} = \frac{0.138 N_{ef}^{\frac{1}{2}} r_h^{\frac{3}{2}}}{(Gm_2)^{\frac{1}{2}} \ln \Lambda} = \Big(\frac{1 + \frac{M_2}{M_1}}{\frac{M_2}{M_1} + \frac{m_2}{m_1}} \Big) t_{rh}.$$

The expansion of the cluster takes place on a timescale, which is a fraction of t_{rh} which is characterized by a factor ζ (if mass loss is negligible and $E \propto GM^2/r_h$) where

$$\frac{\dot{r}_h}{r_h} t_{rh} = \zeta.$$

If we assume (by Hénon's Principle, Section 1.2.4) that the expansion of the system is balanced by the energy generation in the core of the cluster, ζ can be use as a measured of energy generation. The values of ζ for the sets of runs with $m_2/m_1 = 2, 3, 4$ and 5 in Section 2.3.1 are plotted in figure B.1. In figure B.1 as M_2/M_1 decreases ζ reaches a maximum value at approximately $M_2/M_1 \approx 1$, after which it starts to decrease towards the value for a single-component system, i.e. $\zeta_s \approx 0.09$ (Hénon, 1965).

It would be expected that the expansion of the cluster takes place on the timescale of $t_{rh,ef}$, as it is argued in Section 2.4.2 that the energy demand and production are effectively the same

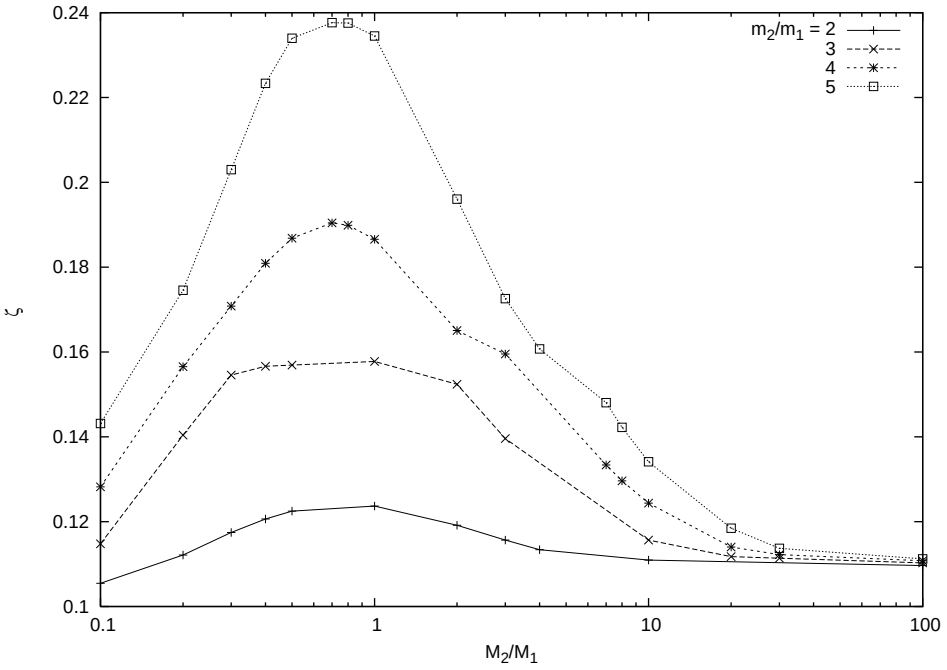

Figure B.1: ζ vs M_2/M_1 for $m_2/m_1 = 2, 3, 4$ and 5

Table B.1: Value of ζ for multi-component models

$m_{max} \backslash \alpha$	**0**	**-0.65**	**-1.3**	**-2.35**
2	0.17	0.23	0.28	0.34
1	0.16	0.21	0.22	0.26

as a in one-component system with N_{ef} stars. The value of ζ would then be expected to be approximately $t_{rh}/t_{rh,ef}\zeta_s$, where ζ_s is the value for the single component model. The predicted values of ζ are compared to the empirical values in figure B.2. Although the predicted curves in figure B.2 are always higher then the corresponding empirical results they do follow the same trend for large M_2/M_1.

For the case $m_2/m_1 = 2$, the empirical value of ζ is less then the predicted value, meaning that the system is generating less energy then expected (see Section 2.4.2). This is consistent with the argument that the predicted N_{crit} for this case is lower then the empirical value, because the predicted value overestimates the energy demand of the system.

B.3 Expansion rate in multi-component systems

The values of ζ were measured for the gas models in Chapter 3, after $2t_{cc}$, and these values are given in Table B.1. The values of ζ increase with decreasing α and there is also a less significant increase with increasing m_{max}.

In a multi-component system the more massive stars are concentrated in the inner regions of the cluster. Therefore, within the half mass radius the average stellar mass is greater than $\bar{m}$. The more massive stars within the half mass radius increases the rate of two body relaxation (i.e. reduces the timescale). If $t_{ef,rh}$ is a better estimate of the half mass relaxation timescale then it would be worthwhile measuring the expansion rate on this timescale. The expansion rate on the $t_{ef,rh}$ timescale is denoted by ζ_2. The value of ζ_2 is related to ζ as follows

$$\zeta_2 = \zeta \frac{t_{ef,rh}}{t_{rh}} = \zeta \frac{N_{ef} \ln \lambda N}{N \ln \lambda N_{ef}}.$$

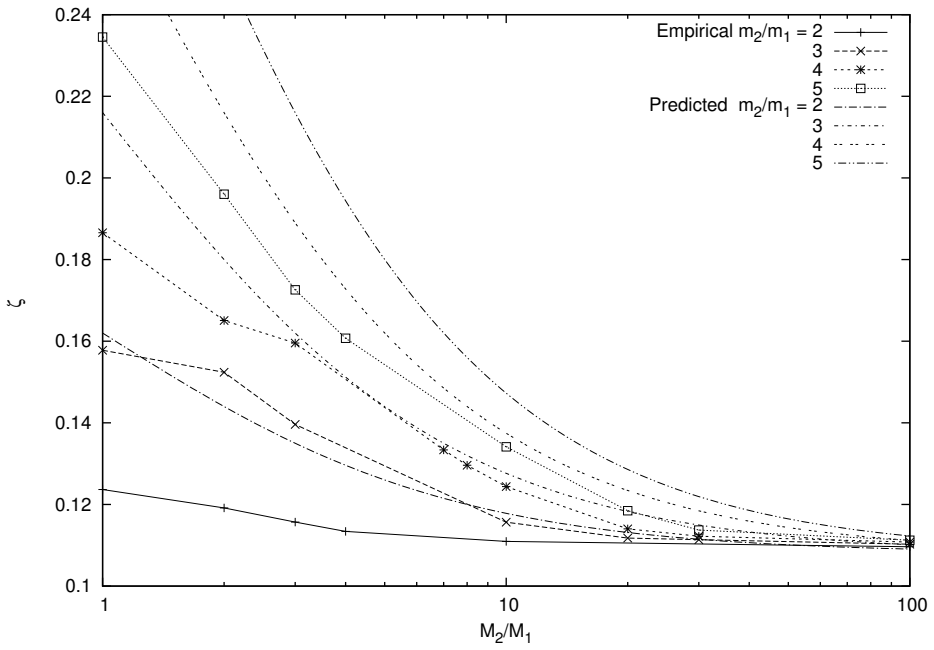

Figure B.2: Predicted values of ζ compared to values empirical; see text for details

Table B.2: Value of ζ_2 for multi-component models

$m_{max}\backslash\alpha$	**0**	**-0.65**	**-1.3**	**-2.35**
2	0.10	0.10	0.09	0.06
1	0.10	0.10	0.09	0.07

The values of ζ_2 are given in Table B.2 and are roughly equal to the value of ζ for a one-component system ($\zeta \approx 0.0926$).

If the total mass of stars with $\sim m_{max}$ is small, then it is unlikely that they would have any significant effect on the timescale of relaxation (e.g. the BH sub-systems considered in Chapter 4). Therefore there is an issue with using a relaxation time based on N_{ef} (as definition in the thesis), as it would then underestimate the relaxation time by as much as a factor $m_{max}/\bar{m}$.

B.4 Core collapse time

Mass segregation plays an important role in the dynamics of multi-component systems. As mass segregation enhances the central density, it is expected that the mass segregation timescale is comparable with the timescale of core collapse. The timescale of mass segregation is roughly t_{rh}/μ, where $\mu = m_{max}/\bar{m}$ (Gürkan et al, 2004). The timescale of mass segregation is also approximately the same as $t_{ef,rh}$ as

$$t_{ef,rh} = \frac{\ln(0.02N)}{\ln(0.02N_{ef})}\frac{N_{ef}}{N}t_{rh} = \frac{\ln(0.02N)}{\ln(0.02N_{ef})}\frac{\bar{m}}{m_{max}}t_{rh} = \frac{\ln(0.02N)}{\ln(0.02N_{ef})}\frac{1}{\mu}t_{rh}.$$

where $\frac{\ln(0.02N)}{\ln(0.02N_{ef})}$ varies from approximately 1 to 2.7 over the mass ranges given in Table B.3.

The core collapse times (t_{cc}) in units of $t_{rh,i}$ are given in Table B.3, where $t_{rh,i}$ is the initial half mass relaxation time. The values of t_{cc} vary with α and to a lesser extent with m_{max}. We can compare values in Table B.3 with the collapse time in units of $t_{ef,rh,i}$ (the initial value of $t_{ef,rh}$), which are given in Table B.4. The values in Table B.4 vary much less than the values in Table B.3.

Gürkan et al (2004) investigated systems with a wide range of initial conditions and mass

Table B.3: Core collapse times (units $t_{rh,i}$)

$(m_{max}, m_{min})\backslash\alpha$	**0**	**-0.65**	**-1.3**	**-2.35**
(2,0.1)	8.4	5.3	3.5	1.6
(1,0.1)	8.2	6.3	4.7	2.8

Table B.4: Core collapse times (units of initial $t_{ef,rh,i}$)

$(m_{max}, m_{min})\backslash\alpha$	**0**	**-0.65**	**-1.3**	**-2.35**
(2,0.1)	13.8	11.4	10.7	9.5
(1,0.1)	13.9	12.3	11.5	10.3

ranges using a Monte Carlo code. They found that the core collapse times of systems were $\propto \mu^{-1.3}$, when given in units of $t_{rh,i}$. However here we are interested in the evolution on the $t_{ef,rh}$ timescale. From the results of Gürkan et al (2004) (see Table 2 of that paper) we have the values of t_{cc} for systems with a range of m_{max} for the Salpeter IMF ($\alpha = -2.35$). These values are given in Table B.5 in units of $t_{rh,i}$ and units of $t_{ef,rh,i}$. The core collapse times vary much less in units of $t_{ef,rh,i}$ than those in units of $t_{rh,i}$. The values in units of $t_{ef,rh,i}$ are of the same order as t_{cc} for a one-component cluster with Plummer model initial conditions, which is approximately $15.5 t_{rh,i}$ (Binney & Tremaine, 2008; Heggie & Hut, 2003).

Table B.5: Core collapse times from Gürkan et al (2004) in units of $t_{rh,i}$ and $t_{ef,rh,i}$. All models had Plummer model initial conditions, a Salpeter IMF and $N = 1.25 \times 10^6$. For full details see Gürkan et al (2004)

(m_{max}, m_{min})	$t_{cc}/t_{rh,i}$	$t_{cc}/t_{ef,rh,i}$
(360,0.2)	0.0795	13.56
(240,0.2)	0.076	9.83
(120,0.2)	0.07	5.52
(90,0.2)	0.0664	4.24
(60,0.2)	0.0786	3.68
(20,0.2)	0.156	3.18
(8,0.2)	0.478	4.90
(5,0.2)	0.805	5.79
(2,0.2)	2.2	8.23
(1,0.2)	4.29	10.37

Appendix C

Evaluation of α and β in one-component models

In Chapter 4 the values of α ($E/(M\phi_c)$) and β ($\dot{E}/(\dot{M}_2\phi_c)$) were used to predicted the rate of mass loss from a BH sub-system. The values were based on the theory of one-component models. In this appendix we will attempt to measure the values of α and β in one-component N-body simulations.

In N-body units $M = 1$, $E = -0.25$ and $\phi_c \approx 1.7$ (for a Plummer model) leading to an initial value of $\alpha \approx 0.15$. However, unlike for systems which contain a BH sub-system, where ϕ_c is not expected to change much from its initial value during the formation of the BH sub-system, one-component systems undergo a much deeper core collapse resulting in a larger value of ϕ_c. The post-collapse value of α for a one-component system with $N = 4k$ was found to be ≈ 0.06 using a gas model.

For the case of BH sub-systems we argued that BH most likely escape after receiving a large velocity increase from an interaction with a BH - BH binary. Particles which escape by this method will be referred to in this appendix as ejected particles. For one-component systems particles also escape from two-body encounters. The difference, as illustrated in Fig C.1, is that two-body evaporation tends to result in escapers with a low velocity and ejected particles tend to escape with a large velocity. For the purpose of this appendix, high velocity escapers are defined as particles which escape with $v^2/<v^2> > 2$. Technically particles can escape by either process above and below this condition, however it is expected that the majority of ejected particle meet this condition and the majority of escapers by evaporation do not.

It is easy to measure the number of ejected particles per binary, by taking the ratio of binary escapers to ejected particles. For the $N = 4k$ run the result is 4.7 ejected particles per binary, which results in a total ejected mass of $6.7m$ per binary (including the binary). The same measurement was taken for a $N = 2k$ one-component run with the same initial conditions, which resulted in a similar value of $6.1m$ per binary.

In chapter 4 we considered $\dot{M}_2$ the rate of mass loss from a BH sub-system. Alternatively we could have considered $\dot{M}_{ej}$ the rate of increase in mass of ejected BH (i.e. $-\dot{M}_2$). In this case M_{ej} would simply be the total mass of ejected particles $M_{ej} = \sum m_{ej}$, where m_{ej} is the stellar mass of each ejected particle. The equation which relates M_{ej} to $\dot{E}$ is then

$$\dot{E} \approx \beta \dot{M}_{ej} |\phi_c| \approx \frac{\beta}{\alpha} \dot{M}_{ej} \frac{|E|}{M}. \tag{C.1}$$

If we assume over a period of time that there is only a small change in energy (ΔE) and that the total mass remains roughly constant, then we can integrate Eq C.1 to get

$$\Delta E \approx \frac{\beta}{\alpha} \frac{\Delta M_{ej}}{M} E_i,$$

where E_i is the initial value of E and ΔE is the change in energy. Rearranging the above

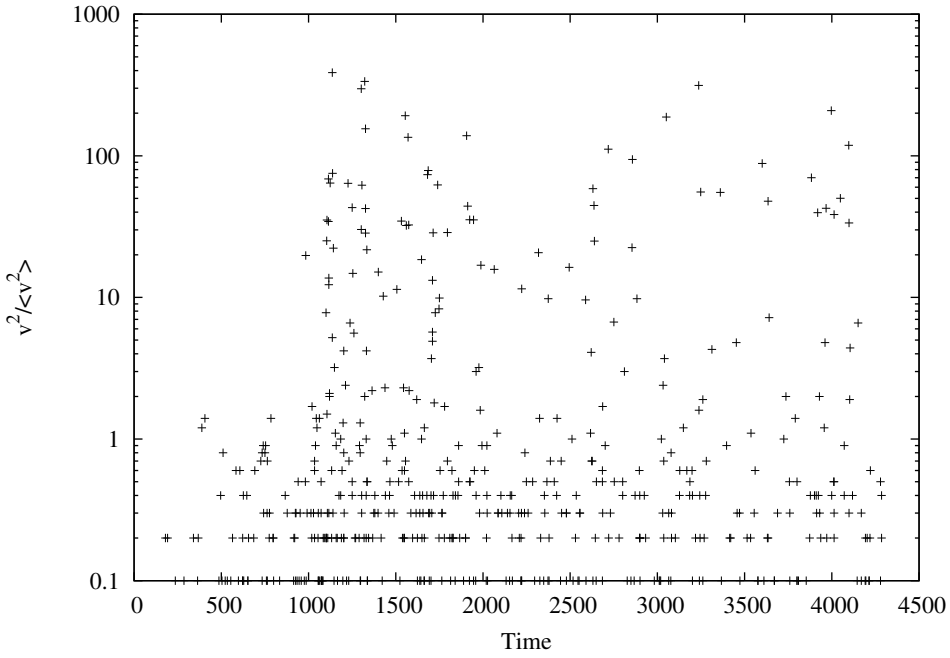

Figure C.1: The relative squared velocity of escaping stars ($v^2/<v^2>$) over time from a $N = 4k$ one-component model. Before t_{cc} ($\approx$ 1125) all escape is due to two-body evaporation as no binaries have yet formed. After t_{cc} particles escape form both two-body evaporation and strong interactions with binaries. Similar plots are given by Baumgardt et al (2002)

equation results in

$$\beta \approx \alpha \frac{\Delta E}{E_i} \Big(\frac{\Delta M_{ej}}{M} \Big)^{-1}.$$

As we are assuming all energy generation is associated with the ejection of stars, ΔE needs to be measured up to a point in time where the binding energy in binaries remaining in the system is small or preferably zero. This is because the binding energy in binaries which have not yet escaped contributes to ΔE and this energy generation might not be associated with any ejection of particles.

Evaluating β for the same run as in Fig C.1 using the above equation results in a value of ≈ 2, which is approximately consistent with the value of β used in Chapter 4.

Appendix D

Energy transport in systems containing a BH sub-system

It has been a fundamental assumption in Chapter 4 that in a system, containing a BH sub-system, the majority of energy generated first flows throughout the BH sub-system and is then transferred to the rest of the system via two-body relaxation. In this section we will discuss the validity of such an assumption. We will do this by considering the energy generated by a BH binary as it hardens and is ultimately ejected from the system, as was done for the one-component case by Heggie & Hut (2003). We shall assume that the BH binary mostly generates energy by encounters with single BH. This is a reasonable assumption as long as there are sufficient BH for the central region to be dominated by them. We can divide the life of the BH binary in the system into five energy generating phases as follows:

(1). After the BH binary is formed the interactions between the binary and the other BH will not be energetic enough to remove either from the sub-system. During this phase all the energy that is generated must be deposited within the BH sub-system.

(2). After phase (1) the binary then starts giving the single BH enough energy to escape the BH sub-system. The single BH will typically receive more kinetic energy from an encounter with a BH binary than the binary itself. During this phase the BH binary remains in the BH sub-system and the increase in the kinetic energy of the centre of mass (c.m.) of the binary is deposited in the BH sub-system. Some of the energy of the single BH, however is deposited directly into the light component though how much is discussed further below.

(3). At some point the c.m. of the BH binary will receive enough kinetic energy that it too can escape from the BH sub-system along with the single BH. As the density is much lower outside the BH sub-system, however, the binary is unlikely to deposit much any energy until it returns to the higher density region in the centre of the BH sub-system.

(4). The single BH starts receiving enough energy to escape from the system. The BH binary still escapes from the BH sub-system but remains bound to the whole system and ultimately returns to the BH sub-system.

(5). Finally the BH binary escapes from the system and the binary contributes no more energy to the system.

Using the same approach as Heggie & Hut (2003, see page 225, Box 32.1), we will now consider where the energy generated by each hard binary is distributed. As stated in Section 4.3.5 the amount of energy generated by each hard binary is expected to be $\sim 10m_2|\phi|$ and we will assume as in Section 4.3.5 that $\frac{\phi_2}{\phi_1} \approx 10^{-1}$. We will consider in turn heating from BH which do not escape the sub-system, from subescapers (BH which escape from the sub-system but not from the system) and finally from BH which escape the system.

Heating from BH which do not escape the sub-system is involved in phases 1 (the single BH and the binary) and 2 (the binary). The amount of energy generated during phase 1 can be

estimated in the same way as was done for the one component case by Heggie & Hut (2003). The result is that only about 3% of the total energy generation per hard binary is generated during this phase. Including the direct heating by the BH binary during phase 2, the total heating from BH which do not escape the sub-system is about 5.5%.

Heating from subescapers is involved in phases 2 (the single BH), 3 (the single BH and the binary) and 4 (the binary). The total amount of energy contributed by subescapers is about 49%. Initially a subescaper indirectly heats the BH sub-system, by $m_2\phi_2$ for a single BH and by $2m_2\phi_2$ in the case of the binary. The number of single subescapers is expected to be approximately 4.3 and the number of encounters which cause the binary to become a subscaper is also approximately 4.3. This is because in both cases 4.3 is the typical number of encounters needed to increase the binding energy of the binary by a factor of 10. This brings the total amount of heating (including the direct heating considered previously) to the BH sub-system to 18%.

What happens to a subescaper once it leaves the BH sub-system is a point of uncertainty. It will indirectly heat the light component up to some maximum radius (which depends on its kinetic energy) reached by the BH. It is possible that afterwards the subescaper remains on a nearly radial orbit and falls back into the BH sub-system, releasing most of its energy there. In the case of one-component systems Spitzer (1987) showed that if a particle is ejected from the core its orbit is perturbed by the other stars in the system, with the result that the particle misses the core at the next pericentre of its orbit. However it is clear that the more massive BH will be less significantly perturbed by the light stars in the system, and may well return to the sub-system at the pericentre of its orbit. If the BH does return to the sub-system then most of its energy will be distributed there, and the same reasoning will also apply to non-escaping BH binaries which are ejected from the core. If almost all the heating from subescapers occurs in the BH sub-system, then the total heating per binary (including the other heating considered previously) to the BH sub-system is now $\approx 54\%$.

Finally it is fairly easy to estimate the amount of energy resulting from escapers, which is $m_2|\phi_c|$ per single BH escaper and $2m_2|\phi_c|$ for the escape of the binary itself. The heating is indirect and heating to each component is proportional to the contribution of each component to the central potential. Per hard binary the percentage of energy generated due to escape is the same as for a one-component system, and is approximate 45%: of this about 10% goes into the heating of the BH sub-system (as $\phi_c - \phi_{c,1} \simeq 0.1\phi_c$). This type of heating is involved in phases 4 (the single BH) and 5 (the binary and single BH). Therefore the heating to the BH sub-system per hard binary may be as much as 59%. We have assumed (Sections 4.3.1 and 4.3.2) that all energy is emitted from the BH sub-system. Clearly this assumption of energy transport is only approximately valid even if the amount of heating to the BH sub-system (per BH binary) is $\sim 59\%$.

Appendix E

Heating in outer Lagrangian shells

In this section we shall consider the heating by the BH caused by the initial mass segregation. In simulations in the Chapter 4 the BH are initially spread throughout the system with the same velocity distribution as the other stars. As the BH are much more massive than the other stars the tendency towards equipartition of kinetic energy causes the BH to lose kinetic energy to the other stars, which in turn causes the BH to fall in the potential well of the cluster, causing an increase in their kinetic energy. As stated in Section 4.3, these systems are usually Spitzer unstable, and therefore equipartition of kinetic energy cannot be achieved: BH continuously fall in the potential well until they are concentrated in the centre of the system. The time this process takes depends on the location of the BH, as the process depends on the local relaxation time, which varies significantly throughout the cluster. For BH which start in the outer parts of the system this process takes the longest, as the relaxation time is longest there and they have to travel the furthest to reach the central region.

If an individual BH is initially the outer part of the system, it will be continuously heated by falling in the potential well, until it reaches a place where the relaxation time is short enough to remove its excess kinetic energy ($\sim r_h$). The amount of energy lost by the BH is $\sim m_2|\phi_{rh} - \phi_t|$, where ϕ_t and ϕ_{rh} are the gravitational potential at the edge of the system and at r_h respectively. We shall assume that $|\phi_{rh}| \gg |\phi_t|$ and so we may neglect ϕ_t; also ϕ_{rh} can be approximated by $\frac{GM}{2r_h} \approx \sigma_1^2$. Therefore the BH arrive at r_h with an energy a factor $\sim \frac{m_2}{m_1}$ greater than the other stars there. As the relaxation time is relative short at and inside r_h the system attempts to reduce the kinetic energy of the BH towards $\sim m_1\sigma_1^2$, forcing the BH towards the centre until it comes into thermal contact with the rest of the BH population.

This behaviour is illustrated in Fig. E.1 with an N-body run. This run uses $\frac{m_2}{m_1} = 5$, which is smaller than would be expected for a BH sub-system; however the small value of $\frac{m_2}{m_1}$ allows for a large value of N_2 (in this case $N_2 = 1000$) which more clearly illustrates the behaviour. As can be seen in Fig. E.1 (Bottom) the squared three dimensional velocity dispersion (v_2^2) initially decreases for the Lagrangian radii within $\sim r_h$ and initially increases for the larger Lagrangian radii. The heating in the Lagrangian radii ends when the radii enter r_h (see Fig. E.1 Top), after which they show a decrease in v_2^2 up until $t \approx 2500$ where there is an increase in v_2^2 which is associated with core collapse. By the time that core collapse has completed (at $t \simeq 3250$) most of the BH (80%) have been segregated to within $\approx 0.2r_h$. At this time the outermost Lagrangian radius (90% of M_2) has the highest value of v_2^2 (Fig. E.1 Bottom). This indicates that the outermost BH are still undergoing mass segregation (though part of the increase may be attributable to BH ejection). Indeed as can be seen in Fig. E.1 (Top) the outermost Lagrangian radius continuously contracts even after core collapse occurs.

The behaviour discussed in this section is not limited to systems containing a BH; in fact any system with a mass spectrum should also exhibit similar behaviour. The important point is that continued mass segregation serves to heat the low-mass component, and this kind of heating may affect the rate of energy generation from out sources, as energy is directly injected into the region near r_h. This effect has not been taken into account in the theory in Section

4.3, however as the values of N_2 are so small in Section 4.3 it is unlikely that this effect is significant.

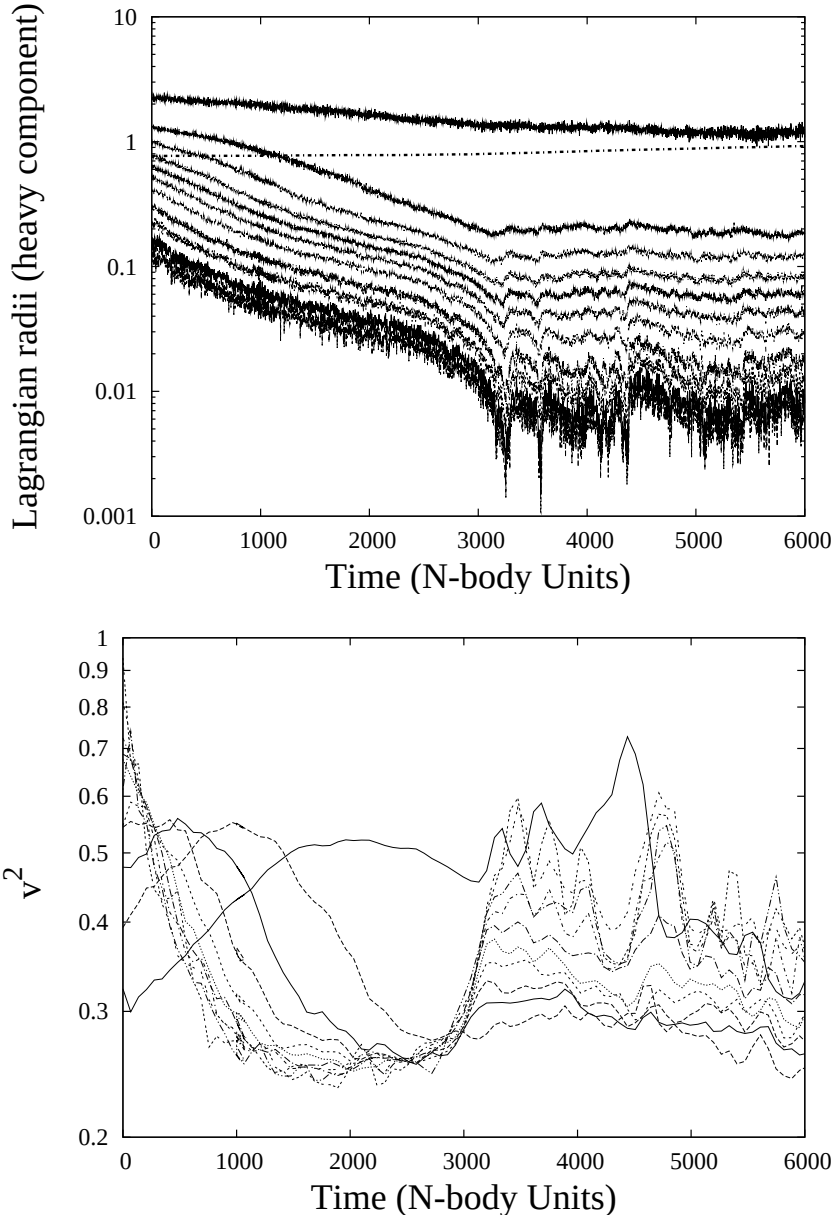

Figure E.1: Evolution of the heavy component in a two component N-body run with $N = 128k$, $\frac{m_2}{m_1} = 5$ and $\frac{M_2}{M_1} \approx 0.038$. The corresponding mass fractions are 1%, 2%, 5%, 10%, 20%, 30%, 40%, 50%, 62.5%, 75% and 90% of M_2. Bottom: Mean square velocity dispersion inside the Lagrangian shell. The 90% shell becomes the hottest shell at $t \simeq 1450$ and remains hotter than the next inner shell until well after t_{cc}. Top: plot of the radii of the Lagrangian shells in the heavy component. The dotted line is r_h the half mass radius of the whole system.